EFFECT OF SWIRL ON FLOW CHARACTERISTICS

A major thesis submitted

In partial fulfillment for the requirements of the award of degree of

Master of Engineering

In

Thermal Engineering

By
VINAY KUMAR JOSHI
ROLL NO. 8574
(Session 2004-06)

Under the Guidance of

Prof. B.B.ARORA Prof. B.D.PATHAK

Department of Mechanical Engineering,
Delhi College of Engineering, University of Delhi
DELHI 110042 INDIA

Candidate's Declaration

I hereby declare that the work which being present in the major thesis entitled "**Effect Of Swirl On Flow Characteristics**" in the partial fulfillment for the award of degree of **MASTER of ENGINEERING** with specialization in "**THERMAL ENGINEERING"** submitted to **Delhi College of Engineering, University of Delhi,** is an authentic record of my own work carried out under the supervisions of Prof B.D.PATHAK and Prof. B.B.ARORA , Department of Mechanical Engineering Delhi College of Engineering, University of Delhi. I have not submitted the matter in this dissertation for the award of any other Degree or Diploma or any other purpose whatever.

(VINAY KUMAR JOSHI)
College Roll No.05/THERMAL/2004
University Roll No: 8574

Certificate

This is to certify that the above statement made by VINAY KUMAR JOSHI is true to the best of our knowledge and belief.

(**B.B.ARORA**)
Astt Professor
Department of Mechanical Engg.
Delhi College of Engineering, Delhi

(**B.D.PATHAK**)
Asst. Professor
Department of Mechanical Engg
Delhi College of Engineering, Delhi

Acknowledgement

It is a great pleasure to have the opportunity to extent my heartiest felt gratitude to everybody who helped me throughout the course of this dissertation.

It is distinct pleasure to express my deep sense of gratitude and indebtedness to my learned supervisors Prof B.D.PATHAK and Prof. B.B.ARORA Department of Mechanical Engineering, Delhi College of Engineering, for their invaluable guidance, encouragement and patient review. Their continuous inspiration only has made me complete this dissertation. .

I would also like to take this opportunity to present my sincere regards to my teachers for their kind support and encouragement.

I am thankful to my friends and classmates for their unconditional support and motivation for this dissertation.

(Vinay Kumar Joshi)

Roll No. 8574

Abstract

A diffuser is a device for converting the kinetic energy of an incoming fluid into pressure. As the flow proceeds through the diffuser there is continuous retardation of the flow resulting in conversion of kinetic energy into pressure energy. Such a process is termed as diffusion. Diffuser forms an important part in flow machinery and structures

The present study involves the CFD analysis of effect of swirl on flow characteristics. The annular diffuser considered in the present case has both the hub and casings are diverging with unequal angles and hub angle keeping constant as 5°. The geometries of all the diffusers are calculated for constant area ratio 4 and equivalent cone angle 10, 15, 20, 25, 30. Swirl angle of 5, 10, 15, 20, 25 are introduced at the inlet. The characteristic quantities such as static pressure distribution at hub and casing walls, velocity profiles at various sections and flow patterns have been presented for studying the effect of swirl.

Introduction of swirl is found to substantially increase the rate of rise of static pressure at casing wall. Advanced turbulence models are required to study the effects of strong swirl at inlet. The difference in static pressure between hub and casing wall increases with increase in swirl angle. For equivalent cone angles up to 15 deg there is no separation observed at the casing wall for no swirl condition. With further increase in angle there is a separation at the casing wall. A high amount of swirl is required to suppress the separation on the casing wall for an equivalent cone angle of 25 degrees.

CONTENTS

List of Tables

List of Figures

List of Colour Maps of Pressure and Velocity

List of Static Pressure graphs at Re = 2.5 × 10^5

Comparative Graphs of Static Pressure at Various Equivalent Cone Angle

Comparative Graphs of Static Pressure at Various Swirl Angle

Graphs of Velocity Distribution at Various Section

Comparative Graphs of Velocity for Varying Swirl Angle

Comparative Graphs of Velocity for Varying Equivalent Cone Angle

Validation Graph

Abbreviations

C_P	Pressure recovery co-efficient
C_{PI}	ideal pressure recovery co-efficient
K	Total pressure loss co-efficient
2θ	Equivalent cone angle
θ_h	Hub angle
θ_c	Casing angle
D_{hi}	Diameter of hub at inlet to the diffuser
D_{ho}	Diameter of hub at outlet of diffuser
D_{ci}	Diameter of casing at inlet to the diffuser
D_{co}	Diameter of casing at outlet of diffuser
AR	Area ratio
B	blockage factor
A_B	Blocked area
A_E	Effective area
D_{eq}	Equivalent flow diameter
U_{in}	Velocity at inlet
U_m	Max. Velocity
P	Static pressure
P_t	Total pressure
Re	Reynolds number
v_x, v_r, v_t	Velocity in longitudinal, radial and tangential direction respectively
u_m	Mean velocity with respect to inlet
ε	Energy dissipation rate
η	Diffuser effectiveness
x,y,z	Cartesian coordinate system
μ	Laminar viscosity
μ_t	Turbulent viscosity
k	Turbulent kinetic energy
ρ	Density

τ	Stress tensor
w	Swirl velocity
ξ	Total pressure loss co-efficient
ν	Kinematic viscosity
S_m	Mass added
g	acceleration due to gravity

Chapter 1

Introduction

A diffuser is a device that increases the pressure of a fluid at the expense of its kinetic energy Japikse and Pampreen (1978). The cross-section area of diffuser increases in the direction of flow, therefore fluid is decelerated as it flows through it causing a rise in static pressure along the stream. Such a process is known as diffusion. The flow process near the diffuser walls is subjected to greater retardation due to the formation and development of the boundary layer. A study of the parameters governing the development of the boundary layer and their relationship with diffuser performance is, therefore vital in optimizing the design of a diffuser Adkin, Jacobsen and chevealier (1983).

Diffusers are extensively used in centrifugal compressors, axial flow compressors, ram jets, combustion chambers, inlet portions of jet engines etc. The energy transfer in these turbo machineries involves the exchange of significant levels of kinetic energy in order to accomplish the intended purpose. As a consequence, very large levels of residual kinetic energy frequently accompany the work input and work extraction processes, sometime as much as 50% of the total energy transferred. A small change in pressure recovery can increases the efficiency significantly. Therefore diffusers are absolutely essential for good turbo machinery performance.

1.1 TYPE OF DIFFUSERS

1.1.1 Axial Diffuser – In axial diffusers, fluid flows along the axis of diffusers and there is continuous retardation of the flow. Axial diffuser is divided in to the following categories-

• Conical diffuser

• Channel diffuser

• Annular diffuser

The basic geometric parameters for these type of diffusers are as follows:

For conical diffuser-

Non dimensional length, L/W_1

Aspect ratio, $AS = b/W_1$

Area ratio, $AR = A_2/A_1$

$$AR = 1 + 2(L/W_1)\tan\theta$$

For channel diffuser- Non dimensional length, L/D_1

Area ratio, $AR = A_2/A_1$

$$AR = [1 + 2(L/D_1)\tan\theta]^2$$

For annular diffuser- Non-dimensional length, $L/\Delta r$ or L/h

Area ratio, $AR = A_2/A_1$

$$AR = 1 + 2(L/h_1)\sin\theta$$ (For equiangular case)

1.2 ANNULAR DIFFUSER

A survey of diffuser research has revealed that considerably more investigations have been carried out on two dimensional and conical diffusers. Much of the extent data covering annular diffusers was done in the experimental laboratory Stafford and James (1957). But, the annular diffusers have a very strong industrial significance and have received attention in recent years. These types of diffuser are very much used in aircraft applications. With the help of annular diffuser the maximum presser recovery is achieved within the shortest possible length. With annular diffuser, good performance is possible with large wall angles since an inner surface is present to guide the flow radially outward. The annular diffuser affords the possibility of introducing many different geometric combinations since there is now an inner surface that can be varied independently of the outer surface. It is more difficult to define the essential geometric parameters for annular diffusers since the numbers of independent variables are large Goebel and Japikse (1981). The essential variables to define the geometry of annular diffuser are two wall angles, area ratio, non-dimensional length and inlet radius ratio. As the number of variables

increases, geometry becomes more complex. This has not been economically possible by experiments and hence led to the development of computational fluid dynamic methods to analyze the performance characteristics of annular diffuser Arora, Pathak and Singh (2005). The present study investigates the unequal angle type of annular diffuser. In these types of annular diffusers both hub and casing are diverging outward with different angle of divergence. Hub angle is kept constant at 5°.

1.3 PERFORMANCE PARAMETERS

Performance parameters are very helpful in designing and predicting the performance of diffusers. These parameters reveal that diffuser geometry will give the desire output or not. The following parameters are important to find out diffuser performance.

1.3.1 Static Pressure Recovery Coefficient –

The pressure recovery coefficient of a diffuser is most frequently defined as the static pressure rise through the diffuser divided by the inlet dynamic head.

$$C_p = \frac{p_2 - p_1}{\frac{1}{2}\rho v^2_{av1}}$$

Where subscripts 1 and 2 refers to diffuser inlet and outlet conditions respectively. v_{av1} represents the average velocity at the inlet. An ideal pressure recovery can be defined if the flow is assumed to be isentropic. Then, by employing the conservation of mass, this relation can be converted to an area ratio for incompressible flow.

$$C_{pi} = 1 - \frac{1}{AR^2}$$

1.3.2 Diffuser Effectiveness –

The diffuser effectiveness is simply the relation between the actual recovery and the ideal pressure recovery.

$$\eta = C_p / C_{pi}$$

This is an excellent parameter for judging the probable level of

performance when it is necessary to estimate the expected performance under unknown conditions, relative to available data.

1.3.3 Total Pressure Loss Coefficient –

The total pressure loss coefficient reflects the efficiency of diffusion and drag of the system. The most common definition of loss coefficient is as the ratio of total pressure rise to the diffuser inlet dynamic head.

$$K = \frac{\overline{p}_{01} - \overline{p}_{02}}{\frac{1}{2}\rho v^2_{av1}}$$

$$K = (\overline{u}_1^{\,2} - \overline{u}_2^{\,2})/U_i^{\,2} - C_p \qquad = (\alpha_1 - \alpha_2 / AR^2) - C_p$$

Where is the total pressure in the core region at the exit, the over bar indicate the mass averaged quantity, and p_{oi} α_1 and α_2 are the kinetic energy parameters at the inlet and exit of the diffuser .

For the case where the velocity profile at the inlet of diffuser is flat with a thin wall boundary layer , $\alpha_1 \approx 1$. However, due to the thickening of boundary layer through the diffuser, α_2 is generally greater than unity. Nonetheless, it is often assumed that kinetic energy coefficient are equal to unity, than

$$K = C_{pi} - C_p$$

Since flow in diffusers are subjected to an adverse pressure gradient there is a potential danger for flow separation to occur which could lead to loss in performance as well as damage of downstream equipment. The aim of design is to keep the adverse pressure gradient as high as possible, but below a critical limit, by controlling the length versus area-ratio of the diffuser.

The design requirements for a good diffuser are as following-

1. Convey the flow efficiently transferring a portion of the kinetic energy into a static pressure rise.

2. It must accept a variety of inlet conditions including extreme swirl, blockage and Mach number.
3. Deliver the fluid with reasonable velocity and angle profiles without separated regions.
4. Wall curvature must not have a deleterious effect upon passage performance.
5. Pressure recovery achieved over a short axial length.

While obtaining the best possible design, some limitations are imposed on a diffuser.
1. Limited length
2. Specified area ratio
3. Specified cross- sectional shape
4. Maximum static pressure recovery
5. Minimum stagnation pressure loss

It is not hard to appreciate that the performance of the diffuser directly and often strongly influences the overall efficiency of the turbo machine. Thus the detailed processes which occur in diffusing elements must be carefully understood and thoroughly optimized if good turbo machinery performance is to be obtained.

Chapter 2

Literature Review

Flow through a diffuser is accompanied by reduction of mean kinetic energy and a consequent increase in pressure. It is more difficult to arrange for an efficient deceleration of flow than it is to obtain an efficient acceleration. There is a natural tendency in a diffusing process for the flow to break away from the walls of the diverging passage, reverse its direction, and flow back in direction of the pressure gradient. If the divergence is too rapid, this may result in the formation of eddies with consequent transfer of some kinetic energy into internal energy and a reduction in useful pressure rise. A small angle of divergence, however, implies a long diffuser and a high value of skin friction loss. Usually, flow separation in a diffuser is sought to be avoided due to the invoked additional pressure loss. Other than in many strongly separated flows, such as the flow over a backward facing step, the point of flow separation, in diffuser, is not defined by the geometry but entirely by the pressure gradient. Hence, diffuser flows are very sensitive and are difficult to predict with numerical means. Diffusers have been studied extensively in the past, since this is a very common flow configuration. Apart from the characterization of diffusers, these flows are used to study fundamental physics of pressure-driven flow separations.

Historically, annular diffusers have ranked after channel and conical diffusers in terms of interest for research and hence fewer works is available upon which to establish the technology base for design and performance evaluation. Although annular diffusers are used in gas turbines and turbo machinery installations, it is only in the last decade that there have been any systematic investigations of there performance characteristics. The most notable contribution is that due to Sovran and Klomp (1967) who tested over one hundred different geometries, nearly all of which had conically diverging center bodies with an inlet radius ratio (R_i/R_o) of 0.55 to 0.70. The tests were carried out with a thin inlet boundary layer and the diffusers have free discharge. The tests were present as

contours of pressure recovery plotted against area ratio and non-dimensional length. Howard et al (1967) also tested symmetrical annular diffusers with center bodies of uniform diameter, using fully developed flow at inlet. The limits of the various flow regimes and the optimum performance lines were established. Besides it, some other researchers also contributed in the field of annular diffuser and concluded various important results. Much of the extent data covering the annular diffusers was done in the experimental laboratory to uncover some of the unusual performance characteristics of annular diffusers. But there are still some important unresolved questions. The reason for it is that the numbers of independent variables are large for annular diffusers. In the annular diffuser the flow take place between two boundary surfaces which can varies independently.

This chapter involves a systematic study of different geometric and flow parameters which influence the overall and internal performance of annular diffusers. In this regard the available literature has been examined with a view to make comments on the state of the art and to recognize the scope of further research on the subject.

2.1 Effect of Geometric Parameters

In an annular diffuser, a number of different geometric variables can influence the variation of pressure recovery and inlet condition of flow. The basic equations of motion reveal the importance of both geometric and aerodynamic parameters on the ultimate performance of annular diffuser. The specification of a wide variety of geometric parameters is essential before the performance of diffuser is given. In this section, the various geometric parameters and there influence on diffuser performance is reviewed.

2.1.1 Passage Divergence and Length

Area ratio and non-dimension length prescribes the overall diffusion and pressure–gradient respectively, which is the principle factor in boundary layer development. The study by Henry and Wood (1958) is useful to understand the subsonic annular diffuser. Two diffusers with area ratio 2.1 and divergence of 5º and 10º were tested at various Mach number. It found by this study that most of data clusters around a line of constant

effectiveness. It is also observed that the inner wall is being starved of fluid. If a higher divergence had been used, then one might anticipate stall on the inner surface. An extensive study is carried out by Kmonicek and Hibs (1974) in which, the pressure loss coefficient is found out on the basis of the work of compression required to meet the static pressure rise, the results are very interesting but difficult to understand due to use of unconventional terminology.

Sovran and Klomp (1967) and Howard et al. (1967) produced the first widely used annular diffuser maps for channel diffusers. Sovran and Klomp conducted a large number of performance measurements which spanned a broad selection of geometric types of diffusers. The map is only a broad representation of the bulk of configurations tested in the vicinity of their best performance areas. The poorer diffusers are not well defined by the map. These maps also show optimal diffuser geometrics under different conditions and two optimum lines are established. The line of C_p^* shows the best area ratio for a given length/passage height ratio, and the line of C_p^{**} shows the best length/ passage height ratio for a given area ratio. The same results were find out by Howard et al (1967). The important difference between this and the Sovran and Klomp (1967) map was that the latter was made for very low inlet aerodynamic blockage whereas the former study was carried out for fully developed inlet profiles, implying high aerodynamic blockage. Along the line of peak recovery there is fairly good agreement between the two maps but in the region of heavy transitory stall the maps disagree substantially.

Johnston (1959) and Johnston (1953) reported a study of four different annular diffusers. Three of the four agree tolerably well with the basics Sovran and Klomp (1967) map, one of them disagree substantially; the case a strong disagreement is probably in stall. Srinath (1968) studied four equiangular annular diffuser with 2θ = 7º, 10º, 15º and 20º respectively. Tests were reported with a variety of $L/\Delta r$ values. The line of best pressure recovery shown as C_P^* by Sovran and Klomp (1967) was again confirmed, and Srinath's map is quite similar to that of Howard et al. (1967). Srinath (1968), also observed that the existence of a down stream pipe improved the pressure recovery of the diffuser itself.

An extensive study of diffusers which, although annular, begin with a circular cross section was reported by Ishikawa and Nakamura (1989). The author found that the performance of the diffuser differed significantly depending on whether it is parallel or diverging for L/r_1 greater than about 2. When both types have the same non dimensional length and area ratio, the parallel diffuser has the higher C_P. The lines of optimum performance are also drawn. The line of C_P^* shows the best area ratio for a given non dimensional length, and the line of C_P^{**} shows the best non dimensional length for a given area ratio. In the case of the latter line, there is no difference between the parallel and diverging diffuser.

Ishikawa and Nakamura (1989), also attempted to compare their results with those of Sovran and Klomp(1967), for a conventional annular diffuser for the same wall length and area ratio, their diffuser was superior, but since the inlet conditions were different in the two studies, this conclusion is only tentative. It was also found that the addition of a conical center body improves the performance of simple conical diffusers with appreciable or large stall. The study carried out by Moller (1965), who designed an axial to radial band with the intention of eliminating diffusion in the inlet region, found that the peak pressure recovery for the entire band and radial diffuser sections was 0.88 and 0.82 for the low blockage and high blockage cases, respectively. Cockrell and Markland (1963), reported that a variation in the area ratio from 2.5 to 8.0 has a small effect on the loss coefficients of conical diffusers.

2.1.2 Wall Contouring

Several annular diffuser studies have been published in which contoured walls were an essential part of the design problem. Thayer (1971), reported that curved wall diffusers had pressure recovery as high as 0.61 to 0.65 for an area ratio of 2.15. An extensive study by Stevens and Williams (1980), reported that for curved wall diffuser, good pressure recovery was found for a loss significantly below the level which would be expected from pressure recovery loss correlation , but pressure recovery values were lower then those which would be expected from the Sovran and Klomp (1967), map. Upon careful examination, it was determined that the boundary layers in this diffuser are different from

those which would be expected in most diffuser studies. Takehira et al (1977), presented extensive data for a large set of both straight annular diffusers and curved wall diffusers, and determined that the use of strong curvature at the exit of diffuser was not debilitating but did produce a penalty compared to noncurved diffusers or diffusers with curvature at the inlet.

An additional study by Japikse (2000) shows that wall contouring is an important parameter regarding pressure recovery. Adkins et al (1983), tested an annular diffuser of constant outer radius and a conical center body with cones of different angles. In general the pressure recovery increases with decreasing cone angle for various area ratios, but the 132º and sometimes the 45º-cone angle produced lower pressure recoveries than an equivalent sudden expansion. This was attributed to a large and rapid separation at the base of the cone where the diffuser starts. Adding a radius to the base of the cone so that it smoothly blended into the upstream hub, was found to improve the performance.

2.2 Effects of Flow Parameters

2.2.1 Aerodynamic Blockage

The aerodynamic blockage on annular diffusers is much less well understood than it is in channel and conical diffusers. Coladipietro et al (1974) reported that for short diffusers, the variation of pressure recovery with blockage was similar to the channel and conical diffusers; that is the pressure recovery decreased with increasing blockage. However, for the long diffusers, higher performance was observed at the higher blockage levels.

Stevens and Williams (1980) determined that pressure recovery initially decreases with increased blockage but then for very long inlet lengths where the flow is able to achieve a fully developed form, the pressure recovery again rises. From a careful study of these data it is evident that not only the inlet boundary layer displacement thickness but also other higher order effects such as turbulence intensity and boundary layer mixing phenomena can greatly alter the measured result. In another study by Geobel and Japikse (1981) found that the pressure recovery reduces as aerodynamic blockage increases. In concluding this section several notes can be made. First, the influence of inlet conditions

on annular diffuser performance is more complicated than for channel and conical diffuser. In this case, both the hub and casing surfaces can develop boundary layers with significantly different histories. The two differing boundary layers will experience different growth processes as they pass through the diffuser. Furthermore, blockage on one wall has the effect of modifying the effective flow area and hence the core flow velocity, thereby influencing the growth of the boundary layer on the opposite wall. Hence complex interactions can develop within the diffuser.

2.2.2 Inlet Swirl

The method of swirl generation can itself influence the performance of an annular diffuser and, therefore, consideration must be given first to this question. Most investigators have chosen to generate swirled in a radial inflow plane in order to take advantage of the simple cascade design geometry. Others have preferred to use axial cascade which have the advantage that they more closely simulate specific turbo machinery flow condition and permit control of the spacing between the diffuser and the vanes in form that may be more typical of an actual turbo machine. On the other hand axial cascade invariably introduces tip and hub leakage since the cascades are of a variable geometry type, an effective sealing is impossible. In addition to inlet swirl, there may be changes in inlet turbulence intensity, velocity or total pressure gradients, vorticity or wake shading, and inlet aerodynamic blockage may change indirectly as a function of the swirl angle as it is varied. In order for firm conclusion to be drawn, the effect of swirl variation must be deciphered from the performance data.

Srinath (1968) considered an axial flow equiangular diffuser with swirl between 0º and 15º. Peak pressure recovery was found at approximately 10º and then decreased rapidly. Hoadley and Hughes (1969) tested an annular diffuser with a cylindrical inner body and reported that best recovery was achieved at approximately 10º of swirl. Divehi and Kartavenko (1975) also reported by the same type of study that the best performance can be achieved between the range of 10º to 20º of inlet swirl angle. A study is presented by Japikse and Pamprreen (1979) of an exhaust diffuser and hood found that substantial recovery has been achieved even up to swirl angle in excess of 40º.

2.2.3 Inlet Turbulence

With long approach pipes diffuser performance rises as approach length increases. This was first noted in the Cockrell and Markland (1963) and attributed this to changes in turbulence which enhances mixing transverse to flow directions, thus reducing the distortions. Indeed, the core turbulence intensity of developing pipe flow rises significantly from L_a /D is equal to 20 to 45 and than remains nearly constant. Two studies have been published which considered variation in inlet turbulence intensity or structure for there impact on annular diffuser performance. The data of Coladieiepro et al (1974) have included both low and high inlet turbulence intensity levels, and this may be explanation for the unusual measurements observed at different blockage. The second study is the work of Williams and Stevens (1969) and Stevens and Fry (1973), which showed that substantial improvements in radial momentum transport were achieved by turbulence producing grids and wall spoilers. Additional results by Hestermann et al (1995), and Klein (1995) also show that increasing the level of turbulence to 6 – 8.5 % is beneficial in increasing the pressure recovery and, in one case of removing the separation of stalled diffuser. The conclusion of above study is that the effect of increasing inlet turbulence intensity is to increase pressure recovery.

2.2.4 Mach Number Influence

Most annular diffuser research has been carried out at low inlet mach numbers. However, several studies have shown measurement at different Mach number. The study by Thayer (1971), Wood and Henry (1958) and Japikse and Pampreen (1979) illustrate virtual independence of recovery with Mach number up to some critical level of approximately 0.80 to 1.1. The actual level depends on method of measurement and the type of inlet. Wood and Henry (1971) show that a shock structure must be presented before the performance begins to deteriorate, but the reference Mach number may have little to do with the actual shock location and shock structure. In most cases, the reduction of performance with Mach number is very slight but in a few cases there can be a degradation of five or ten point of performance recovery.

2.2.5 Reynolds Number Influence

Viscosity is an important parameter in any fluid dynamic process and normally appears in the form of a Reynolds number. Typically, diffusers are characterized by a Reynolds number based on an inlet hydraulic diameter. All studies reported that the Reynolds number is a comparatively weak parameter as long as the flow is in the fully turbulent regime. Crockrell and Markland (1963) state that a variation of the inlet Reynolds number has no significant effect on the diffuser performance if this variation is uncoupled from its effects on the inlet boundary layer parameters. For Reynolds number variation within the range of 2×10^4–7×10^5, they also pointed out that the diffuser performance would be practically independent of Reynolds number provided the inlet boundary parameters remain constant. Sharan (1972) reported that for thick boundary layers, there is no change in pressure recovery as the Reynolds number increases.

2.3 Boundary Layer Parameter

The flow in diffuser is governed by the behavior of the boundary layers at the diffuser walls. The deceleration of the flow through the diffuser produces a pressure rise in the stream wise direction. The wall shear layers are therefore subjected to a positive or adverse pressure gradient. As is well known, an adverse pressure gradients cause the wall boundary layers to thicken and possibly separate from the diffuser walls, forming areas of backflow in the diffuser. The net result of thinking of the wall boundary layers or the formation of regions of backflow is the blockage of flow area which reduces the effective area available to the flow. Reduction in effective flow area in turn results in a reduced pressure rise through the diffuser.

2.3.1 Boundary Layer Suction

The effect of suction consists in the removal of decelerated fluid particles from the boundary layer before they are given a chance to cause separation. Wilbur and Higginbotham (1957) investigated the suction phenomenon and found that a suction flow rate of 2.3% increased the static pressure rise by 25 – 60% and decreased the measured total pressure loss by 63%. In another study by Wilbur and Higginbotham (1955), it is shown that suction control is not efficient when applied in an extensive backflow region

such as exists immediately downstream of an abruptly turned body. Experiments by Juhasz (1974), on short annular diffuser showed that the diffuser exit profiles could be shifted either towards the hub or towards the casing of annulus by bleeding off a small fraction of the flow through the inner and outer wall respectively. Boundary Layer Suction is also adopted by Ackert (1967), for both channel and conical diffuser with large divergence angle.

2.3.2 Blowing and Injection

Wilbur and Higginbotham (1955), found that at an injection rate of 3.4%, a 33% increases in the measured static pressure rise and a 50% decrease in the measured total pressure loss can be obtained. Juhasz (1974), have reported results of their investigations on the effect of injecting secondary fluid into wild angle conical diffusers through annular slot at inlet. Injection was found to result in considerable improvement in the uniformity of exit flow as well as in the magnitude of pressure recovery.

CHAPTER 3

Mathematical Formulation

The present study involves various models and basic laws of fluid mechanics to attain the results. FLUENT provides comprehensive modeling capabilities for a wide range of incompressible laminar and turbulent fluid problems. In fluent, a broad range of mathematical models for transport phenomena (like heat transfer swirl and chemical reactions) is combined with the ability to model complex geometries. The range of problems that can be addressed is very wide. The turbulence models provided have broad range of applicability without the need for fine tuning to a specific application.

3.1 Conservation principals

Conservation laws can be derived considering a given quantity of matter or control mass and its extensive properties, such as mass, momentum and energy. This approach is used to study the dynamics of solid bodies. In fluid flows, however it is difficult to follow a parcel of matter. It is more convenient to deal with the flow within a certain spatial region we call a control volume, rather than a parcel of matter, which quickly passes through the region of interest. For all fluid flows the two extensive properties mass and momentum are solved. Flows involving heat and mass transfer or compressibility, an additional equation of energy conservation are solved. Additional flow transport equations are solved when the flow is turbulent.

3.1.1 The Mass Conservation Equation

The equation for conservation of mass, or continuity equation, can be written as follows:

$$\frac{\partial \rho}{\partial t} + \nabla \cdot (\rho \vec{v}) = S_m$$

Equation is the general form of the mass conservation equation and is valid for incompressible as well as compressible flows. The source S_m is the mass added to the

continuous phase from the dispersed second phase (e.g., due to vaporization of liquid droplets) and any user-defined sources.

For 2D ax symmetric geometries, the continuity equation is given by

$$\frac{\partial \rho}{\partial t} + \frac{\partial}{\partial x}(\rho v_x) + \frac{\partial}{\partial r}(\rho v_r) + \frac{\rho v_r}{r} = S_m$$

Where x is the axial coordinate, r is the radial coordinate, v_x is the axial velocity, and v_r is the radial velocity.

3.1.2 Momentum Conservation Equations

Conservation of momentum in an inertial (non-accelerating) reference frame

$$\frac{\partial}{\partial t}(\rho \vec{v}) + \nabla \cdot (\rho \vec{v}\vec{v}) = -\nabla p + \nabla \cdot (\overline{\overline{\tau}}) + \rho \vec{g} + \vec{F}$$

where p is the static pressure, τ is the stress tensor (described below), and ρg and F are the gravitational body force and external body forces (e.g., that arise from interaction with the dispersed phase), respectively. F also contains other model-dependent source terms such as porous-media and user-defined sources.

The stress tensor τ is given by 2

$$\overline{\overline{\tau}} = \mu \left[(\nabla \vec{v} + \nabla \vec{v}^{\,\mathrm{T}}) - \frac{2}{3} \nabla \cdot \vec{v} I \right]$$

Where μ is the molecular viscosity, I is the unit tensor, and the second term on the right hand side is the effect of volume dilation.

For 2D ax symmetric geometries, the axial and radial momentum conservation equations and v_z is the swirl velocity.

$$\frac{\partial}{\partial t}(\rho v_x) + \frac{1}{r}\frac{\partial}{\partial x}(r\rho v_x v_x) + \frac{1}{r}\frac{\partial}{\partial r}(r\rho v_r v_x) = -\frac{\partial p}{\partial x} + \frac{1}{r}\frac{\partial}{\partial x}\left[r\mu\left(2\frac{\partial v_x}{\partial x} - \frac{2}{3}(\nabla \cdot \vec{v})\right)\right] + \frac{1}{r}\frac{\partial}{\partial r}\left[r\mu\left(\frac{\partial v_x}{\partial r} + \frac{\partial v_r}{\partial x}\right)\right] + F_x$$

3.2 TURBULENCE MODELS

Turbulent flows are characterized by fluctuating velocity fields. These fluctuations mix with transported quantities such as momentum, energy, and species concentration, and cause the transported quantities to fluctuate as well. Since these fluctuations can be of small scale and high frequency, they are too computationally expensive to simulate directly in practical engineering calculations. Instead, the instantaneous (exact) governing equations can be time-averaged, ensemble-averaged, or otherwise manipulated to remove the small scales, resulting in a modified set of equations that are computationally less expensive to solve. However, the modified equations contain additional unknown variables, and turbulence models are needed to determine these variables in terms of known quantities. FLUENT provides the following choices of turbulence models:

- Spalart-Allmaras model
- k-ε models
- Standard k-ε model
- Renormalization-group (RNG) k-ε model
- Realizable k-ε model
- k-ω models
- Standard k-ω model
- Shear-stress transport (SST) k-ω model
- Reynolds stress model (RSM)
- Large eddy simulation (LES) model

3.2.1 The Standard k-ε Model

The standard k- ε model is a semi-empirical model based on model transport equations for the turbulence kinetic energy (k) and its dissipation rate (ε). The model transport equation for k is derived from the exact equation, while the model transport equation for ε was obtained using physical reasoning and bears little resemblance to its mathematically exact counterpart.

In the derivation of the k- ε model, it was assumed that the flow is fully turbulent, and the effects of molecular viscosity are negligible. The standard k-ε model is therefore valid only for fully turbulent flows.

Transport Equations for the Standard k-ε Model

The turbulence kinetic energy, k, and its rate of dissipation, ε, are obtained from the following transport equations:

$$\frac{\partial}{\partial t}(\rho k) + \frac{\partial}{\partial x_i}(\rho k u_i) = \frac{\partial}{\partial x_j}\left[\left(\mu + \frac{\mu_t}{\sigma_k}\right)\frac{\partial k}{\partial x_j}\right] + G_k + G_b - \rho\epsilon - Y_M + S_k$$

and

$$\frac{\partial}{\partial t}(\rho \epsilon) + \frac{\partial}{\partial x_i}(\rho \epsilon u_i) = \frac{\partial}{\partial x_j}\left[\left(\mu + \frac{\mu_t}{\sigma_\epsilon}\right)\frac{\partial \epsilon}{\partial x_j}\right] + C_{1\epsilon}\frac{\epsilon}{k}\left(G_k + C_{3\epsilon}G_b\right) - C_{2\epsilon}\rho\frac{\epsilon^2}{k} + S_\epsilon$$

In these equations, G_k represents the generation of turbulence kinetic energy due to the mean velocity gradients. G_b is the generation of turbulence kinetic energy due to buoyancy. Y_M represents the contribution of the fluctuating dilatation in compressible turbulence to the overall dissipation rate. $C_{1\varepsilon}$, $C_{2\varepsilon}$, and $C_{3\,\varepsilon}$ are constants. σ_k and $\sigma\varepsilon$ are the turbulent Prandtl numbers for k and ε , respectively. S_k and S_ε are user-defined source terms.

Modeling the Turbulent Viscosity

The turbulent (or eddy) viscosity, μ_t, is computed by combining k and ε as follows:

$$\mu_t = \rho C_\mu \frac{k^2}{\epsilon}$$

where C_μ is a constant.

The model constants $C_{1\varepsilon}$, $C_{2\varepsilon}$, C_μ, σ_k, and σ_v have the following default values :

$C_{1\varepsilon} = 1.44$, $C_{2\varepsilon} = 1.92$, $C_\mu = 0.09$, $\sigma_k = 1.0$,$\sigma_\varepsilon = 1.3$

These default values have been determined from experiments with air and water for fundamental turbulent shear flows including homogeneous shear flows and decaying isotropic grid turbulence. They have been found to work fairly well for a wide range of wall-bounded and free shear flows.

Although the default values of the model constants are the standard ones most widely accepted, you can change them (if needed) in the Viscous Model panel.

3.2.2 The RNG k- ε Model

The RNG-based k-ε turbulence model is derived from the instantaneous Navier-Stokes equations, using a mathematical technique called "renormalization group" (RNG) methods. The analytical derivation results in a model with constants different from those in the standard k-ε model, and additional terms and functions in the transport equations for k and ε . It is similar in form to the standard k-ε model, but includes the following refinements:

The RNG model has an additional term in its ε equation that significantly improves the accuracy for rapidly strained flows.

The effect of swirl on turbulence is included in the RNG model, enhancing accuracy for swirling flows.

The RNG theory provides an analytical formula for turbulent Prandtl numbers, while the standard k-ε model uses user-specified, constant values.

While the standard k-ε model is a high-Reynolds-number model, the RNG theory

provides an analytically-derived differential formula for effective viscosity that accounts for low-Reynolds-number effects. Effective use of this feature does, however, depend on an appropriate treatment of the near-wall region.

These features make the RNG k-ε model more accurate and reliable for a wider class of flows than the standard k-ε model.

Transport Equations for the RNG k-ε Model

The RNG k- ε model has a similar form to the standard k-ε model:

$$\frac{\partial}{\partial t}(\rho k) + \frac{\partial}{\partial x_i}(\rho k u_i) = \frac{\partial}{\partial x_j}\left(\alpha_k \mu_{\text{eff}} \frac{\partial k}{\partial x_j}\right) + G_k + G_b - \rho\epsilon - Y_M + S_k$$

and

$$\frac{\partial}{\partial t}(\rho \epsilon) + \frac{\partial}{\partial x_i}(\rho \epsilon u_i) = \frac{\partial}{\partial x_j}\left(\alpha_\epsilon \mu_{\text{eff}} \frac{\partial \epsilon}{\partial x_j}\right) + C_{1\epsilon}\frac{\epsilon}{k}(G_k + C_{3\epsilon}G_b) - C_{2\epsilon}\rho\frac{\epsilon^2}{k} - R_\epsilon + S_\epsilon$$

In these equations, G_k represents the generation of turbulence kinetic energy due to the mean velocity gradients. G_b is the generation of turbulence kinetic energy due to buoyancy. Y_M represents the contribution of the fluctuating dilatation in compressible turbulence to the overall dissipation rate,. The quantities α_k and α_ε are the inverse effective Prandtl numbers for k and ε, respectively. S_k and S_ε are user-defined source terms.

Modeling the Effective Viscosity

The scale elimination procedure in RNG theory results in a differential equation for turbulent viscosity:

$$d\left(\frac{\rho^2 k}{\sqrt{\epsilon\mu}}\right) = 1.72\frac{\hat{\nu}}{\sqrt{\hat{\nu}^3 - 1 + C_\nu}}d\hat{\nu}$$

where

$$\begin{aligned} \hat{\nu} &= \mu_{\text{eff}}/\mu \\ C_\nu &\approx 100 \end{aligned}$$

Equation is integrated to obtain an accurate description of how the effective turbulent transport varies with the effective Reynolds number (or eddy scale), allowing the model to better handle low-Reynolds-number and near-wall flows.

In the high-Reynolds-number limit, Equation gives

$$\mu_t = \rho C_\mu \frac{k^2}{\epsilon}$$

with C_μ =0.0845, derived using RNG theory. It is interesting to note that this value of Cμ is very close to the empirically-determined value of 0.09 used in the standard k- ε model.

CHAPTER 4

CFD ANALYSIS

FLUENT is a state-of-the-art computer program for modeling fluid flow and heat transfer in complex geometries. FLUENT provides complete mesh flexibility, solving your flow problems with unstructured meshes that can be generated about complex geometries with relative ease. Supported mesh types include 2D triangular/quadrilateral, 3D tetrahedral/hexahedral/pyramid/wedge, and mixed (hybrid) meshes. FLUENT also refine or coarsen grid based on the flow solution.

4.1 Program Capabilities

The FLUENT solver has the following modeling capabilities:

- 2D planar, 2D axisymmetric, 2D axisymmetric with swirl (rotationally symmetric), and 3D flows
- Quadrilateral, triangular, hexahedral (brick), tetrahedral, prism (wedge), pyramid, and mixed element meshes
- Steady-state or transient flows
- Incompressible or compressible flows, including all speed regimes (low subsonic, transonic, supersonic, and hypersonic flows)
- Inviscid, laminar, and turbulent flows
- Newtonian or non-Newtonian flows
- Heat transfer, including forced, natural, and mixed convection, conjugate (solid/fluid) heat transfer, and radiation
- Lumped parameter models for fans, pumps, radiators, and heat exchangers
- Inertial (stationary) or non-inertial (rotating or accelerating) reference frames
- Multiple reference frame (MRF) and sliding mesh options for modeling multiple moving frames
- Mixing-plane model for modeling rotor-stator interactions, torque converters, and similar turbomachinery applications with options for mass conservation

4.2 Planning CFD Analysis

The following consideration should be taken while planning CFD analysis:

Definition of the Modeling Goals:

What specific results are required from the CFD model and how will they be used? What degree of accuracy is required from the model?

Choice of the Computational Model:

How will you isolate a piece of the complete physical system to be modeled? Where will the computational domain begin and end? What boundary conditions will be used at the boundaries of the model? Can the problem be modeled in two dimensions or is a three-dimensional model required? What type of grid topology is best suited for this problem?

Choice of Physical Models:

Is the flow inviscid, laminar, or turbulent? Is the flow unsteady or steady? Is heat transfer important? Will you treat the fluid as incompressible or compressible? Are there other physical models that should be applied?

Determination of the Solution Procedure:

Can the problem be solved simply, using the default solver formulation and solution parameters? Can convergence be accelerated with a more judicious solution procedure? Will the problem fit within the memory constraints of your computer, including the use of multigrid? How long will the problem take to converge on your computer?

Careful consideration of these issues before beginning CFD analysis will contribute significantly to the success of modeling effort.

Problem Solving Steps

Once the important features of the problem are determined, the basic procedural steps are as follows:

- Create the model geometry and grid.
- Start the appropriate solver for 2D or 3D modeling.
- Import the grid.
- Check the grid.

- Select the solver formulation.
- Choose the basic equations to be solved: laminar or turbulent (or inviscid), chemical species or reaction, heat transfer models, etc. Identify additional models needed: fans, heat exchangers, porous media, etc.
- Specify material properties.
- Specify the boundary conditions.
- Adjust the solution control parameters.
- Initialize the flow field.
- Calculate a solution.
- Examine the results.
- Save the results.
- If necessary, refine the grid or consider revisions to the numerical or physical model.

4.3 Overview of Numerical Schemes

FLUENT allows you to choose either of two numerical methods:

- Segregated solver
- Coupled solver

Using either method, FLUENT will solve the governing integral equations for the conservation of mass and momentum, and (when appropriate) for energy and other scalars such as turbulence and chemical species. In both cases a control-volume-based technique is used that consists of:

- Division of the domain into discrete control volumes using a computational grid.
- Integration of the governing equations on the individual control volumes to construct algebraic equations for the discrete dependent variables ("unknowns") such as velocities, pressure, temperature, and conserved scalars.
- Linearization of the discretized equations and solution of the resultant linear equation system to yield updated values of the dependent variables.

The two numerical methods employ a similar discretization process (finite-volume), but the approach used to linearize and solve the discretized equations is different.

4.3.1 Segregated Solution Method

The governing equations are solved sequentially (i.e., segregated from one another). Because the governing equations are non-linear (and coupled), several iterations of the solution loop must be performed before a converged solution is obtained. The various steps of iterations are as follows:

- Fluid properties are updated, based on the current solution. (If the calculation has just begun, the fluid properties will be updated based on the initialized solution.)
- The u, v, and w momentum equations are each solved in turn using current values for pressure and face mass fluxes, in order to update the velocity field.
- Since the velocities obtained in Step 2 may not satisfy the continuity equation locally, a "Poisson-type" equation for the pressure correction is derived from the continuity equation and the linearized momentum equations. This pressure correction equation is then solved to obtain the necessary corrections to the pressure and velocity fields and the face mass fluxes such that continuity is satisfied.
- Where appropriate, equations for scalars such as turbulence, energy, species, and radiation are solved using the previously updated values of the other variables.
- When interphase coupling is to be included, the source terms in the appropriate continuous phase equations may be updated with a discrete phase trajectory calculation.
- A check for convergence of the equation set is made.
- These steps are continued until the convergence criteria are met.

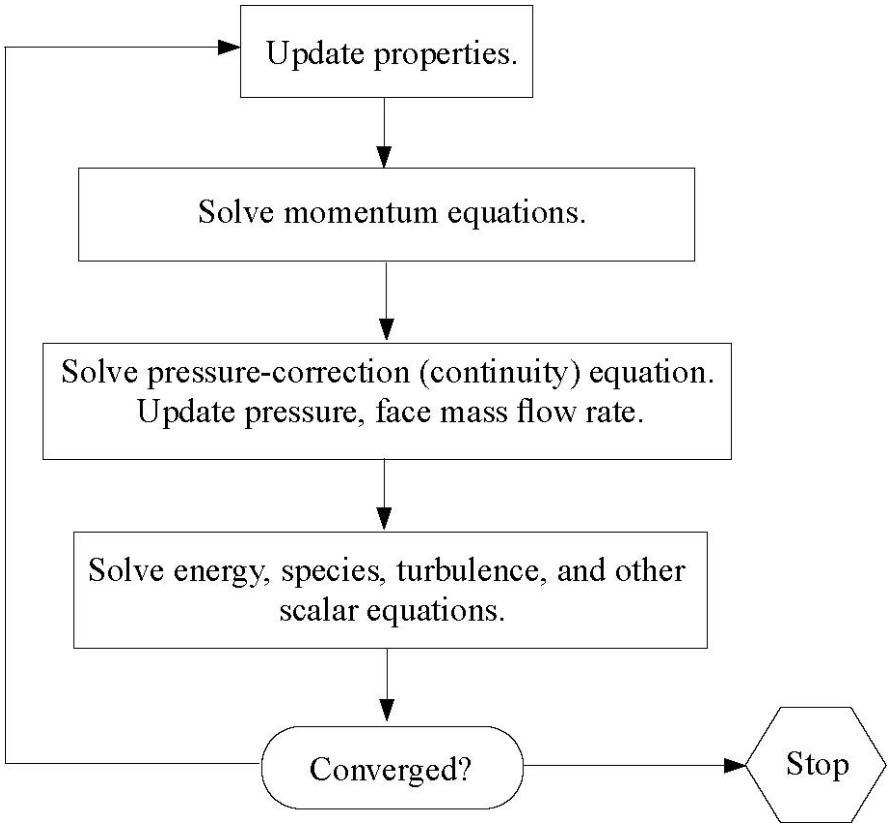

Overview of the Segregated Solution Method

4.3.2 Coupled Solution Method

The coupled solver solves the governing equations of continuity, momentum, and (where appropriate) energy and species transport simultaneously (i.e., coupled together). Governing equations for additional scalars will be solved sequentially (i.e., segregated from one another and from the coupled set) using the procedure described for the segregated solver Because the governing equations are non-linear (and coupled), several iterations of the solution loop must be performed before a converged solution is obtained. The steps of iterations are as follows:

- Fluid properties are updated, based on the current solution. (If the calculation has just begun, the fluid properties will be updated based on the initialized solution.)

- The continuity, momentum, and (where appropriate) energy and species equations are solved simultaneously.

- Where appropriate, equations for scalars such as turbulence and radiation are solved using the previously updated values of the other variables.

- When interphase coupling is to be included, the source terms in the appropriate continuous phase equations may be updated with a discrete phase trajectory calculation.

- A check for convergence of the equation set is made.

- These steps are continued until the convergence criteria are met.

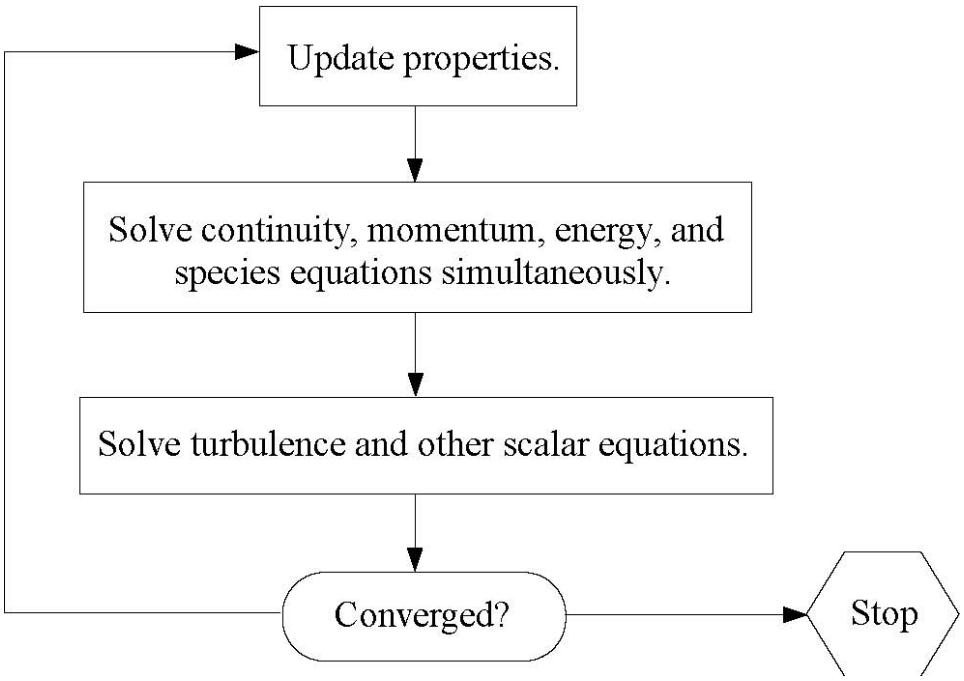

Overview of the Coupled Solution Method

4.4 Linearization: Implicit vs. Explicit

In both the segregated and coupled solution methods the discrete, non-linear governing equations are linearized to produce a system of equations for the dependent variables in every computational cell. The resultant linear system is then solved to yield an updated flow-field solution.

The manner in which the governing equations are linearized may take an "implicit" or "explicit" form with respect to the dependent variable (or set of variables) of interest. By implicit or explicit we mean the following:

Implicit: For a given variable, the unknown value in each cell is computed using a relation that includes both existing and unknown values from neighboring cells. Therefore each unknown will appear in more than one equation in the system, and these equations must be solved simultaneously to give the unknown quantities.

Explicit: For a given variable, the unknown value in each cell is computed using a relation that includes only existing values. Therefore each unknown will appear in only one equation in the system and the equations for the unknown value in each cell can be solved one at a time to give the unknown quantities.

4.5 Discretization

The governing equations are converted into algebraic equations with the help of the finite volume technique that can be solved numerically. This control volume technique consists of integrating the governing equations about each control volume, yielding discrete equations that conserve each quantity on a control-volume basis.

Discretization of the governing equations can be illustrated most easily by considering the steady-state conservation equation for transport of a scalar quantity φ. This is demonstrated by the following equation written in integral form for an arbitrary control volume V as follows:

$$\oint \rho\phi\,\vec{v}\cdot d\vec{A} = \oint \Gamma_\phi \nabla\phi \cdot d\vec{A} + \int_V S_\phi\, dV$$

where

ρ = density

v = velocity vector A = surface area vector

Γ_φ = diffusion coefficient for φ

∇_φ = gradient of φ

S_φ = source of φ per unit volume

Above equation is applied to each control volume, or cell, in the computational domain. Discretization of Equation on a given cell yields

$$\sum_f^{N_{faces}} \rho_f \vec{v}_f \phi_f \cdot \vec{A}_f = \sum_f^{N_{faces}} \Gamma_\phi (\nabla\phi)_n \cdot \vec{A}_f + S_\phi V$$

Where

N_{faces} = number of faces enclosing cell

φf = value of φ convected through face f

$\rho_f v_f A_f$ = mass flux through the face

A_f = area of face f, $|A$

$(\nabla\varphi)_n$ = magnitude of ∇φ normal to face f

V = cell volume

The equations take the same general form as the one given above and apply readily to multi-dimensional, unstructured meshes composed of arbitrary polyhedral, the discrete values of the scalar φ at the cell centers. However, face values φ_f is required for the convection terms in Equation and must be interpolated from the cell center values. This is accomplished using an upwind scheme.

Up winding means that the face value φf is derived from quantities in the cell upstream, or "upwind," relative to the direction of the normal velocity v_n

4.6 Under relaxation

In the iterative solution of the algebric or in the overall iterative scheme employed for handling nonlinearity, it is often desirable to speed up the changes, from iteration to iteration, in the values of dependent variables. This process is called under relaxation. It is a powerful device to avoid divergence in the iterative solution of strongly non linear problems. If unstable or divergent behavior is observed for a particular value of relaxation factors reduce the value of the factors for better convergence of the solution.

4.7 Convergence criteria

Finally, one needs to set the convergence criteria for the iterative method. Usually, there are two levels of iterations, within which the linear equations are solved and outer iteration that deal with the non-linearity and coupling of the equations. Deciding when to stop the iterative process on each level is important, from both the efficiency and accuracy point of view. A numerical is said to be convergent if the solution of the discretized equations tend to exact the solution of the differential as the grid spacing tends to be zero. For convergence criteria around 10^{-6} for X velocity variable, the results are stable in the present problem.

4.8 Implementation of boundary conditions

Each CV provides one algebric equation. Volume integrals are calculated for every control volume, but flux through Cv faces coinciding with the domain boundary requires special treatment. These boundary fluxes must be known, or be expressed as a combination of interior values and boundary data. Two types of boundary conditions need to be specified.

Dirchlet conditions where variable values are given at boundary nodes.

Neuman conditions where the boundary fluxes are incorporated at the boundary.

4.8.1 Inlet boundary condition

The present analysis involves the velocity with and without swirl. The incorporation of velocity without swirl can be specified by any one of the velocity specification methods described in FLUENT. Turbulence intensity is specified as

$$I = 0.16(Re_{DH})^{-1/8} \times 100$$

The inlet based on the Reynolds number with respect to equivalent flow diameter.

Where, Re_{DH} is the Reynolds number based on the hydraulic diameter.

For specifying the velocity in case of flow with swirl, tangential component of velocity will also have to be defined along with axial component. Velocity components are calculated on the basis of inlet swirl angle. In the present case swirl angle of 5, 10, 15, 20, 25 degrees are considered. Inlet velocity of 50 m/s with flat profile is considered for both the cases.

4.8.2 Outlet boundary condition

Atmospheric pressure condition is applied at the outlet boundary condition and set a "back flow" conditions is also specified if the flow reverses direction at the pressure outlet boundary during the solution process. In the "back flow" condition turbulence intensity is specified based on the equivalent flow diameter.

4.8.3 Wall boundary condition

Wall boundary conditions are used to bind fluid and solid regions. In viscous flows the no slip boundary condition is enforced at the walls. Wall roughness affects the drag (resistance) and heat and mass transfer on the walls. Hence roughness effects were considered for the present analysis and a specified roughness based on law of wall modified for roughness is considered. Two inputs to be specified are the physical roughness height and the roughness constant. And the default roughness constant (0.5) is assigned which indicates the uniform sand grain roughness.

4.8.4 Axis boundary condition

The present analysis is modeled with axisymmetric geometry. Hence the centre line of geometry is specified as the axis boundary condition.

4.9 SWIRLING FLOWS

4.9.1 Physics of Swirling and Rotating Flows

In swirling flows, conservation of angular momentum (rw or $r^2\Omega$ = constant) tends to create a free vortex flow, in which the circumferential velocity, w, increases sharply as the radius, r, decreases (with w finally decaying to zero near r = 0 as viscous forces begin to dominate). A tornado is one example of a free vortex. Figure depicts the radial distribution of w in a typical free vortex.

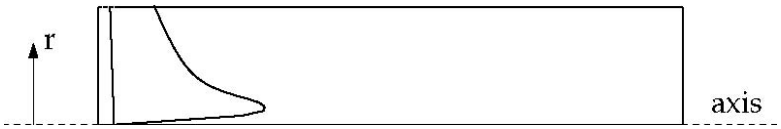

Typical Radial Distribution of w in a Free Vortex

It can be shown that for an ideal free vortex flow, the centrifugal forces created by the circumferential motion are in equilibrium with the radial pressure gradient:

$$\frac{\partial p}{\partial r} = \frac{\rho w^2}{r} \qquad (8.4\text{-}2)$$

As the distribution of angular momentum in a non-ideal vortex evolves, the form of this radial pressure gradient also changes, driving radial and axial flows in response to the highly non-uniform pressures that result. Thus, as you compute the distribution of swirl in your FLUENT model, you will also notice changes in the static pressure distribution and corresponding changes in the axial and radial flow velocities. It is this high degree of coupling between the swirl and the pressure field that makes the modeling of swirling flows complex.

In flows that are driven by wall rotation, the motion of the wall tends to impart a forced vortex motion to the fluid, wherein w/r or Ω is constant. An important characteristic of such flows is the tendency of fluid with high angular momentum (e.g., the flow near the wall) to be flung radially outward. This is often referred to as “radial pumping”, since the rotating wall is pumping the fluid radially outward.

4.9.2 Method of swirl generation

Methods of including rotation in a stream of fluid can be divided into three principle category:

- Tangential entry of the fluid stream, or a part of it ,into the cylindrical duct.
- The use of guide vanes in axial tube flow.
- Rotation of mechanical devices which impart swirling motion to the fluid passing through them. this includes rotating vanes or grids and rotating tubes.

4.9.3 Turbulence Modeling in Swirling Flows

If you are modeling turbulent flow with a significant amount of swirl (e.g., cyclone flows, swirling jets), you should consider using one of FLUENT's advanced turbulence models: the RNG k-ε model, realizable k- ε model, or Reynolds stress model. The appropriate choice depends on the strength of the swirl, which can be gauged by the swirl number. The swirl number is defined as the ratio of the axial flux of angular momentum to the axial flux of axial momentum:

$$S = \frac{\int rw\vec{v} \cdot d\vec{A}}{\bar{R}\int u\vec{v} \cdot d\vec{A}}$$

where R is the hydraulic radius.

For swirling flows encountered in devices such as cyclone separators and swirl combustors, near-wall turbulence modeling is quite often a secondary issue at most. The fidelity of the predictions in these cases is mainly determined by the accuracy of the turbulence model in the core region. However, in cases where walls actively participate in the generation of swirl (i.e., where the secondary flows and vortical flows are generated by pressure gradients), non-equilibrium wall functions can often improve the predictions since they use a law of the wall for mean velocity sensitized to pressure gradients.

4.9.4 Modeling Axisymmetric Flows with Swirl or Rotation

A 2D axisymmetric problem that includes the prediction of the circumferential or swirl velocity can be solved. The assumption of axisymmetry implies that there are no circumferential gradients in the flow, but that there may be non-zero circumferential velocities

4.9.5 Solution Strategies for Axisymmetric Swirling Flows

The difficulties associated with solving swirling and rotating flows are a result of the high degree of coupling between the momentum equations, which is introduced when the influence of the rotational terms is large. A high level of rotation introduces a large radial pressure gradient which drives the flow in the axial and radial directions. This, in turn, determines the distribution of the swirl or rotation in the field. This coupling may lead to instabilities in the solution process, and you may require special solution techniques in order to obtain a converged solution. Solution techniques that may be beneficial in swirling or rotating flow calculations include the following:

(Segregated solver only) Use the PRESTO! scheme (enabled in the Pressure list for Discretization in the Solution Controls panel), which is well-suited for the steep pressure gradients involved in swirling flows.

Ensure that the mesh is sufficiently refined to resolve large gradients in pressure and swirl velocity.

(Segregated solver only) Change the under-relaxation parameters on the velocities, perhaps to 0.3–0.5 for the radial and axial velocities and 0.8–1.0 for swirl.

(Segregated solver only) Use a sequential or step-by-step solution procedure, in which some equations are temporarily left inactive (see below).

If necessary, start the calculations using a low rotational speed or inlet swirl velocity, increasing the rotation or swirl gradually in order to reach the final desired operating condition (see below).

4.9.6 Step-By-Step Solution Procedures for Axisymmetric Swirling Flows

Often, flows with a high degree of swirl or rotation will be easier to solve if you use the following step-by-step solution procedure, in which only selected equations are left active in each step. This approach allows you to establish the field of angular momentum, then leave it fixed while you update the velocity field, and then finally to couple the two fields by solving all equations simultaneously.

! Since the coupled solvers solve all the flow equations simultaneously, the following procedure applies only to the segregated solver.

In this procedure, you will use the Equations list in the Solution Controls panel to turn individual transport equations on and off between calculations.

1. If your problem involves inflow/outflow, begin by solving the flow without rotation or swirl effects. That is, enable the Axisymmetric option instead of the Axisymmetric Swirl option in the Solver panel, and do not set any rotating boundary conditions. The resulting flow-field data can be used as a starting guess for the full problem.

2. Enable the Axisymmetric Swirl option and set all rotating/swirling boundary conditions.

3. Begin the prediction of the rotating/swirling flow by solving only the momentum equation describing the circumferential velocity. This is the Swirl Velocity listed in the Equations list in the Solution Controls panel. Let the rotation “diffuse” throughout the flow field, based on your boundary condition inputs. In a turbulent flow simulation, you may also want to leave the turbulence equations active during this step. This step will establish the field of rotation throughout the domain.

4. Turnoff the momentum equations describing the circumferential motion (Swirl Velocity). Leaving the velocity in the circumferential direction fixed, solve the momentum and continuity (pressure) equations (Flow in the Equations list in the Solution Controls panel) in the other coordinate directions. This step will establish the axial and

radial flows that are a result of the rotation in the field. Again, if your problem involves turbulent flow, you should leave the turbulence equations active during this calculation.

5. Turn on all of the equations simultaneously to obtain a fully coupled solution. Note the under-relaxation controls suggested above.

In addition to the steps above, you may want to simplify your calculation by solving isothermal flow before adding heat transfer or by solving laminar flow before adding a turbulence model. These two methods can be used for any of the solvers (i.e., segregated or coupled).

Gradual Increase of the Rotational or Swirl Speed to Improve Solution Stability

Because the rotation or swirl defined by the boundary conditions can lead to large complex forces in the flow, your FLUENT calculations will be less stable as the speed of rotation or degree of swirl increases. Hence, one of the most effective controls you can apply to the solution is to solve your rotating flow problem starting with a low rotational speed or swirl velocity and then slowly increase the magnitude up to the desired level. The procedure for accomplishing this is as follows:

1. Set up the problem using a low rotational speed or swirl velocity in your inputs for boundary conditions. The rotation or swirl in this first attempt might be selected as 10% of the actual operating conditions.

2. Solve the problem at these conditions, perhaps using the step-by-step solution strategy outlined above.

3. Save this initial solution data.

4. Modify your inputs (boundary conditions). Increase the speed of rotation, perhaps doubling it.

5. Restart the calculation using the solution data saved in step 3 as the initial solution for the new calculation. Save the new data.

6. Continue to increment the speed of rotation, following steps 4 and 5,until you reach the desired operating condition.

CHAPTER 5

Solution Procedure

The present study involves the CFD analysis of effect of swirl on flow characteristics. The annular diffuser considered in the present case has both the hub and casings are diverging with unequal angles and hub angle keeping constant as 5°. The geometries of all the diffusers are calculated for constant area ratio 4 and equivalent cone angle 10, 15, 20, 25, 30. Swirl angle of 5, 10, 15, 20, 25 are introduced at the inlet. The steps taken were

(STEP 1) Modeling (In Gambit):

- Geometry was created
- Stabilizing length equal to D was attached at inlet.
- Boundary layer was attached to both the hub and casing wall with growth factor 1.1 and 10 rows.
- The model has been meshed with quadratic-mesh. Fine meshing with spacing one was done and mesh elements range from 12000 – 55000 elements.
- Boundary conditions were externally specified.
- Boundary conditions taken were for velocity at inlet, pressure at outlet and wall type for both the hub and casing.
- Fluid was specified for the continuum type and the mesh was exported to fluent for post processing.

(STEP 2) Post Processing (In Fluent):

- Grid was checked and scaled.
- 2D axisymmetric solver and segregated solution method was chosen.
- Air was chosen as the fluid for flow, and its properties were selected.
- k-ε model was selected for non-swirling flows and RNG k-ε model was selected for swirling flows
- At air inlet section, the inlet velocity of 50 m/s with flat velocity profile was specified. For analyzing the swirling flows, Tangential component of velocity, based on the inlet swirl angle, along with the axial component was also specified.

- Turbulence intensity of 3% based on inlet flow diameter was specified.
- At the exit section, the pressure was specified being equal to atmospheric pressure.
- Second order upwind scheme was selected to solve continuity and momentum equations.
- Convergence criteria of 10^{-6} were taken.
- Solution was initialized at inlet and made to iterate until converged.
- Once solution is converged, various data for pressure and velocity were obtained and graphs were plotted.

5.1 Model Calculations:

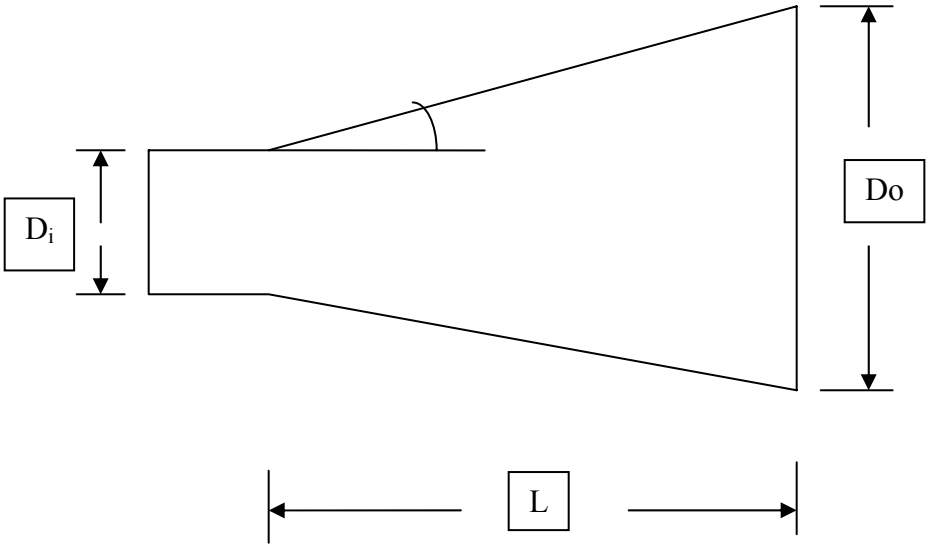

Fig 1a Conical Diffuser

AR=4

Equivalent cone angle = 15°

$D_i = 0.0135$ m

$D_o^2/D_1^2 = 4$

$D_o = 0.027$ m

$\text{Tan } 7.5 = (D_o - D_i) / 2L$

$L = (D_o - D_i) / 2\text{Tan } 7.5$

L = 0.51271

Both hub and casing diverging unequal angles :

$\pi/4(D_{co}^2 - D_{ho}^2) = \pi/4\ D_o^2$

$(D_{co}^2 - D_{ho}^2) = .000729$

$\theta_h = 5°$

$\tan \theta_h = (D_{ho} - D_{hi}) / 2L$

$D_{ho} = 0.08285$

$(D_{co}^2 - D_{ho}^2) = .000729$

$D_{co}^2 = D_{ho}^2 + 0.000729$

$D_{co}^2 = 0.158$

$\text{Tan } \theta_c = (D_{co} - D_{ci}) / 2L$

$\theta_c = 8°55'54''$

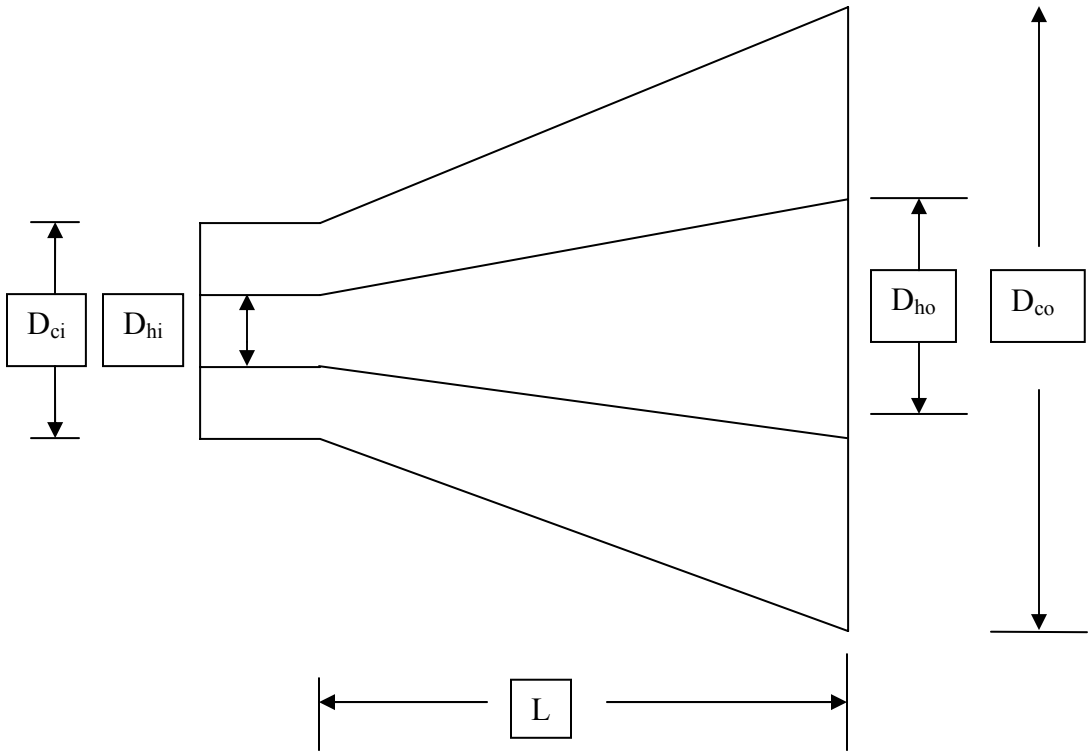

Fig 1b Diffuser with Unequal Angle Hub and Casing

5.2 Validation of Fluent Code

Different models and Boundary conditions are used to analyze the problem in FLUENT, because the exact equations for the complex phenomenon (e.g. turbulence, Swirl, Combustion) are not available. In order to choose better models and boundary conditions we have to rely on experimental data. Hence the validation of the results of scientific analysis must be compared with the experimental data.

For validation area ratio 4 with equivalent cone angle 10 degrees and swirl angle 25 deg is considered at three sections are considered. For validation work the parameters are non dimensionalised. Velocity u is converted into u/Um where u is velocity at any section and Um is the maximum velocity at that section. Similarly position parameters x & y are non dimensionalised to x/L and y/Ym respectively. Validation graphs are shown in figs 75, 76, 77. From the graphs we can see that the scientifically analyzed results are having close proximity to the experimental one. More accurate turbulence model can be chosen to correctly analyze the swirling flows.

S.no	AR	Equivalent Cone Angle(2θ)	Length(m)	Hub(m)		Casing(m)		Hub Angle θ_h	Casing Angle θ_c	Swirl Angle θ_s
				Inlet Dia(D_{hi})	Outlet Dia(D_{ho})	Inlet Dia(D_{ci})	Outlet Dia(D_{co})			
1	4	10	0.7712	0.038	0.1055	0.0775	0.1714	5°	6°56’32”	0°
			0.7712	0.038	0.1055	0.0775	0.1714	5°	6°56’32”	5°
			0.7712	0.038	0.1055	0.0775	0.1714	5°	6°56’32”	10°
			0.7712	0.038	0.1055	0.0775	0.1714	5°	6°56’32”	15°
			0.7712	0.038	0.1055	0.0775	0.1714	5°	6°56’32”	20°
			0.7712	0.038	0.1055	0.0775	0.1714	5°	6°56’32”	25°
		15	0.512	0.038	0.083	0.0775	0.158	5°	8°55’54’’	0°
			0.512	0.038	0.083	0.0775	0.158	5°	8°55’54’’	5°
			0.512	0.038	0.083	0.0775	0.158	5°	8°55’54’’	10°
			0.512	0.038	0.083	0.0775	0.158	5°	8°55’54’’	15°
			0.512	0.038	0.083	0.0775	0.158	5°	8°55’54’’	20°
			0.512	0.038	0.083	0.0775	0.158	5°	8°55’54’’	25°
		20	0.383	0.038	0.0715	0.0775	0.153	5°	11°7’20’’	0°
			0.383	0.038	0.0715	0.0775	0.153	5°	11°7’20’’	5°
			0.383	0.038	0.0715	0.0775	0.153	5°	11°7’20’’	10°
			0.383	0.038	0.0715	0.0775	0.153	5°	11°7’20’’	15°
			0.383	0.038	0.0715	0.0775	0.153	5°	11°7’20’’	20°
			0.383	0.038	0.0715	0.0775	0.153	5°	11°7’20’’	25°

Table 1 Annular Diffuser Geometries for Area Ratio 4

S.no	AR	Equivalent Cone Angle(2θ)	Length(m)	Hub(m)		Casing(m)		Hub Angle θ_h	Casing Angle θ_c	Swirl Angle θ_s
				Inlet Dia(D_{hi})	Outlet Dia(D_{ho})	Inlet Dia(D_{ci})	Outlet Dia(D_{co})			
	4	25	0.305	0.038	0.065	0.0775	0.150	5°	13°20’6’’	0°
			0.305	0.038	0.065	0.0775	0.150	5°	13°20’6’’	5°
			0.305	0.038	0.065	0.0775	0.150	5°	13°20’6’’	10°
			0.305	0.038	0.065	0.0775	0.150	5°	13°20’6’’	15°
			0.305	0.038	0.065	0.0775	0.150	5°	13°20’6’’	20°
			0.305	0.038	0.065	0.0775	0.150	5°	13°20’6’’	25°
		30	0.252	0.038	0.060	0.0775	0.1645	5°	15°34’21’’	0°
			0.252	0.038	0.060	0.0775	0.1645	5°	15°34’21’’	5°
			0.252	0.038	0.060	0.0775	0.1645	5°	15°34’21’’	10°
			0.252	0.038	0.060	0.0775	0.1645	5°	15°34’21’’	15°
			0.252	0.038	0.060	0.0775	0.1645	5°	15°34’21’’	20°

Table 1 Annular Diffuser Geometries for Area Ratio 4

CHAPTER 6

RESULTS AND DISCUSSION

Subsonic turbulent flows inside the unequal hub and casing angle annular diffusers with the effects of inlet swirl have been predicted using the FLUENT code. The following conclusions can be drawn from the results

1. For equivalent cone angles up to 15 deg there is no separation observed at the casing wall for no swirl condition. With further increase in angle there is a separation at the casing wall. Figs 2, 8, 14, 20 & 26 can be referred.
2. For an equivalent cone angle -20 deg the optimum swirl is found to be 15 deg and formation of recirculation zone near the hub wall occurs at 25 deg. Figs 14, 15, 16, 17, 18 & 19 can be referred.
3. For equivalent cone angle of 10 deg there is no separation at the hub wall for a maximum swirl angle of 25 deg but a higher recirculation zone starts near the hub wall just at 15 deg swirl angle for the equivalent cone angle of 25 deg. Fig 7 & 23 can be referred.
4. Separation at the casing wall is observed at an equivalent cone angle of 25 deg for no swirl flows. With the introduction of swirl of 10 deg, the separation is almost suppressed near the casing wall. With further increase in swirl angle a large recirculation zone is observed near the hub wall as can be seen from figs 20, 22 & 25.
5. For the equivalent cone angle of 30 deg a large recirculation zone occurs near the casing wall for 0 deg swirl angle and near the hub wall for 20 deg swirl angle. Figs 28 & 29 can be referred.
6. The difference in static pressure between hub and casing wall increases with increase in swirl angle as can be seen from figs 30, 31, 32, 33, 34, &35.
7. The static pressure distribution increases uniformly along the length of diffuser for both hub and casing walls when there is no separation or recirculation on the walls. There is an abrupt change in the static pressure whenever there is separation or recirculation on the walls as can be seen from figs 41, 46, 47 & 53.

8. The rate of rise of static pressure also increases with increase in equivalent cone angle as can be seen from fig 58, 59 & 60.
9. The rate of rise of static pressure at casing wall increases with increase in swirl angle as can be seen from fig 61, 62 & 63.
10. Fig 64, 65 & 66 shows the distribution of velocity at various section of diffuser during the flow for various equivalent cone angles. It can be seen from figures that the velocity reduces as the flow precedes towards the outlet and with increases in equivalent cone angle the point of maximum velocity shifts towards the hub because of separation at casing wall.
11. With the increase in swirl angle for constant equivalent cone angle the point of maximum velocity shifts towards the casing wall. Swirl causes the flow to divert towards the casing wall to reduce the zone of separation but after 15 deg of swirl angle the flow start separating near the hub wall as can be seen from fig 67, 68, 69, & 70.
12. The swirl angle that can withstand without a recirculation zone at the hub wall depends on the equivalent cone angle. Swirl angle decreases with increase in the equivalent cone angle as can be seen from figs 71, 72, 73, & 74.
13. Turbulence is affected by the swirl in the mean flow; hence in order to account for the effects of swirl the turbulent viscosity in k-ε model must be modified for swirling flows. The effect of swirl on the flow is well predicted by considering the advanced turbulence model (RNG k-ε) available in FLUENT code which yields an appreciable improvement in flow characteristics over the standard k-ε model.

CHAPTER 7

RECOMMENDATIONS FOR FUTURE WORK

- The present analysis is done for an area ratio of 4 for different divergence angle. As the area ratio is an important parameter, which indicates the overall diffusion and hence varying the area ratio can extend further studies.

- The effect of hub-generated swirl can be considered for future study.

- The effect of Mach number can be studied.

- Modeling of the geometry can be modified by attaching a tailpipe at the exit to recover some of the excess kinetic energy of a non-uniform diffuser exit profile in to pressure energy.

- The analysis is basically performed with an advanced k-ε model for swirling flows. Higher order discretization schemes and still better turbulence models can be used for better results in case of swirling flows.

REFERENCES

1. Ackert ,J. 1967. Aspect Of Internal Flow. Fluid Mechanics Of Internal Flow ,Ed. Sovaran G., Elsvier Amsterdum,pp1.

2. Adkins R.C ,Jacobsen OH , Chevealier P 1983 A Premilary Study of Annular Diffuser With Constant Diameter Outer Wall. ASME paper no. 83-GT-218

3. Adkins R.C.,1983. A simple Method For Design Optimum Annular Diffusers. ASME Paper No. 83-GT-42.

4. Arora, B.B.,Pathak, B.D.,2005 "Flow characteristics of parallel hub diverging casing axial annular diffusers". ISME publication pp 794-798

5. Cockrell, D.J., Markland, E., 1963 .A Review of Incompressible Diffuser Flow. Aircraft Engg. Volume 35 , pp 286.

6. Coladipietro, R., Schneider, J.M., Sridhar, K.1974. "Effects of Inlet Flow Conditions on the Performance of Equiangular Annular Diffusers," Trans. CSME 3 (2): pp. 75-82.

7. Dovzhik, S.A., Kartavenko, V.M.,1975. "Measurement of the Effect of Flow Swirl on the Efficiency of Annular Ducts and exhaust Nozzles of Axial Turbomachines," Fluid Mechanics/Soviet Research 4(4): 156-172.

8. Goebel, J. H., Japikse, D., "The Performance of an Annular Diffuser Subject to Various Inlet Blockage and Rotor Discharge Effects," Consortium Final Report, Creare TN-325, March 1981.

9. Hesterman R, Kim S ,Ban Khalid A, Wittigs 1995. Flow Field And Performances Characteristics Of Combustor Diffusers: A Basic Study. Trans. ASME Journal Engineering for Gaas Turbine and Power 117: pp 686-694.

10. Hoadley D,1970. Three Dimensional Turbulent Boundary Layers in an Annular Diffuser. PhD Thesis University of Canbrige.

11. Hoadley, D., Hughes, D.W.,1969. “Swirling Flow in an Annular Diffuser,” University of Cambridge, Department of Engineering, Report CUED/A-Turbo/TR5.

12. Howard, J. H. G., Thorton –Trump A. B., Henseler H. J. 1967” Performance And Flow Regime For Annular Diffusers”.ASME paper no . 67-WA/FE-21.

13. Ishkawa K,Nakamura I 1989”An Experimental Study on The Performance of Mixed Flow Type Conical Wall Annular Diffuser “ ASME FED-69.

14. Japikse, D., 1986. “A New Diffuser Mapping Technique – Studies in Component Performance: Part 1,” ASME Paper No. 84-GT-237, Amsterdam, June 1984; also, Journal of Fluids Engineering, Vol. 108, No. 2. pp. 148-156.

15. Japikse, D., and Pampreen, R., “Annular Diffuser Performance for an Automotive Gas Turbine,” ASME Publication 78-GT-147. 1978.

16. Japikse, D.,1980. “The Influence of Inlet Turbulence on Diffuser Performance,” Concepts ETI, Inc., Design Data Sheet No. 1, .

17. Japikse, D.,2000. “Performance of Annular Diffusers Subject to Inlet Flow Field Variations and Exit Distortion,” presented at the ISROMAC conference in Honolulu, Hawaii, March 26-30,.

18. Johanston I.H.,1959. Effect Of Inlet Conditions On The Flow In Annular Diffusers. National Gas Turbine Establishment Memo No.167,Cp No.178

19. Jonston J P 1959 “Summary of Results of Test on Short Conical Diffuser With Flow Control Inserts: as of June 1,1959.Ingersoll – Rand TN no 71.

20. Juhasz,A.J. 1974. Performance Of An Asymmetric Annular Diffuser With Non Diverging Inner Wall Using Sution .NASA TN -7575.

21. kamonicek V, Hibs M,1974.Results Of Experimental And Theoretical Investigation Of Annular Diffuser. CSIRO,Division of Mechanical Engg.

22. Klein, A., 1995. Characteristics of Combustor Diffusers. Prog .Aerospace Sci. 31: 171-271

23. Moller E.S,1965. Radial Diffuser Using Incompressible Flow Between Disks. ASME paper no. 65-FE-12.

24. Moller E.S.,1965.Radial Flow Without Swirl Between Parallel Disks Havimg Both Supersonic And Subsonic Resions .ASME paper no. 65-FE-11.

25. Shaalan, M.R.A., Shabaka, I.M.M.,1975. “An Experimental Investigation of the Swirling Flow Performance of an Annular Diffuser at Low Speed,” ASME Paper No. 75-WA/FE-17.

26. Sharan V K, 1972.Diffuser Performance Co-Relations. JASI, Volume 24,pp415.

27. Sovran, G., Klomp, E.D.,1967. “Experimentally Determined Optimum Geometries for Rectilinear Diffusers with Rectangular, Conical or Annular Cross-Section,” Fluid Dynamics of Internal Flow, Elsevier Publishing Company.

28. Srinath T 1968 “ An Investigation of The Effects of Swirl on The Flow Regimes and Performance of Annular Diffuser With Equal Inner and Outer Cone Angles .” M.A. Science Thesis , University of Waterloo Canada

29. Stafford ,W . Willber, Jams T. Higginbothom, 1955. Investigation of Two Short Annular Diffuser Configurations Utilizing Suction and Injection as Means of Boundary

Layer Control. NACA RM L54K18.

30. Stafford W.Willbur, James T.H.1957. Investigation Of Short Annular Diffuser Configuration Utilizing Suction As A Means Of Boundary Layer Control. NACA TN-3996

31. Stevan S. J., Williams G.J., 1980. The Influence of Inlet Conditions on the Performance of Annular Diffuser. Trans. ASME Journal Fluids Engg. 102, 357-363.

32. Steven S.J.,Williams G.J.,1969. Performance Of Annular Diffusers. Gas Turbine Collaboration Committee Report No. 299.

33. Stevens S.J., Fry P.,1973 . Measurements of The Boundary Layer Growth in Annular Diffusers . Journal Aircraft Feb., pp 73-89.

34. Sultanian,B.K.Nagao,S.,Sakamato,T., "Experimental and three dimensional CFD investigation in a gas turbine exhaust system",ASME Journal of engineering for gas turbines and power,121, pp.364-374,1999.

35. Takehira, A., et al. "An Experimental Study of the Annular Diffusers in Axial-Flow Compressors and Turbines," Japan Society of Mechanical Engineers, Paper No.39, 1977.

36. Thayer E B 1971"Evaluationof Curved Wall Annular Diffuser " ASME paper no .71-WA/FE-35

37. Wood, C .C., Henary, J.R., 1958. Effects of Shock Boundary Layer Interaction on The Long and Short Subsonic Annular Diffuser .NACA RM L58A31.

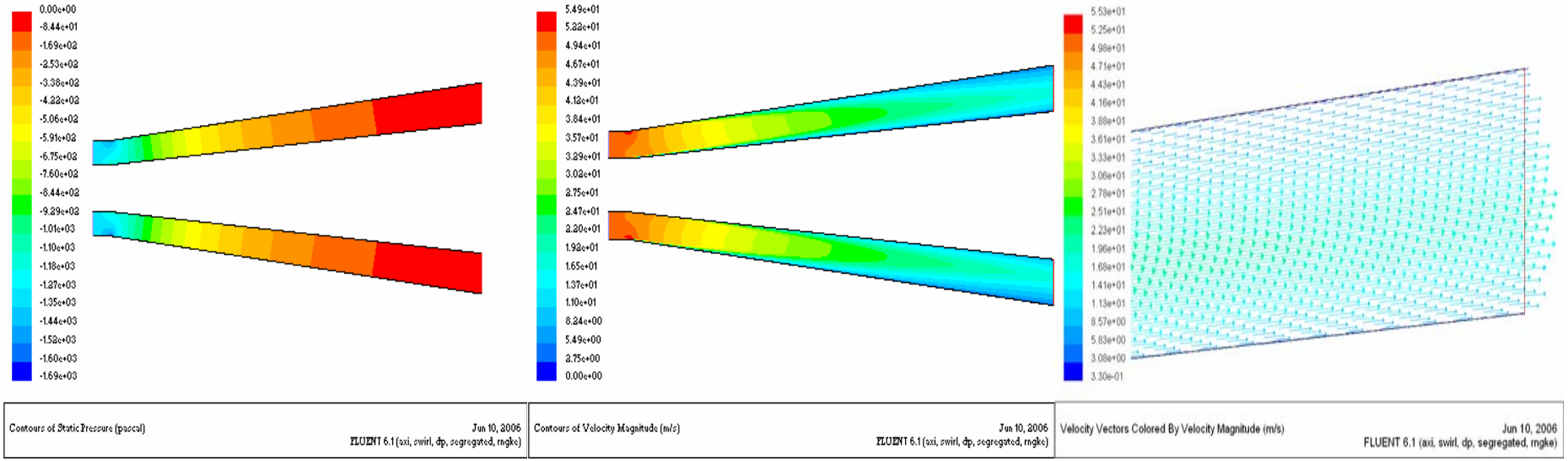

Static Pressure Contours **Velocity Contours** **Velocity Vectors**

Fig 2 AR= 4, Equivalent cone Angle = 10 deg, Swirl Angle = 0 deg, Velocity = 50m/s

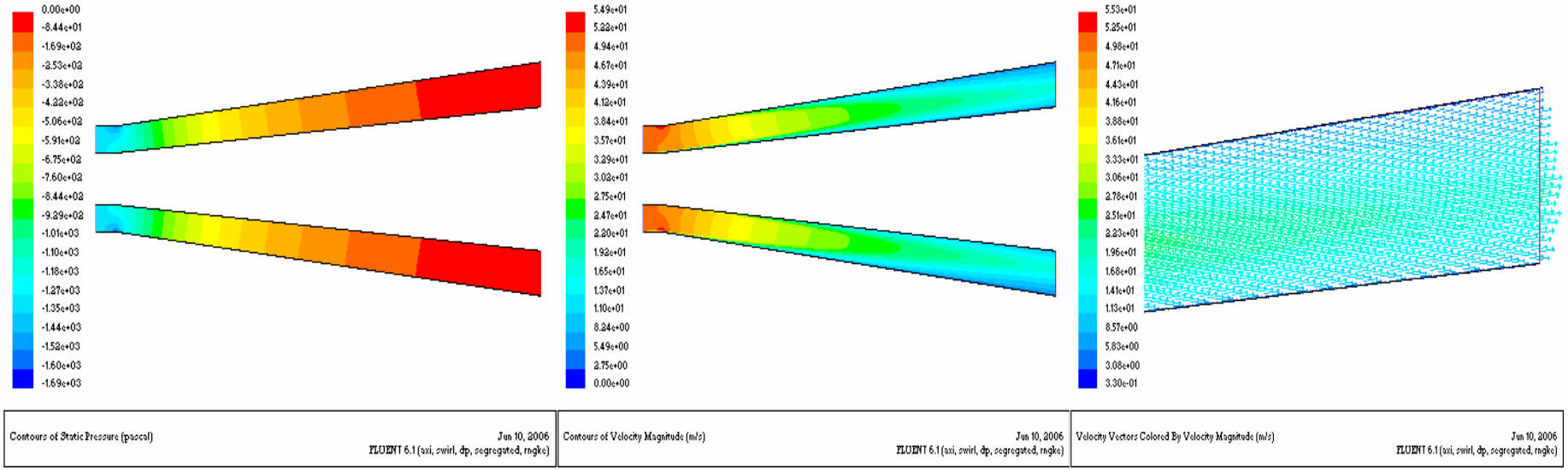

Static Pressure Contours **Velocity Contours** **Velocity Vectors**

Fig 3 AR= 4, Equivalent cone Angle = 10 deg, Swirl Angle = 5 deg, Velocity = 50m/s

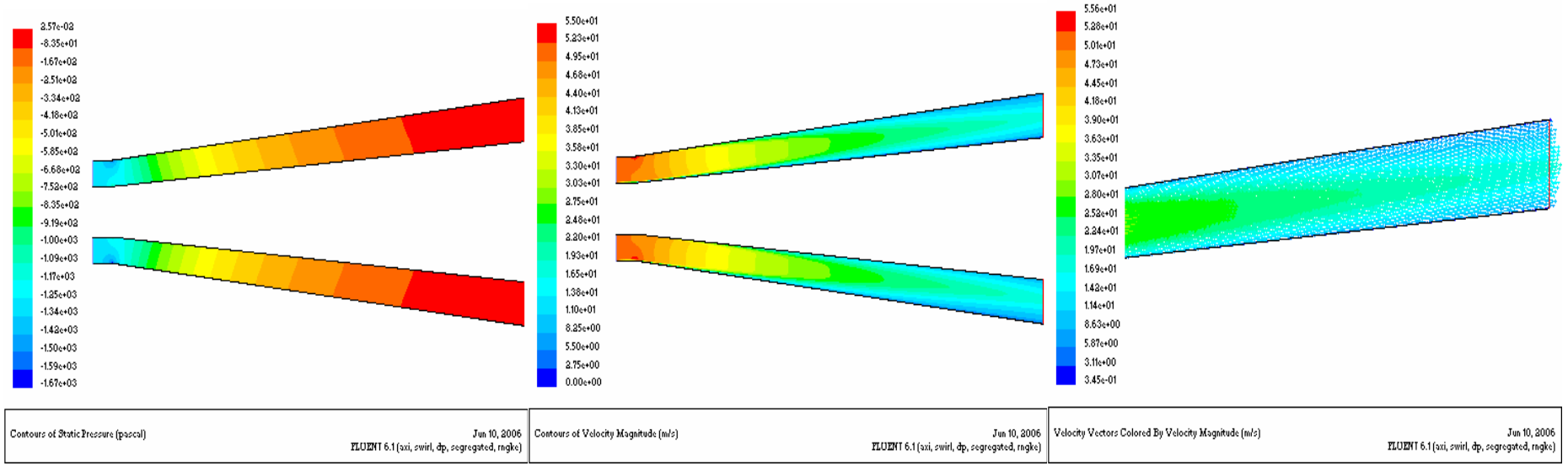

Static Pressure Contours **Velocity Contours** **Velocity Vectors**

Fig 4 AR= 4, Equivalent cone Angle = 10 deg, Swirl Angle = 10 deg, Velocity = 50m/s

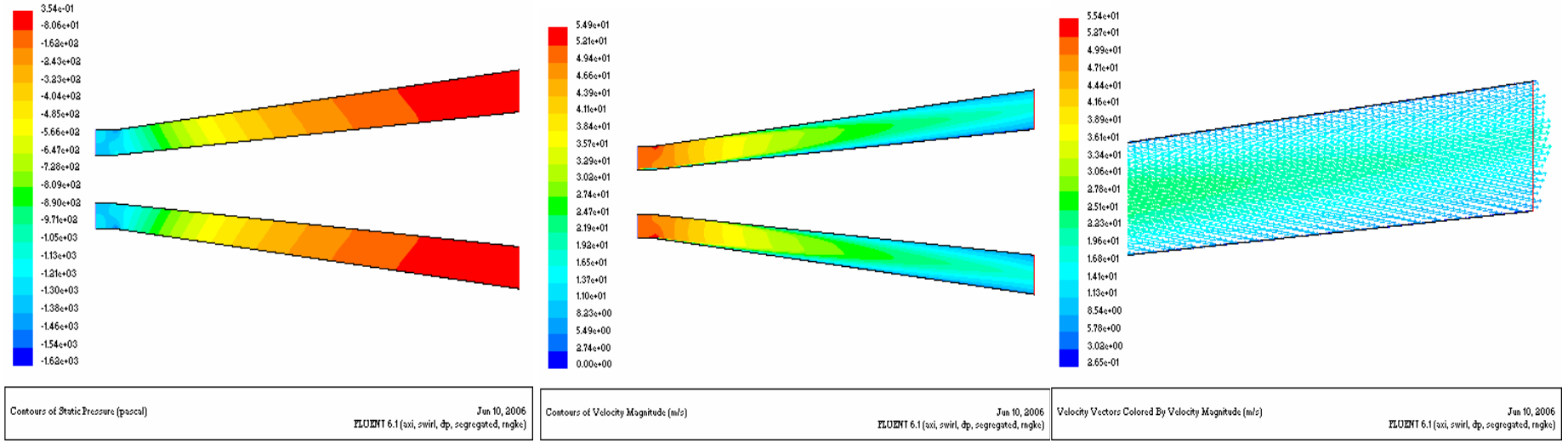

Static Pressure Contours **Velocity Contours** **Velocity Vectors**

Fig 5 AR= 4, Equivalent cone Angle = 10 deg, Swirl Angle = 15 deg, Velocity = 50m/s

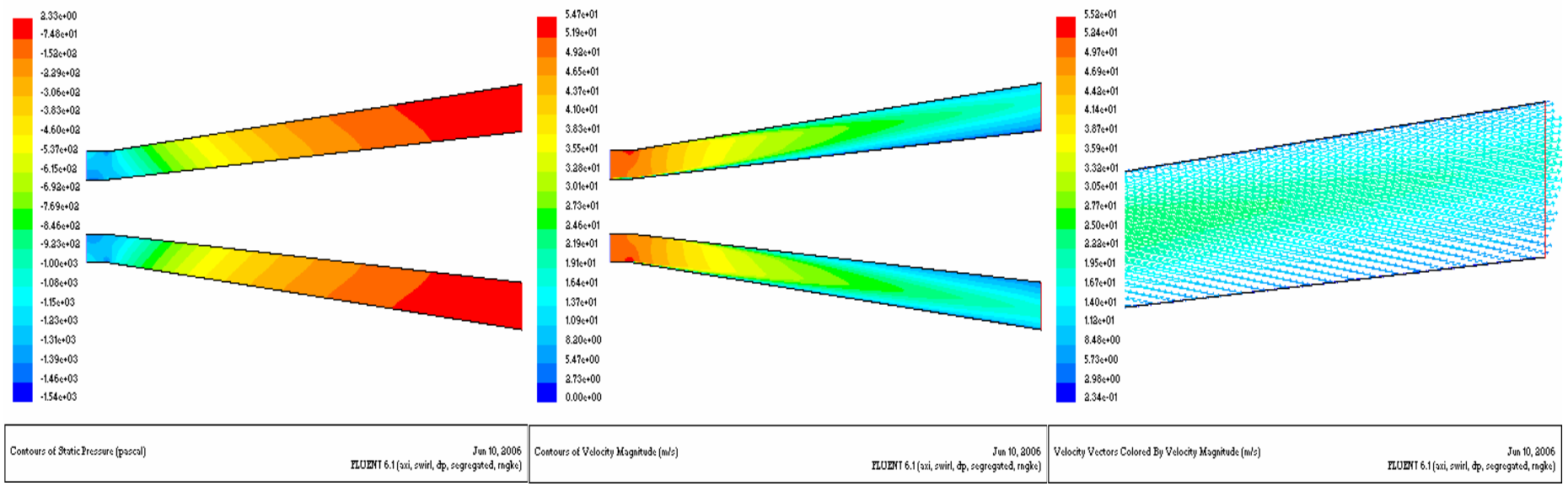

Static Pressure Contours **Velocity Contours** **Velocity Vectors**

Fig 6 AR= 4, Equivalent cone Angle = 10 deg, Swirl Angle = 20 deg, Velocity = 50m/s

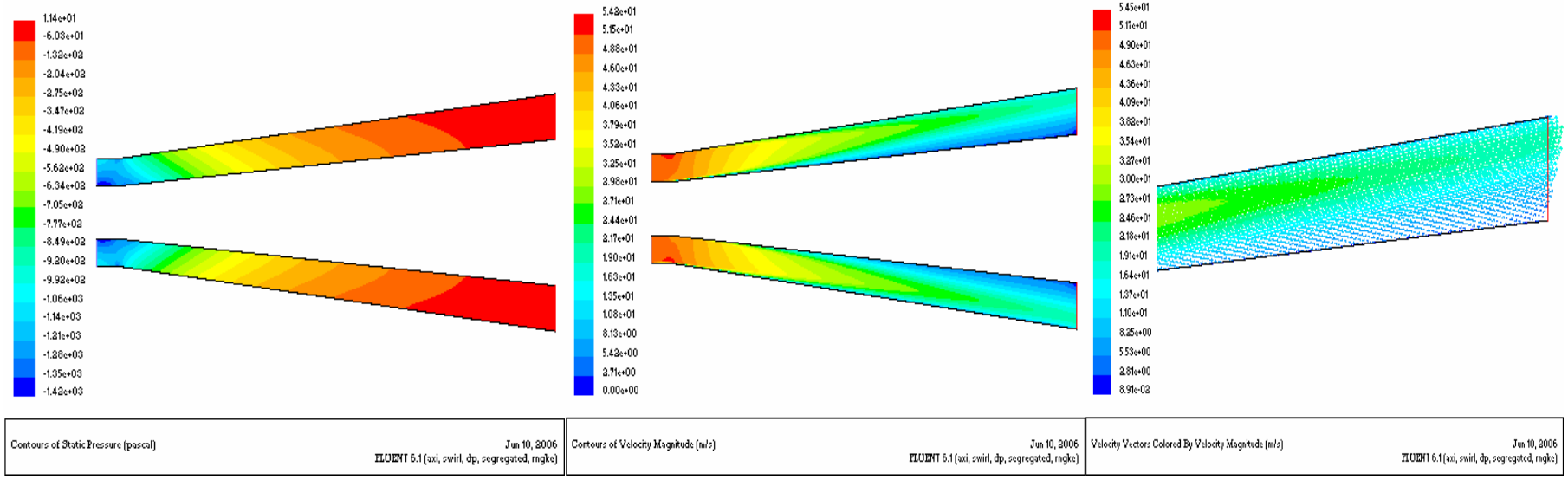

Static Pressure Contours **Velocity Contours** **Velocity Vectors**

Fig 7 AR= 4, Equivalent cone Angle = 10 deg, Swirl Angle = 25 deg, Velocity = 50m/s

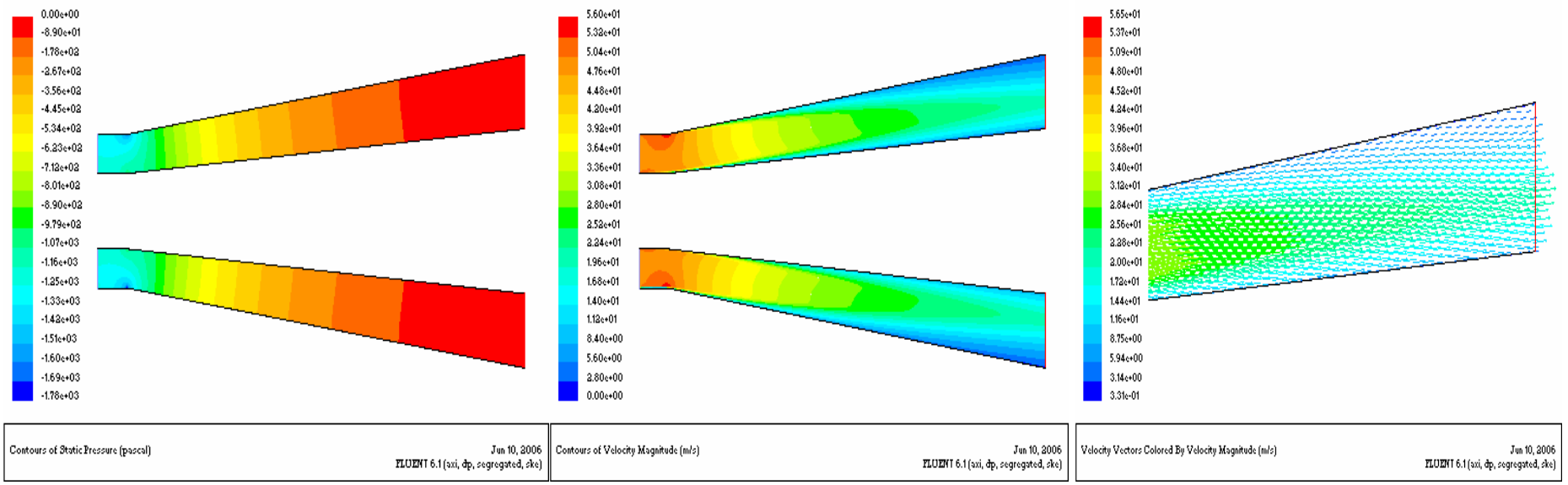

Static Pressure Contours **Velocity Contours** **Velocity Vectors**

Fig 8 AR= 4, Equivalent cone Angle = 15 deg, Swirl Angle = 0 deg, Velocity = 50m/s

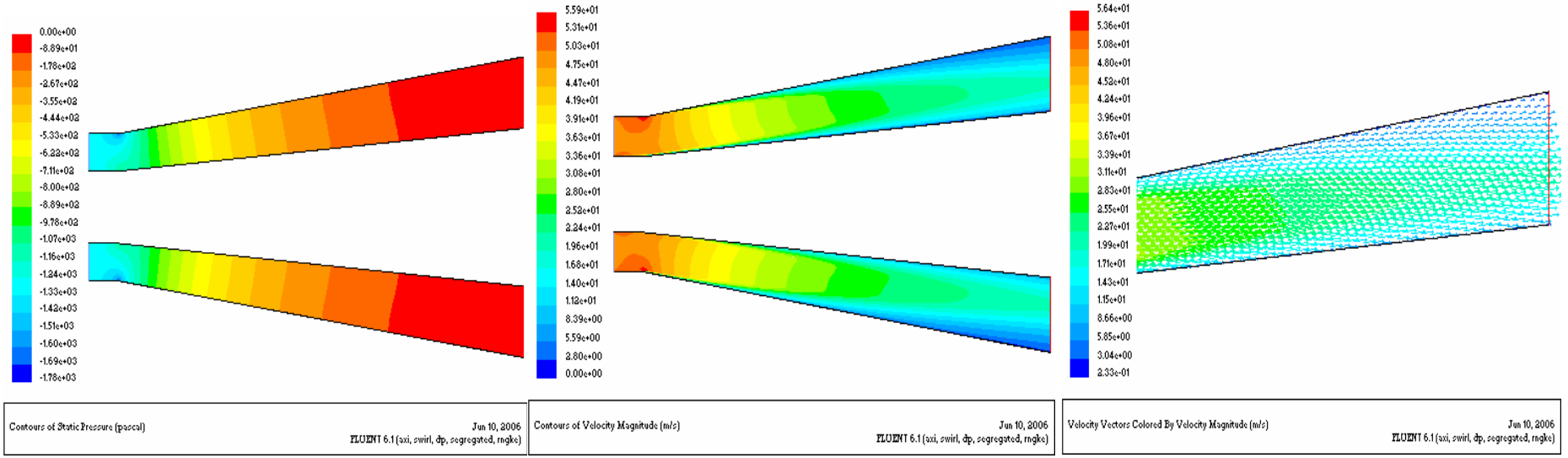

Static Pressure Contours **Velocity Contours** **Velocity Vectors**

Fig 9 AR= 4, Equivalent cone Angle = 15 deg, Swirl Angle = 5 deg, Velocity = 50m/s

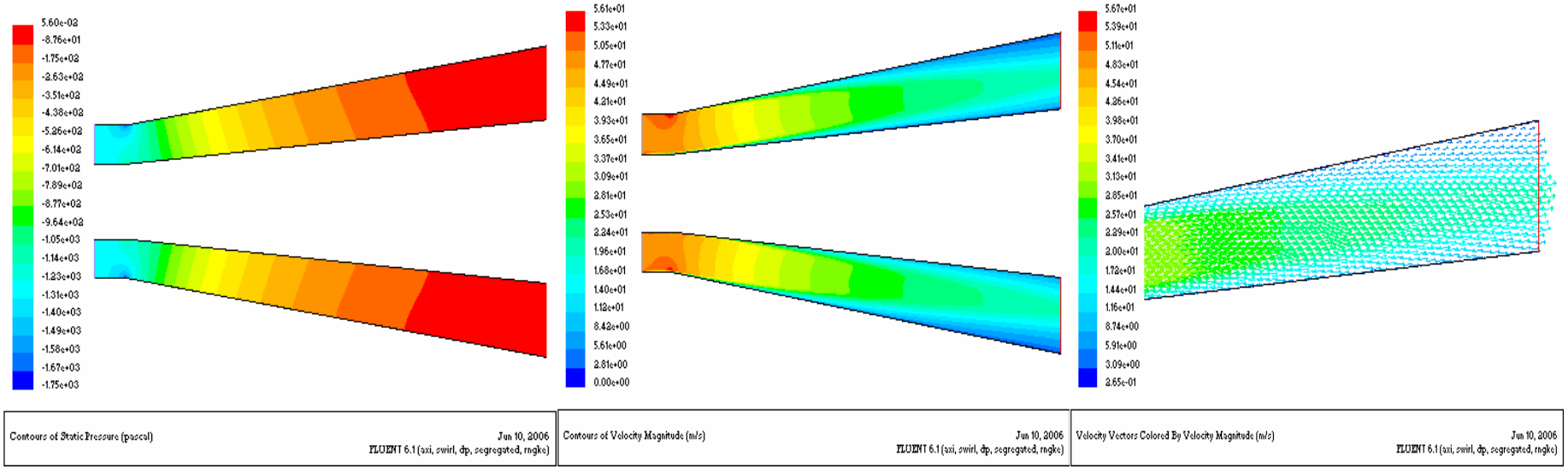

Static Pressure Contours **Velocity Contours** **Velocity Vectors**

Fig 10 AR= 4, Equivalent cone Angle = 15 deg, Swirl Angle = 10 deg, Velocity = 50m/s

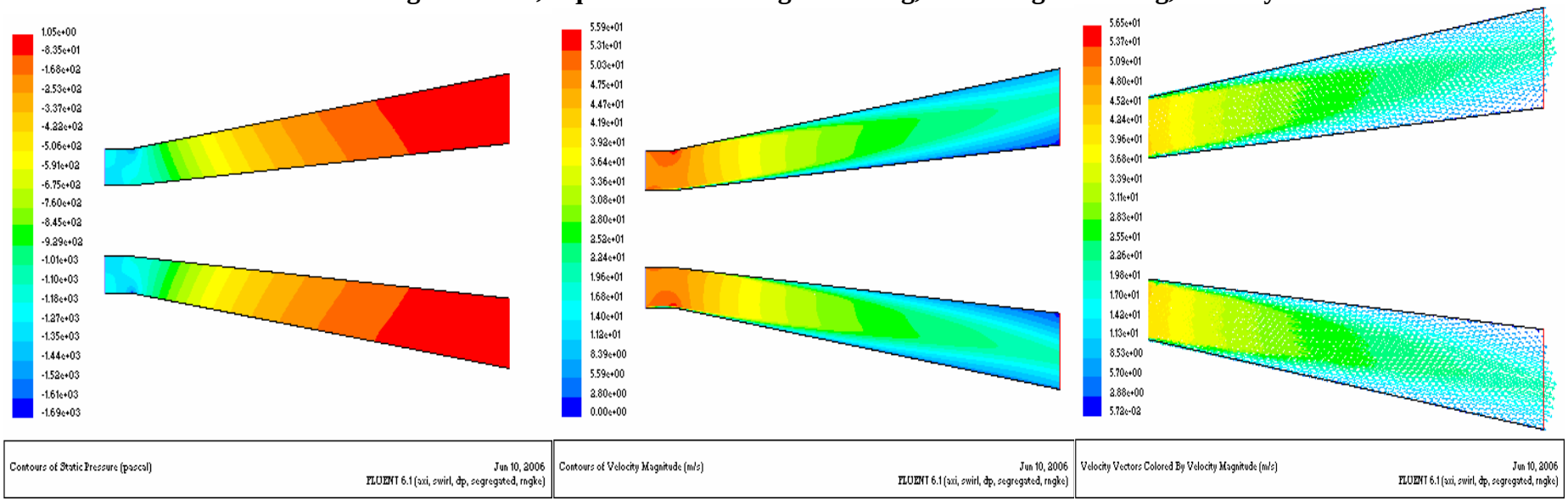

Static Pressure Contours **Velocity Contours** **Velocity Vectors**

Fig 11 AR= 4, Equivalent cone Angle = 15 deg, Swirl Angle = 15 deg, Velocity = 50m/s

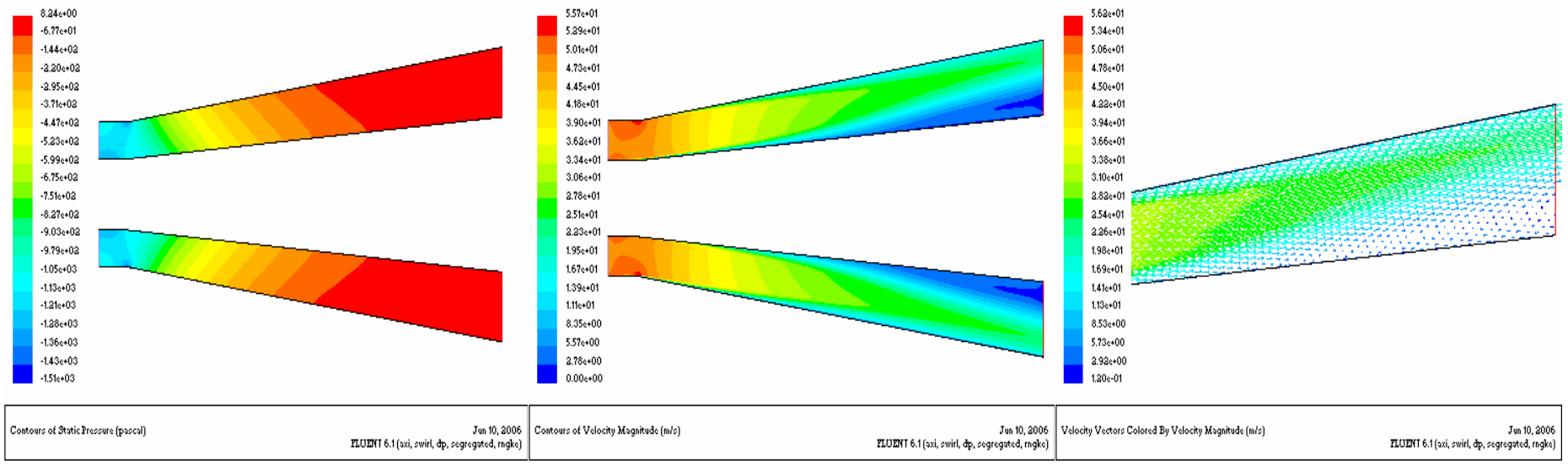

Static Pressure Contours **Velocity Contours** **Velocity Vectors**

Fig 12 AR= 4, Equivalent cone Angle = 15 deg, Swirl Angle = 20 deg, Velocity = 50m/s

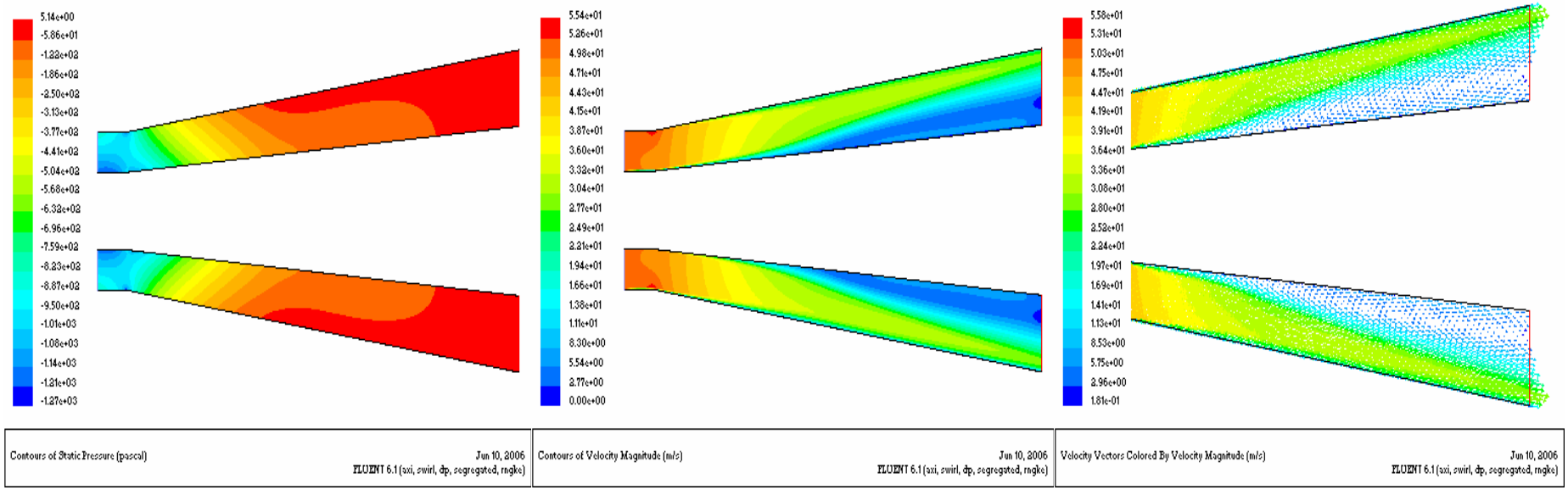

Static Pressure Contours **Velocity Contours** **Velocity Vectors**

Fig 13 AR= 4, Equivalent cone Angle = 15 deg, Swirl Angle = 25 deg, Velocity = 50m/s

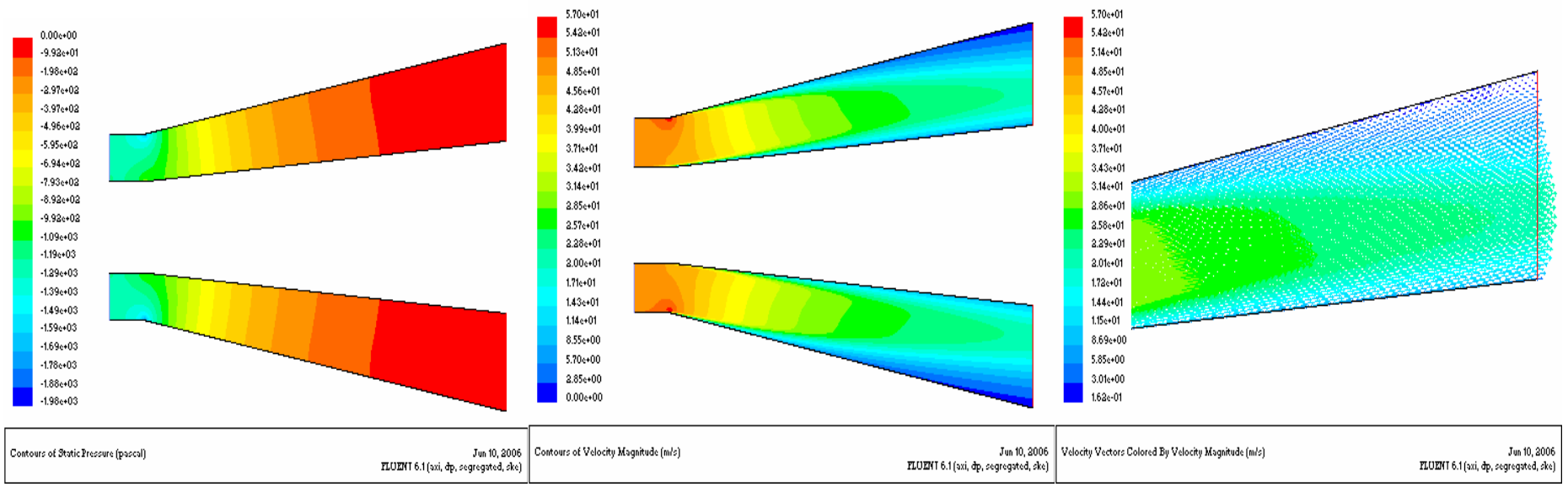

Static Pressure Contours **Velocity Contours** **Velocity Vectors**

Fig 14 AR= 4, Equivalent cone Angle = 20 deg, Swirl Angle = 0 deg, Velocity = 50m/s

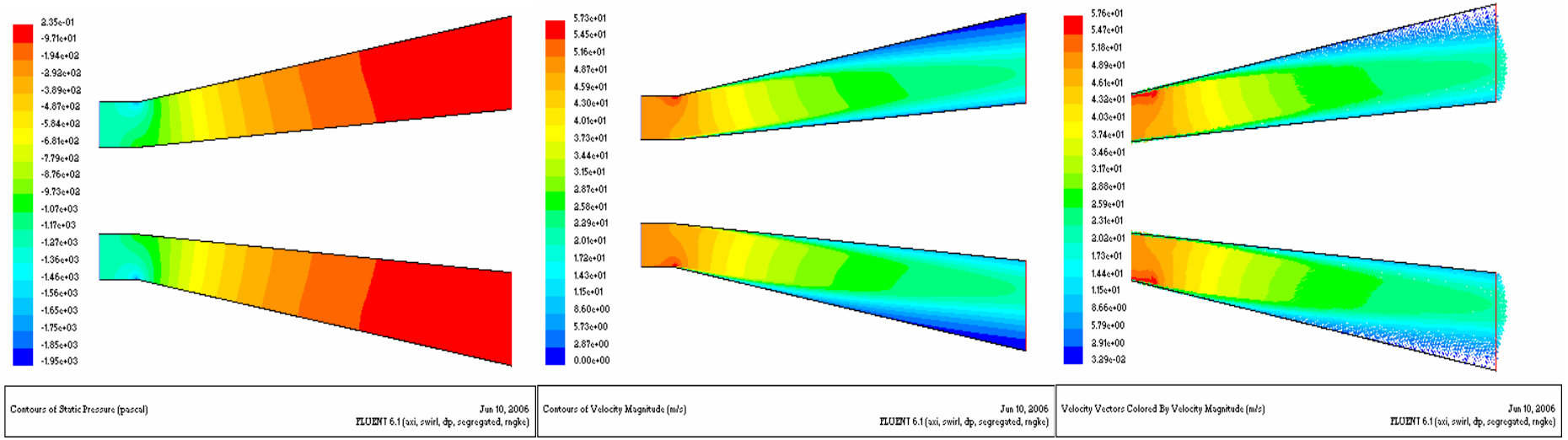

Static Pressure Contours **Velocity Contours** **Velocity Vectors**

Fig 15 AR= 4, Equivalent cone Angle = 20 deg, Swirl Angle = 5 deg, Velocity = 50m/s

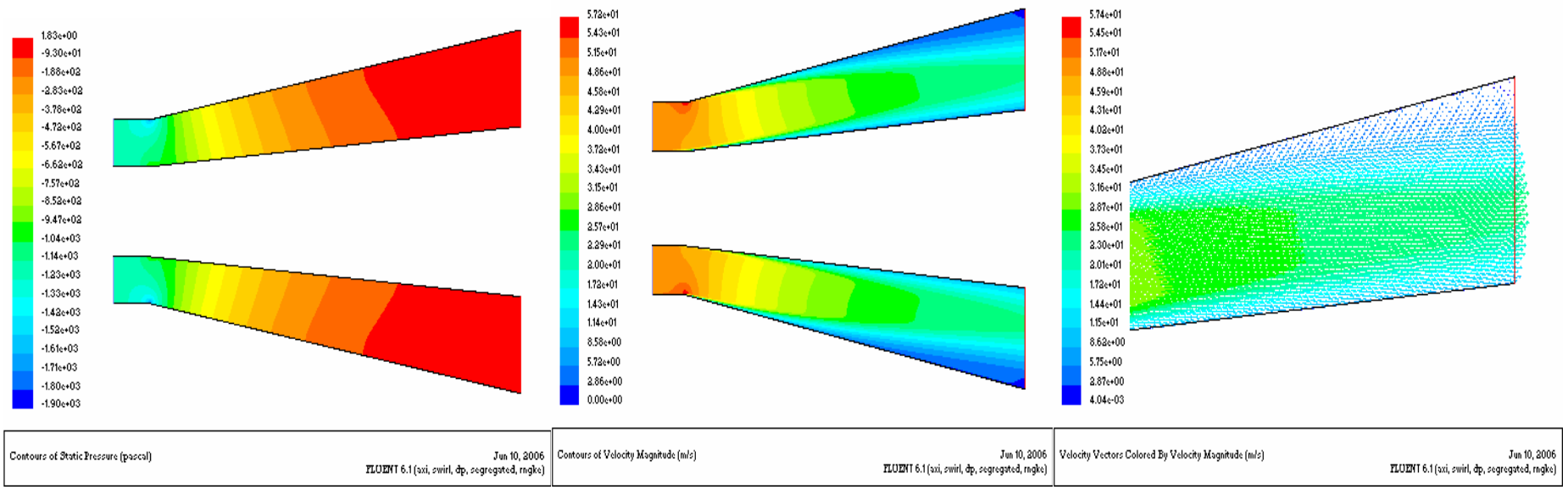

Static Pressure Contours **Velocity Contours** **Velocity Vectors**

Fig 16 AR= 4, Equivalent cone Angle = 20 deg, Swirl Angle = 10 deg, Velocity = 50m/s

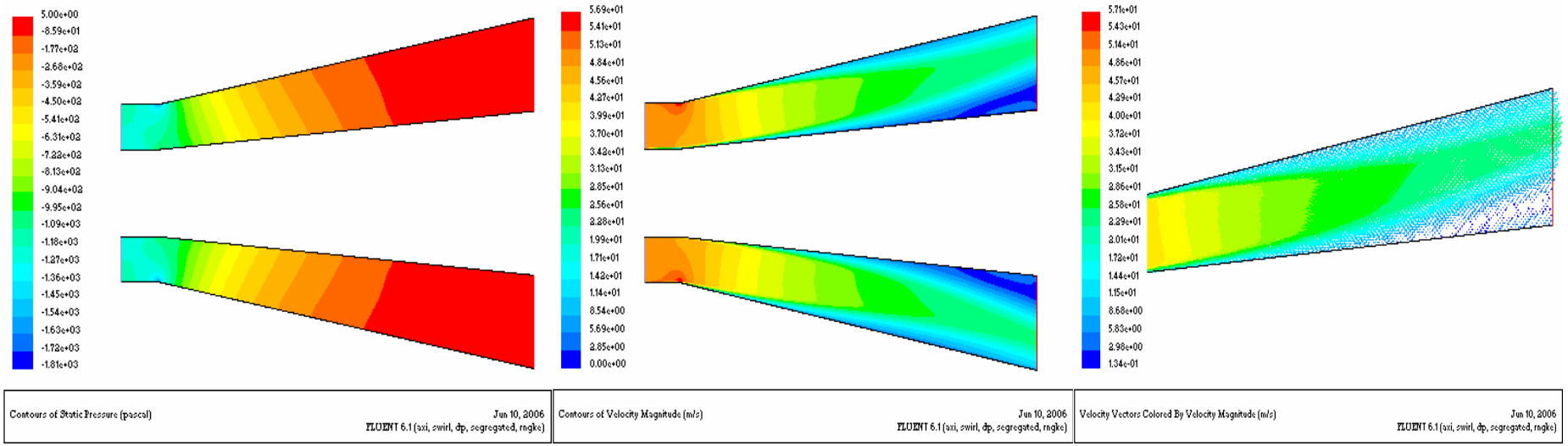

Static Pressure Contours **Velocity Contours** **Velocity Vectors**

Fig 17 AR= 4, Equivalent cone Angle = 20 deg, Swirl Angle = 15 deg, Velocity = 50m/s

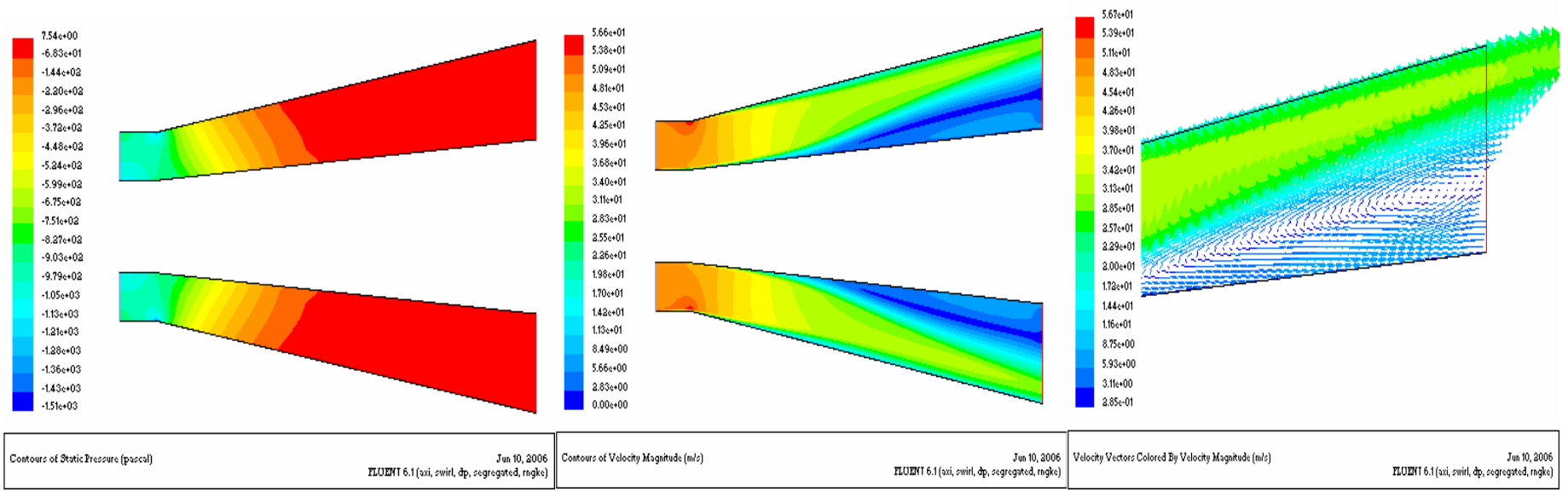

Static Pressure Contours **Velocity Contours** **Velocity Vectors**

Fig 18 AR= 4, Equivalent cone Angle = 20 deg, Swirl Angle = 20 deg, Velocity = 50m/s

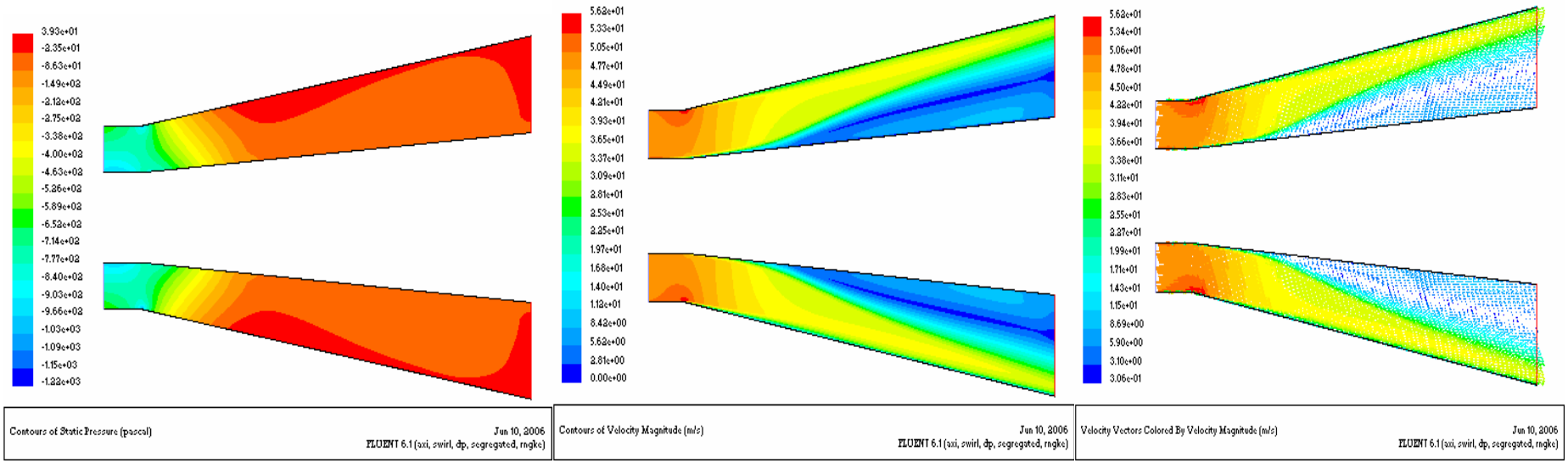

Static Pressure Contours **Velocity Contours** **Velocity Vectors**

Fig 19 AR= 4, Equivalent cone Angle = 20 deg, Swirl Angle = 25 deg, Velocity = 50m/s

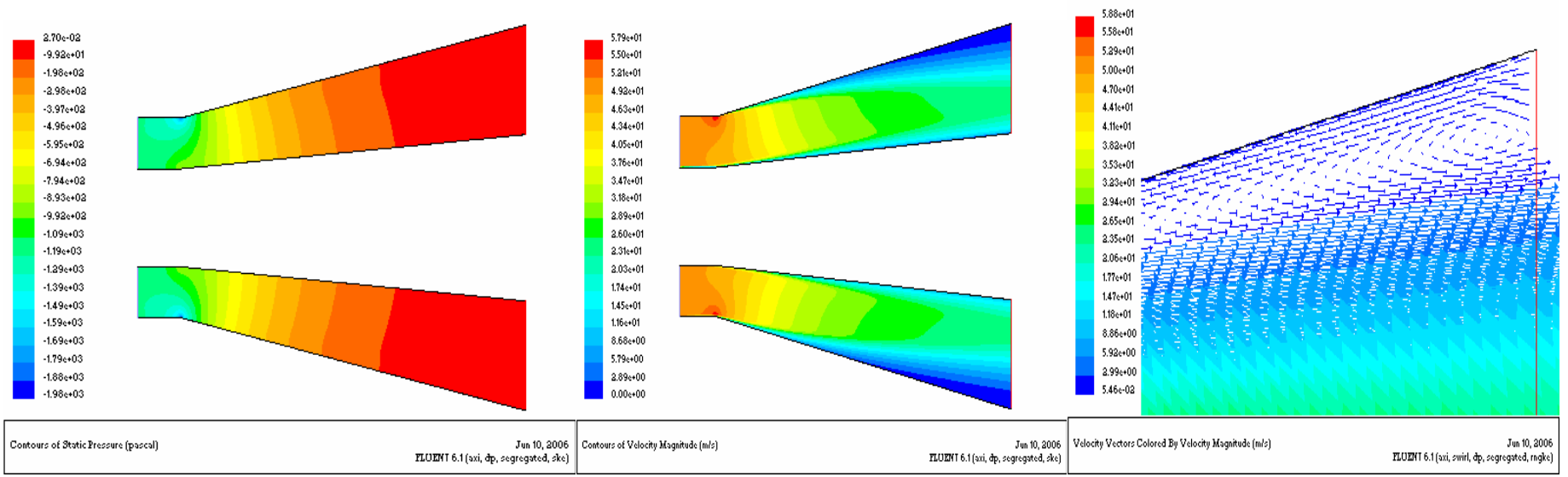

Static Pressure Contours **Velocity Contours** **Velocity Vectors**

Fig 20 AR= 4, Equivalent cone Angle = 25 deg, Swirl Angle = 0 deg, Velocity = 50m/s

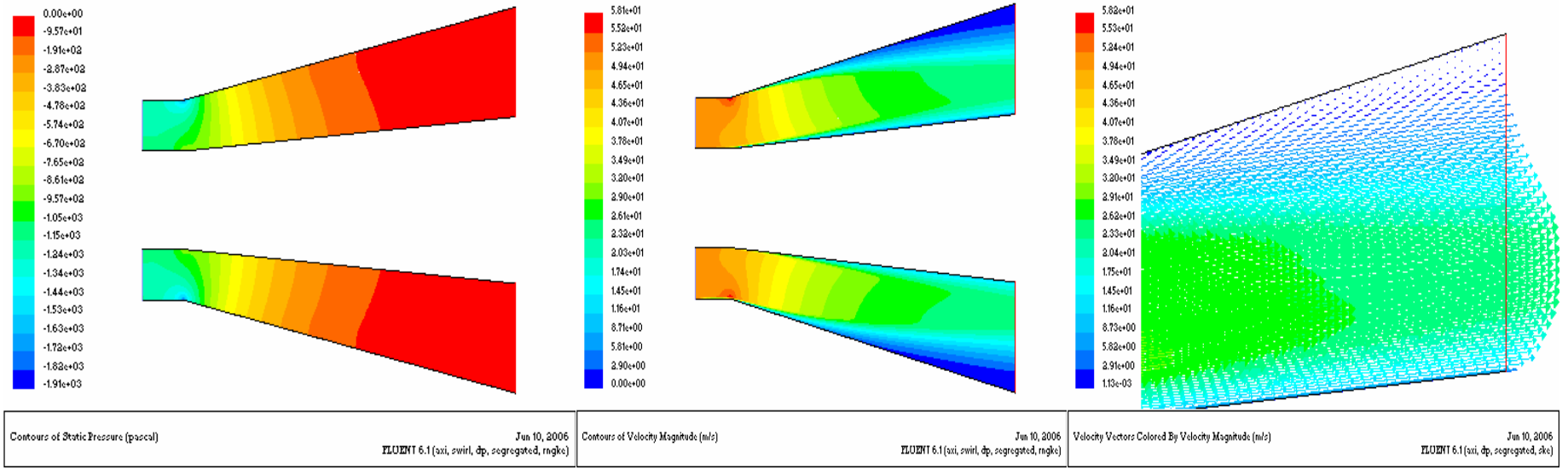

Static Pressure Contours **Velocity Contours** **Velocity Vectors**

Fig 21 AR= 4, Equivalent cone Angle = 25 deg, Swirl Angle = 5 deg, Velocity = 50m/s

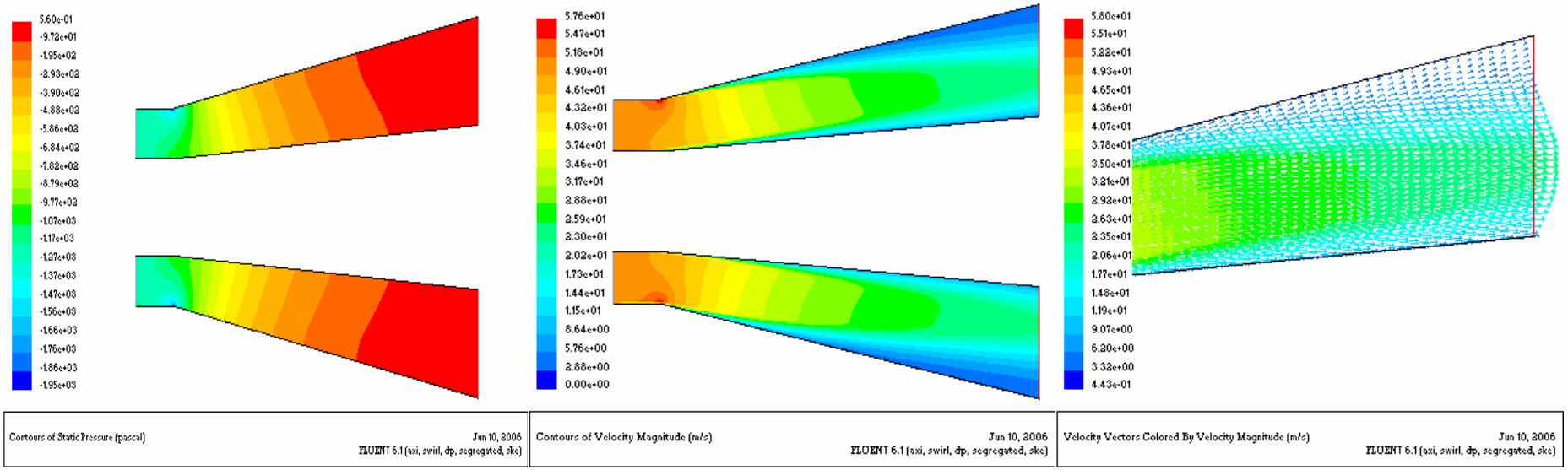

Static Pressure Contours **Velocity Contours** **Velocity Vectors**

Fig 22 AR= 4, Equivalent cone Angle = 25 deg, Swirl Angle = 10 deg, Velocity = 50m/s

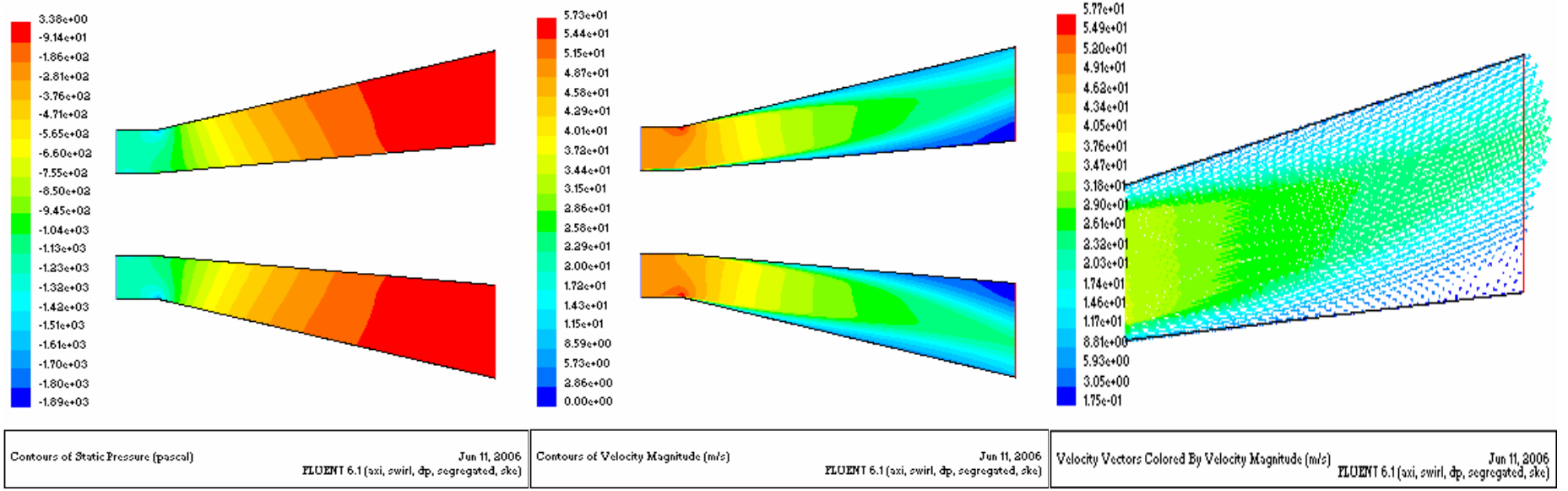

Static Pressure Contours **Velocity Contours** **Velocity Vectors**

Fig 23 AR= 4, Equivalent cone Angle = 25 deg, Swirl Angle = 15 deg, Velocity = 50m/s

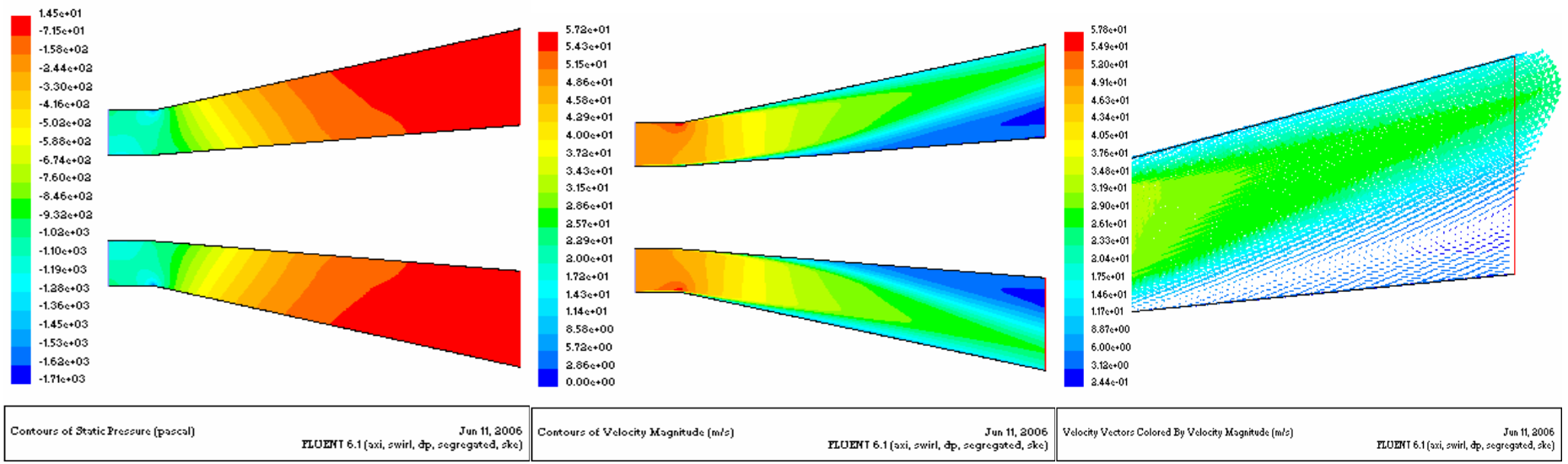

Static Pressure Contours **Velocity Contours** **Velocity Vectors**

Fig 24 AR= 4, Equivalent cone Angle = 25 deg, Swirl Angle = 20 deg, Velocity = 50m/s

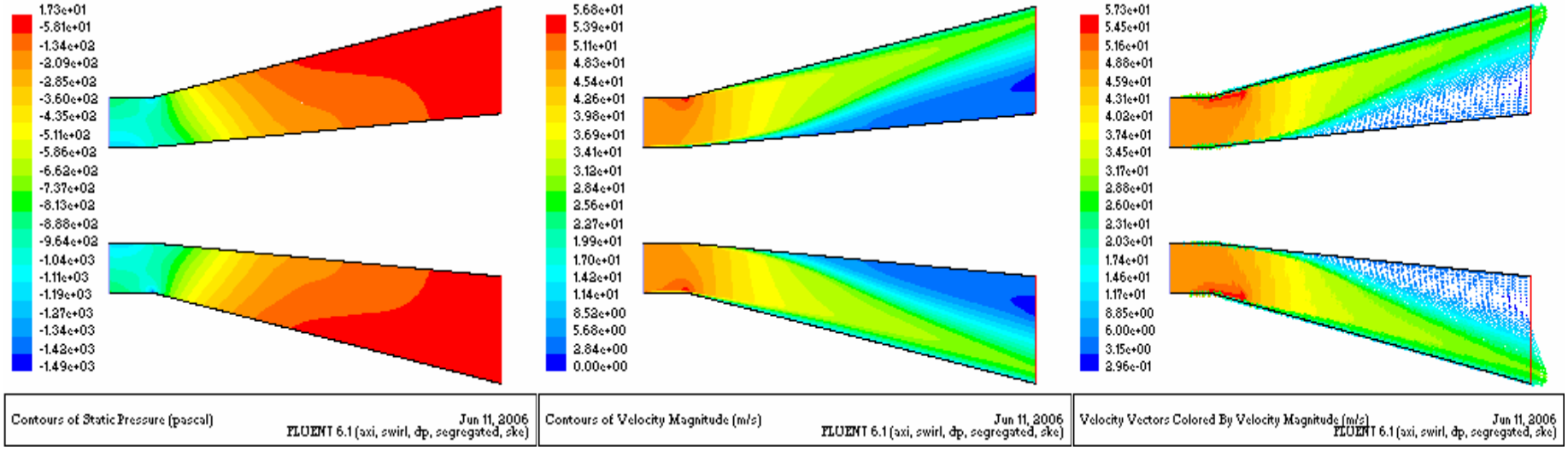

Static Pressure Contours **Velocity Contours** **Velocity Vectors**

Fig 25 AR= 4, Equivalent cone Angle = 25 deg, Swirl Angle = 25 deg, Velocity = 50m/s

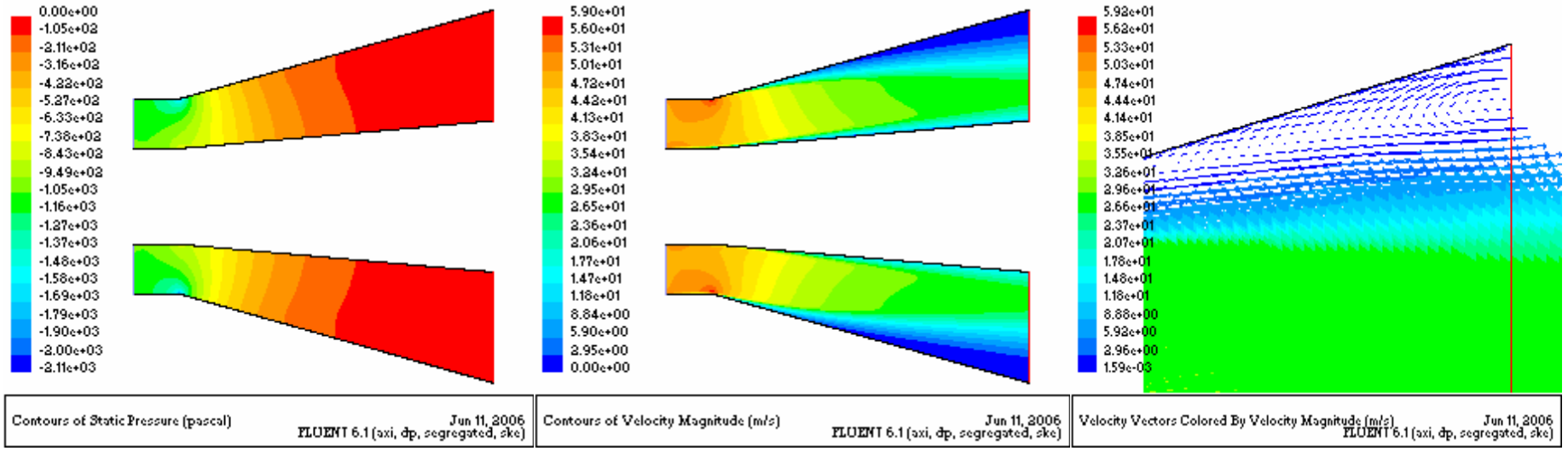

Static Pressure Contours **Velocity Contours** **Velocity Vectors**

Fig 26 AR= 4, Equivalent cone Angle = 30 deg, Swirl Angle = 0 deg, Velocity = 50m/s

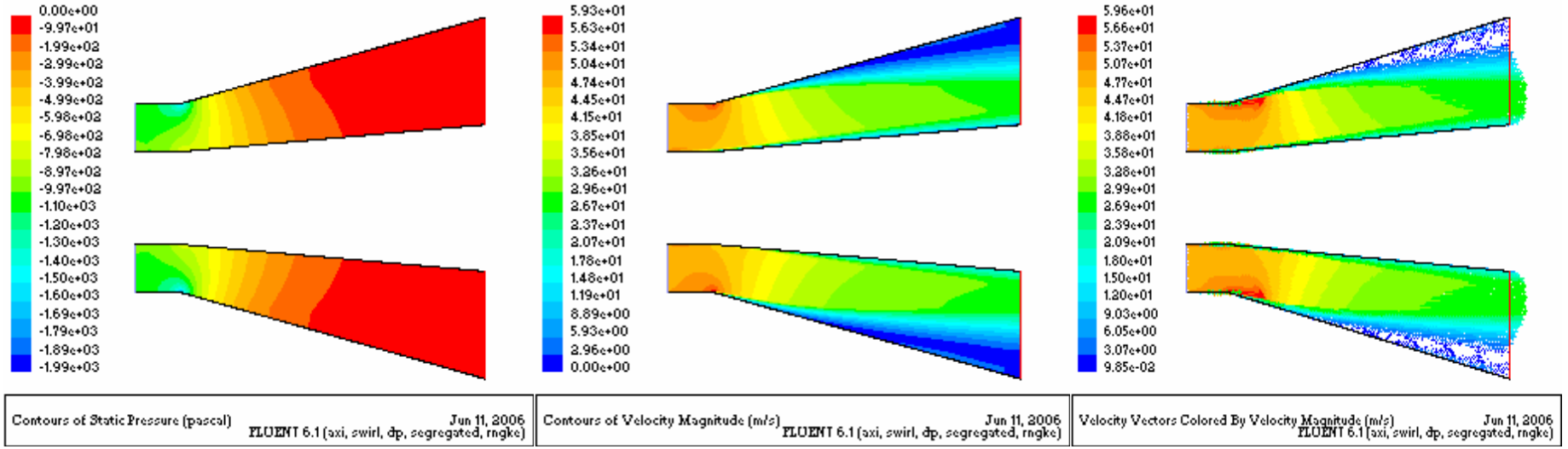

Static Pressure Contours **Velocity Contours** **Velocity Vectors**

Fig 27 AR= 4, Equivalent cone Angle = 30 deg, Swirl Angle = 5 deg, Velocity = 50m/s

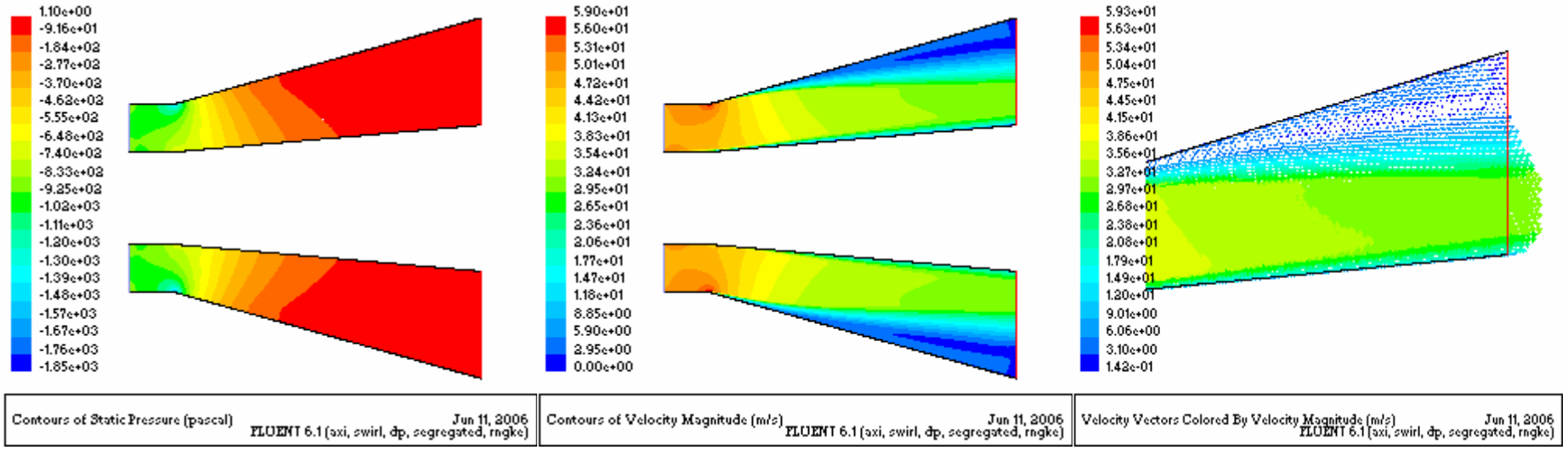

Static Pressure Contours **Velocity Contours** **Velocity Vectors**

Fig 28 AR= 4, Equivalent cone Angle = 30 deg, Swirl Angle = 0 deg, Velocity = 50m/s

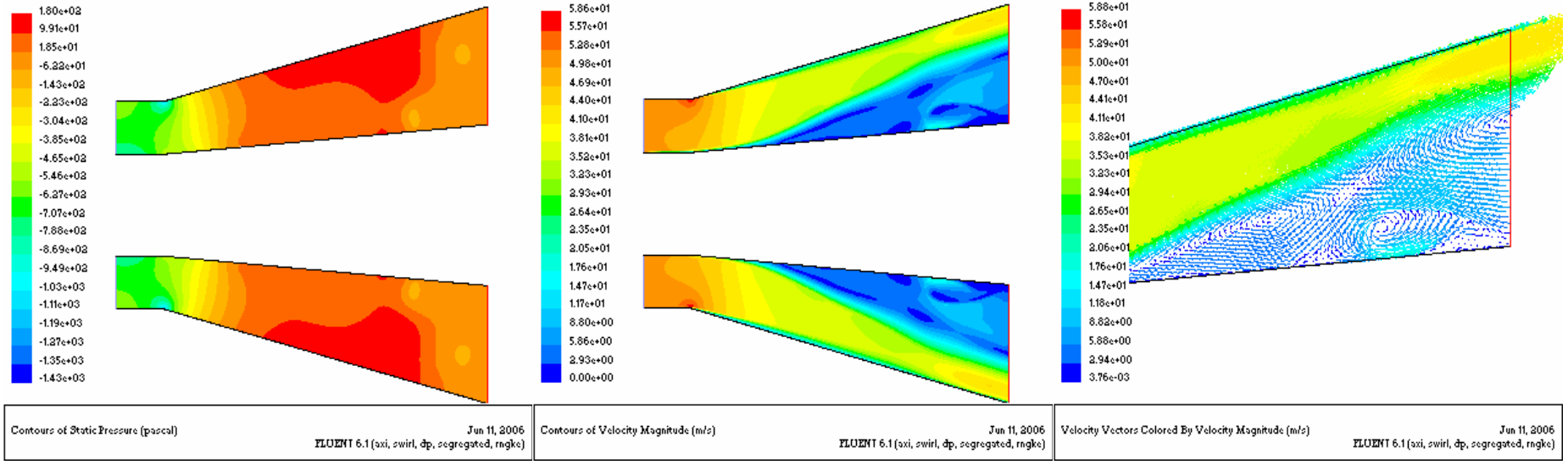

Static Pressure Contours **Velocity Contours** **Velocity Vectors**

Fig 29 AR= 4, Equivalent cone Angle = 30 deg, Swirl Angle = 20 deg, Velocity = 50m/s

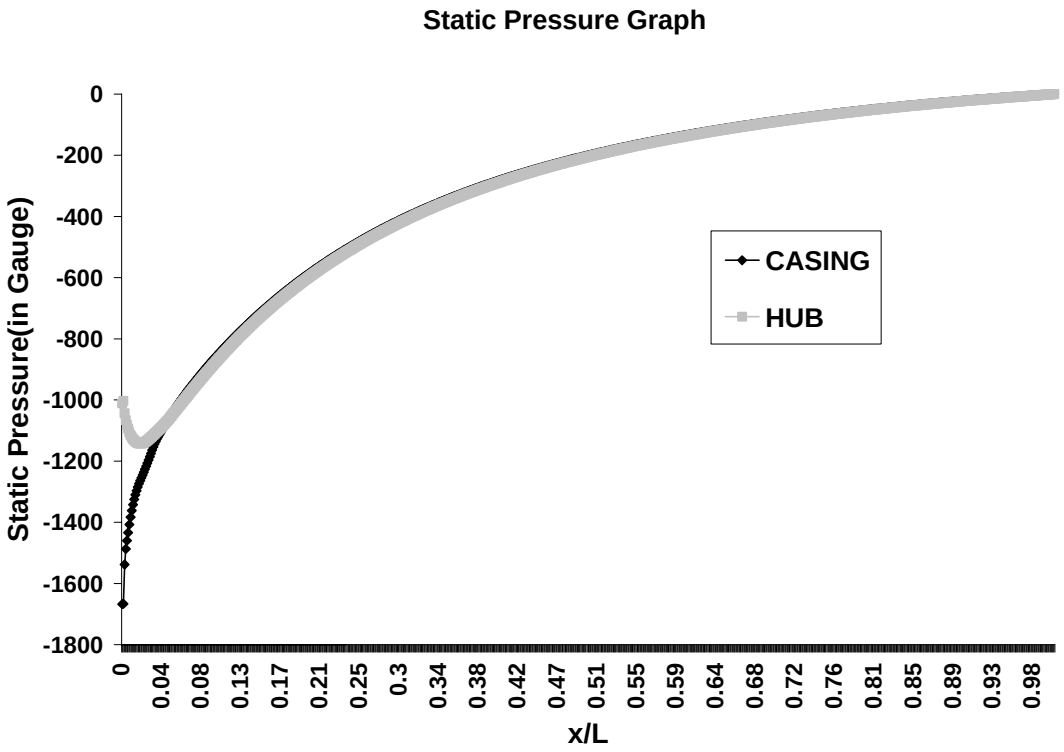

Fig 30

AR = 4, Equivalent Cone Angle = 10 deg, Swirl Angle = 0 deg, Re = 2.5×10^5

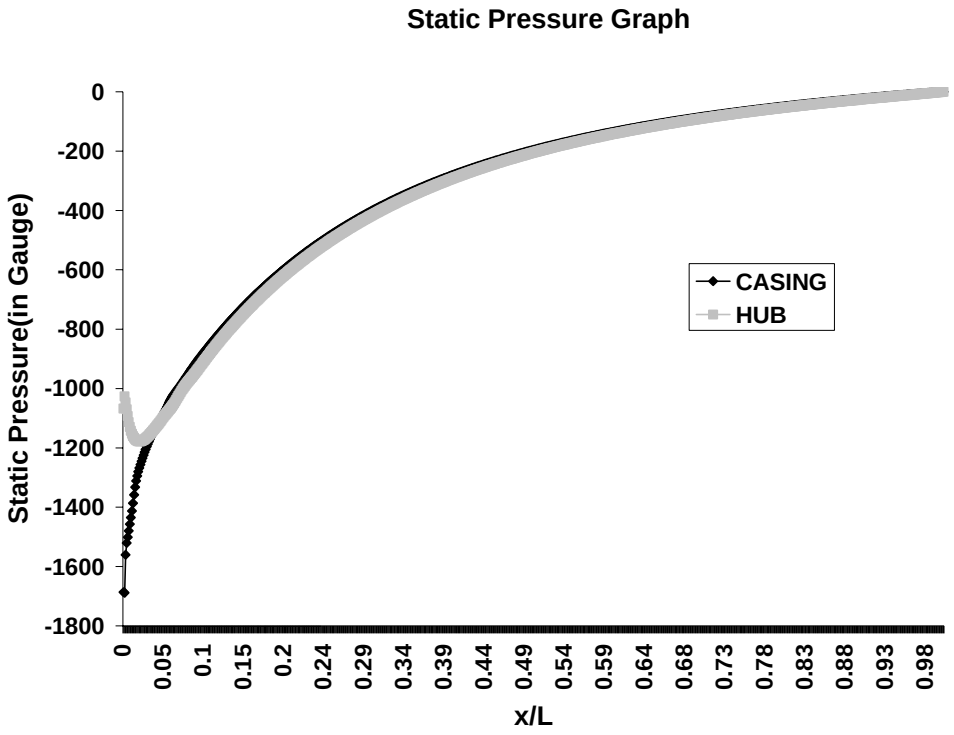

Fig 31

AR = 4, Equivalent Cone Angle = 10 deg, Swirl Angle = 5 deg, Re = 2.5×10^5

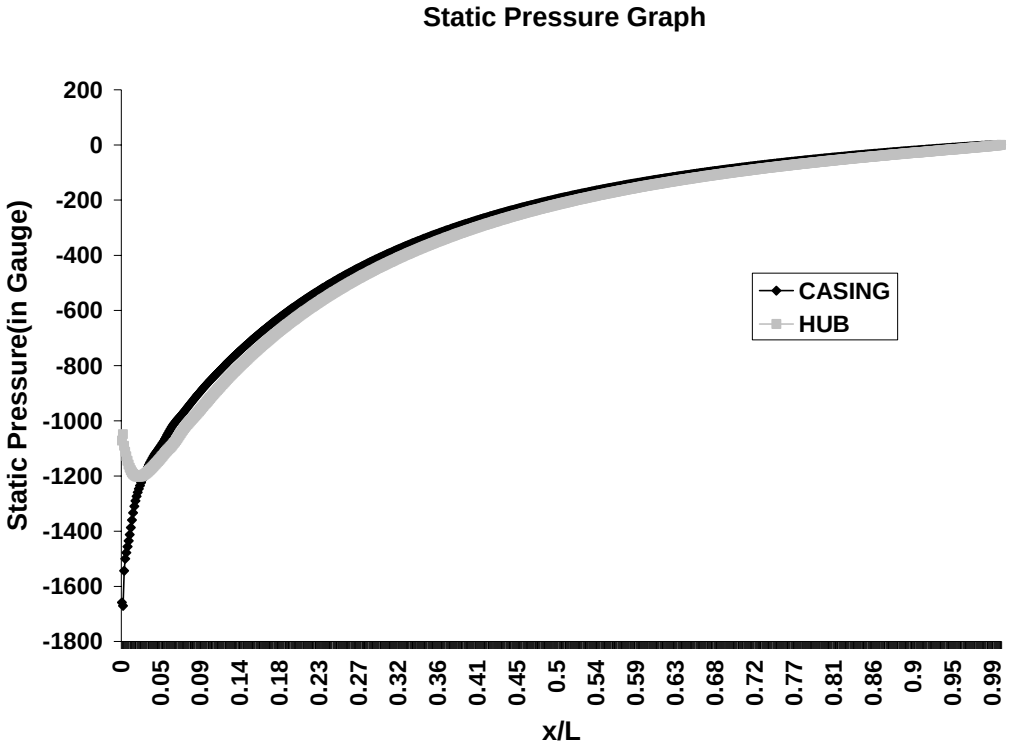

Fig 32

AR = 4, Equivalent Cone Angle = 10 deg, Swirl Angle = 10 deg, Re = 2.5×10^5

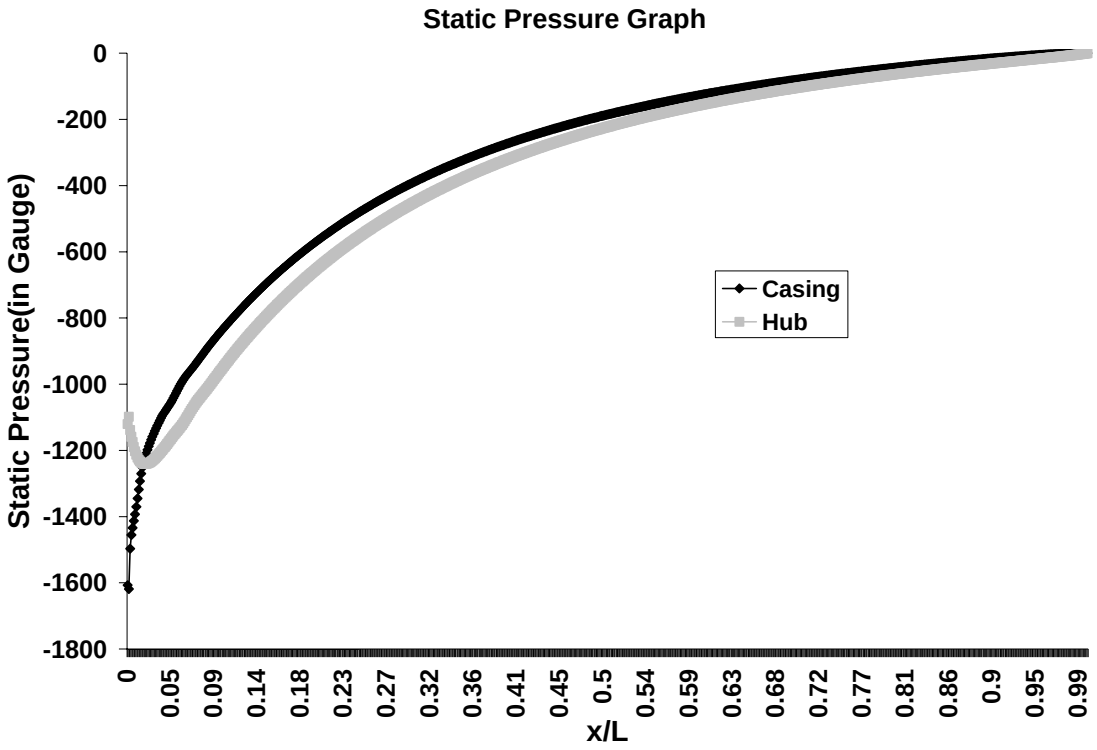

Fig 33

AR = 4, Equivalent Cone Angle = 10 deg, Swirl Angle = 15 deg, Re = 2.5 × 10^5

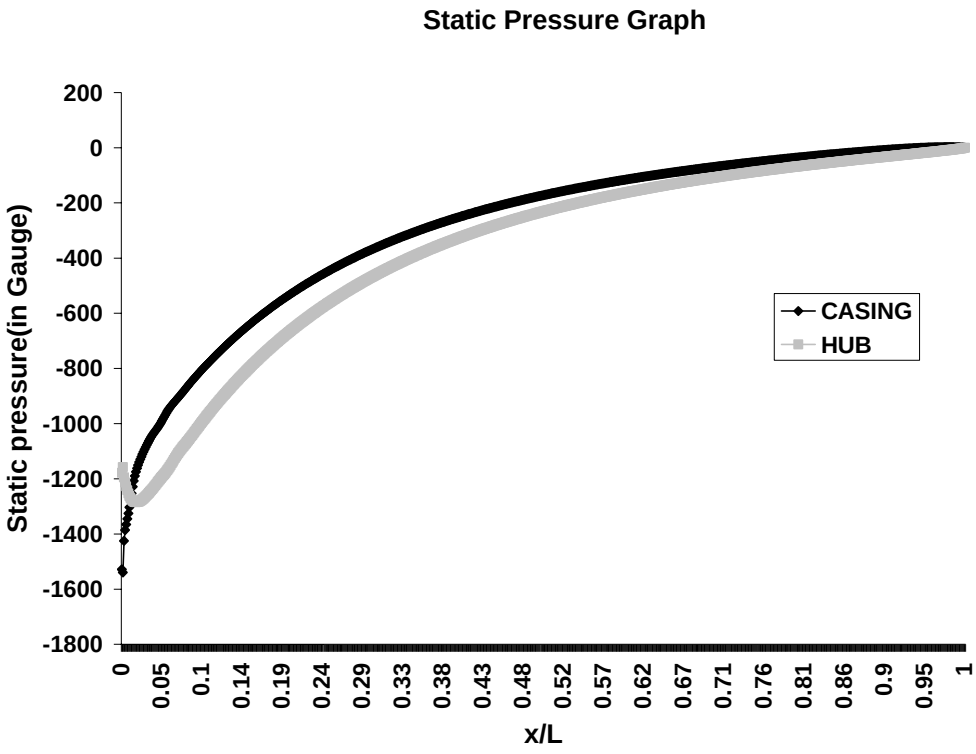

Fig 34

AR = 4, Equivalent Cone Angle = 10 deg, Swirl Angle = 20 deg, Re = 2.5×10^5

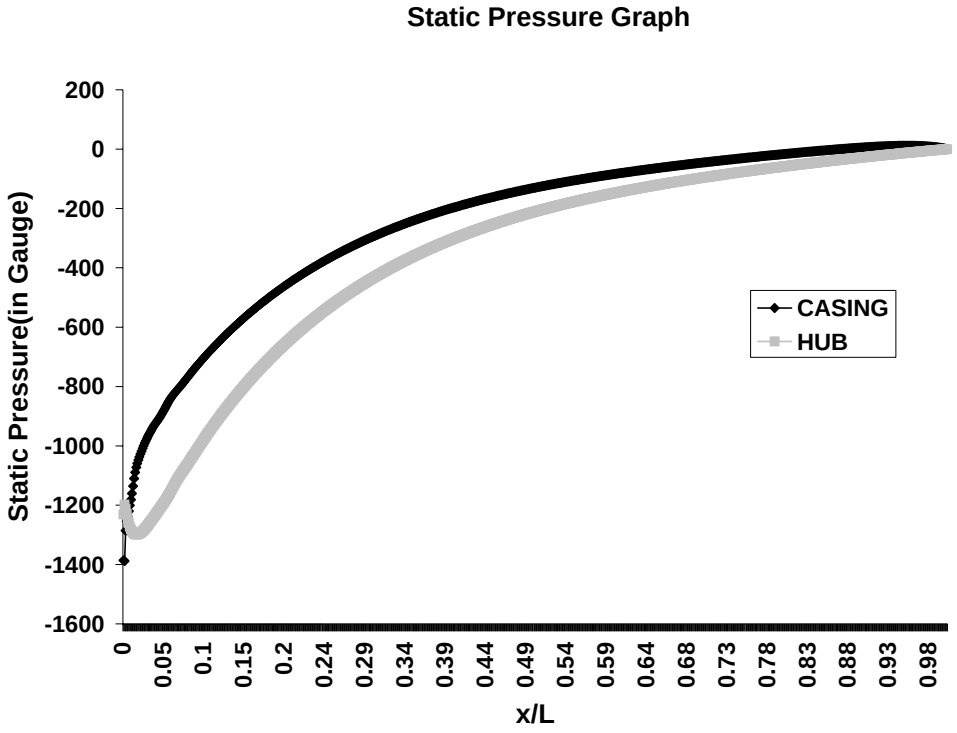

Fig 35

AR = 4, Equivalent Cone Angle = 10 deg, Swirl Angle = 25 deg, Re = 2.5×10^5

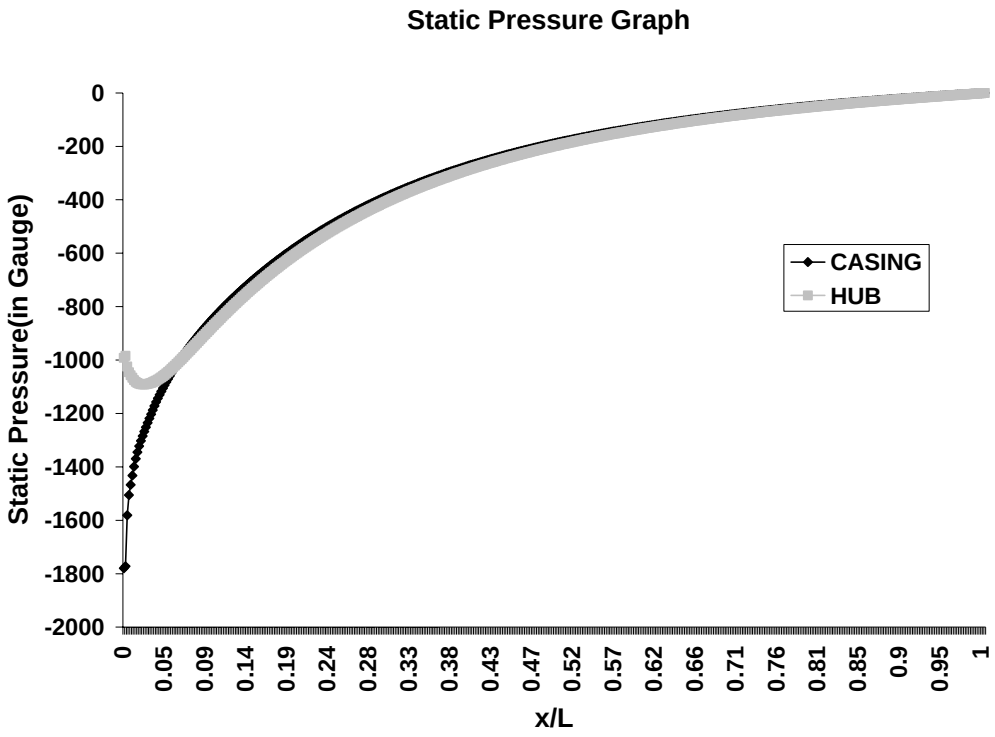

Fig 36

AR = 4, Equivalent Cone Angle = 15 deg, Swirl Angle = 0 deg, Re = 2.5×10^5

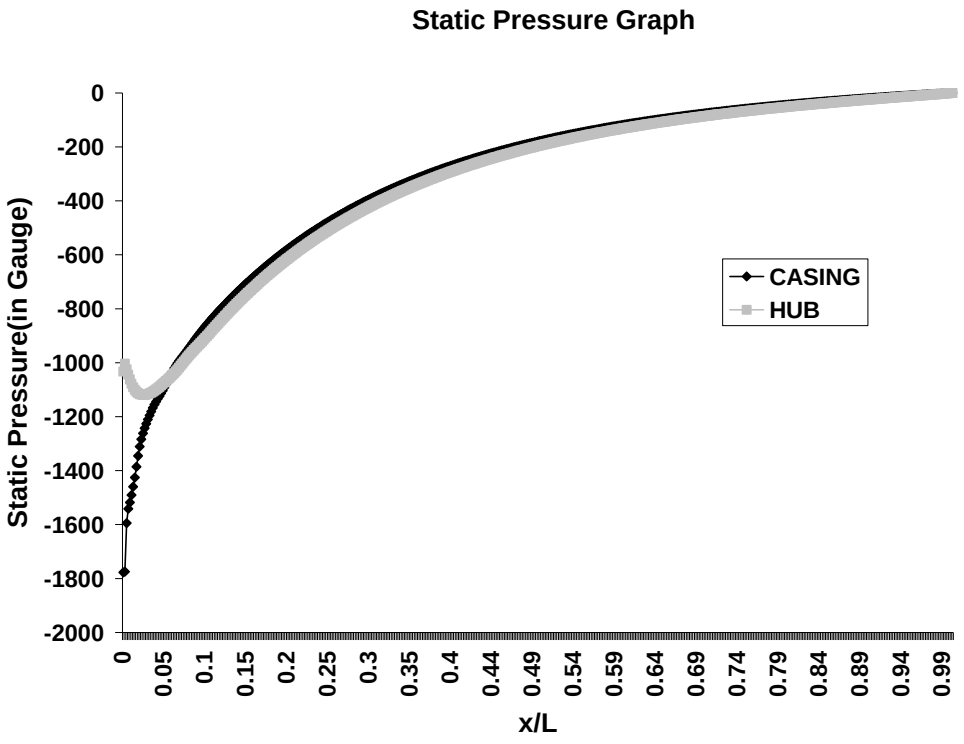

Fig 37

AR = 4, Equivalent Cone Angle = 15 deg, Swirl Angle = 5 deg, Re = 2.5×10^5

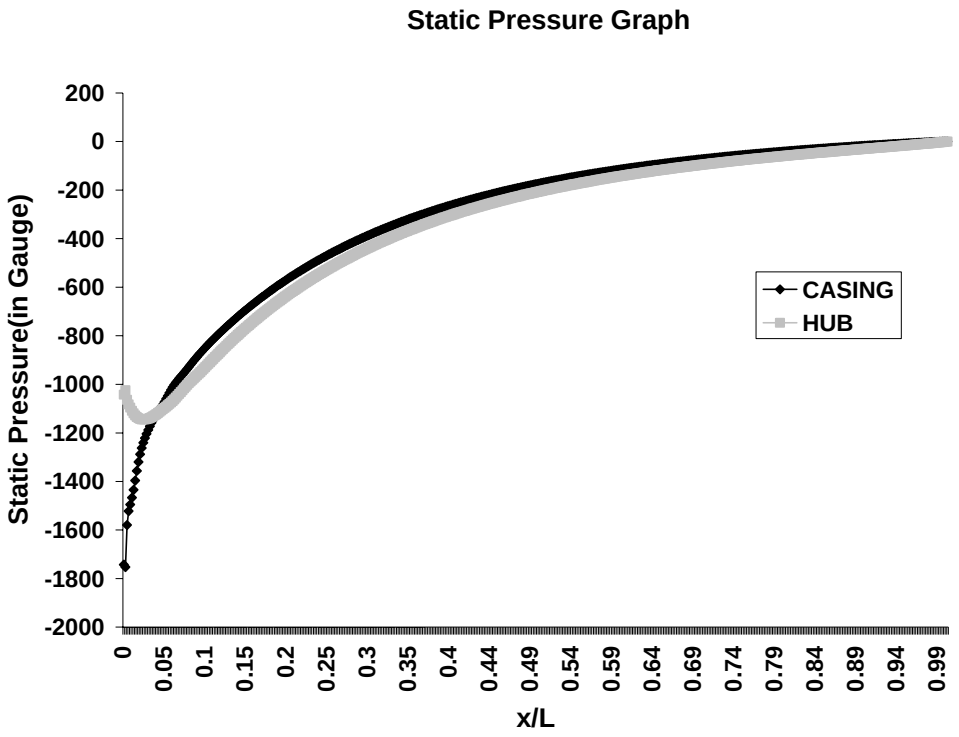

Fig 38

AR = 4, Equivalent Cone Angle = 15 deg, Swirl Angle = 10 deg, Re = 2.5×10^5

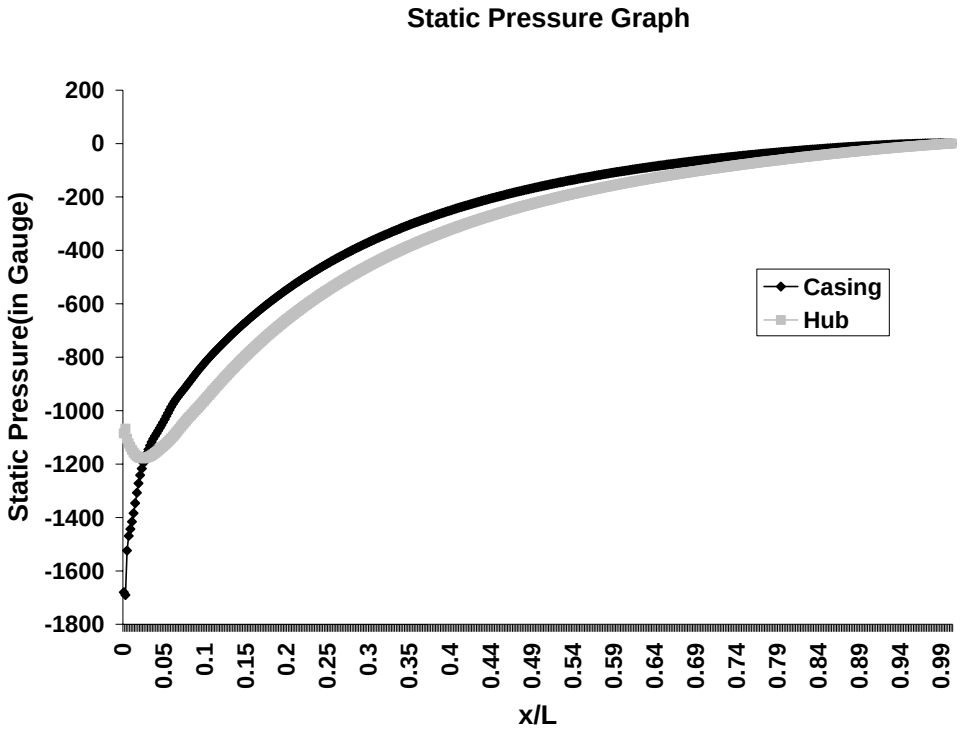

Fig 39

AR = 4, Equivalent Cone Angle = 15 deg, Swirl Angle = 15 deg, Re = 2.5×10^5

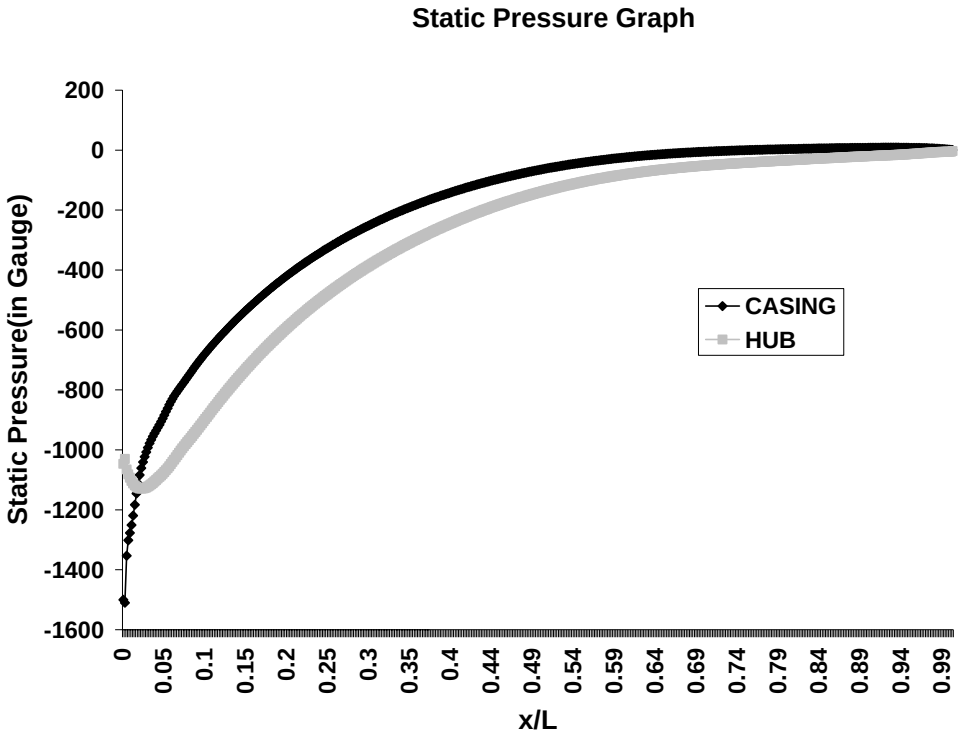

Fig 40

AR = 4, Equivalent Cone Angle = 15 deg, Swirl Angle = 20 deg, Re = 2.5 × 10^5

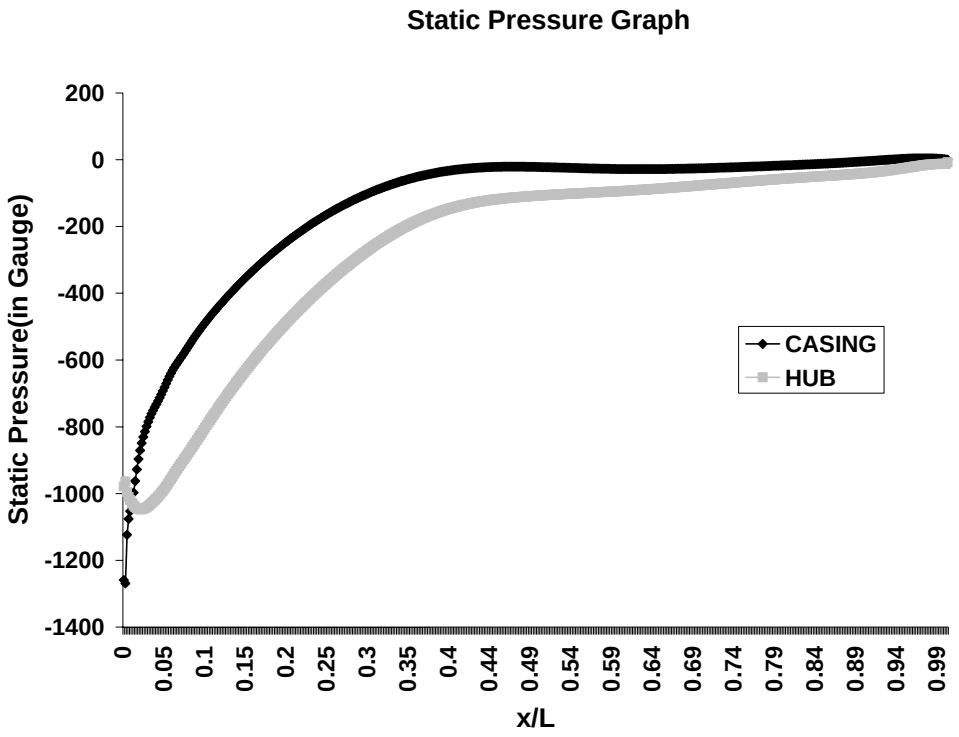

Fig 41

AR = 4, Equivalent Cone Angle = 15 deg, Swirl Angle = 25 deg, Re = 2.5×10^5

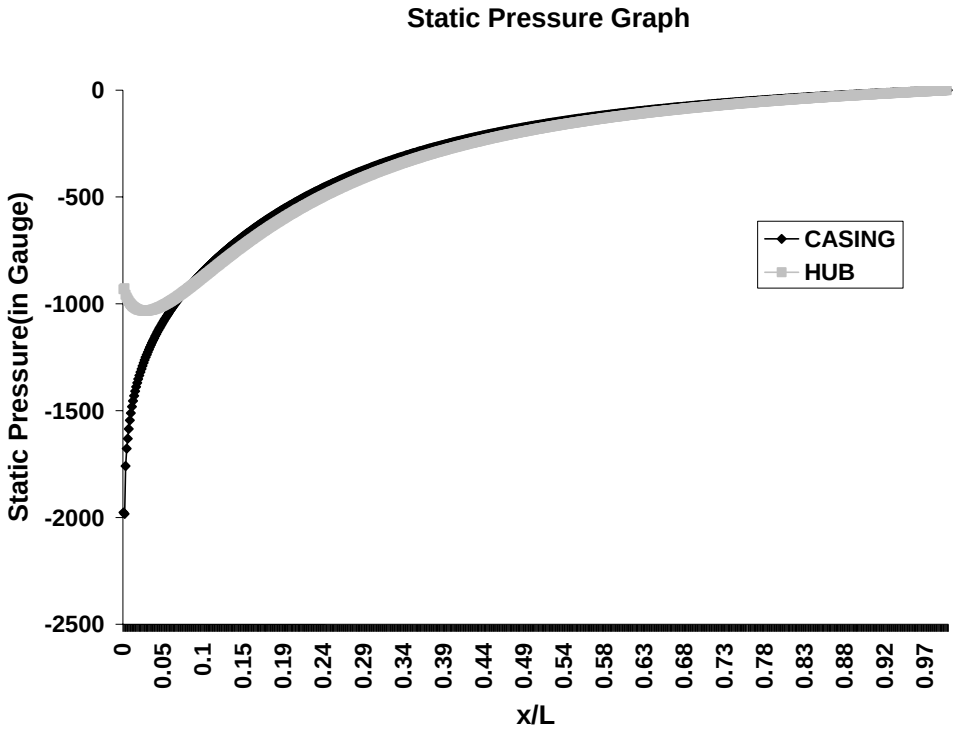

Fig 42

AR = 4, Equivalent Cone Angle = 20 deg, Swirl Angle = 0 deg, Re = 2.5×10^5

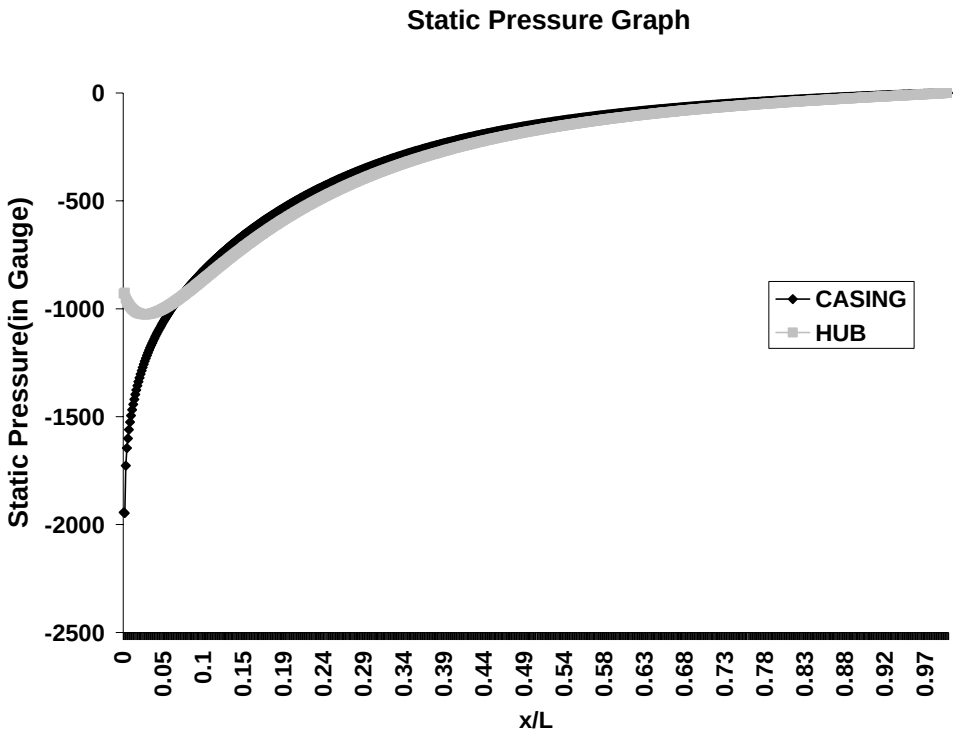

Fig 43

AR = 4, Equivalent Cone Angle = 20 deg, Swirl Angle = 5 deg, Re = 2.5×10^5

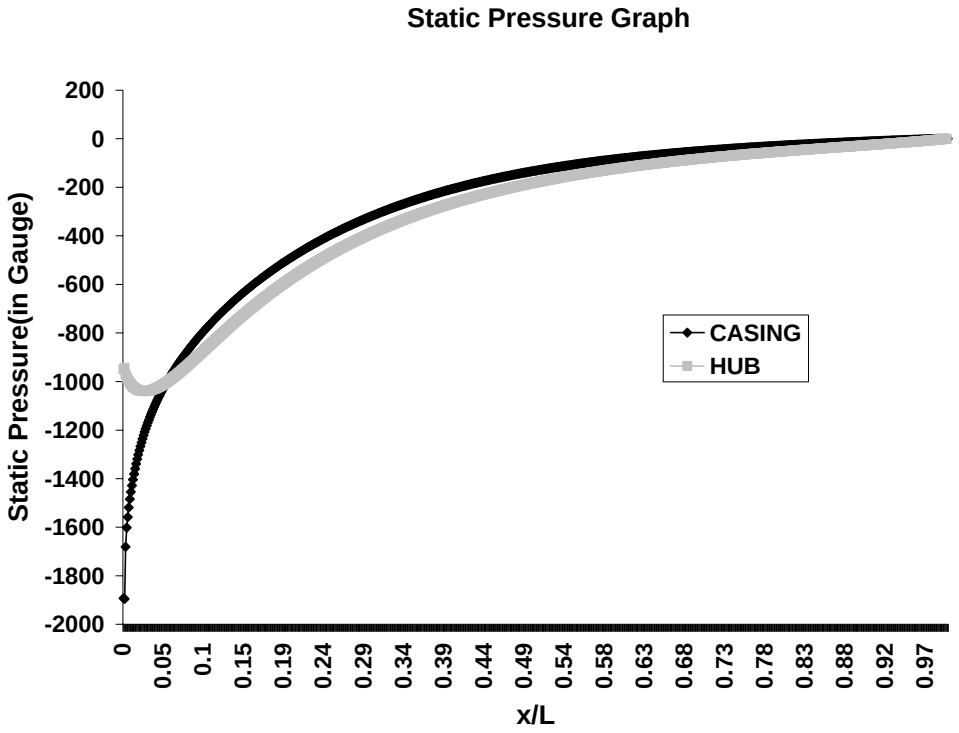

Fig 44

AR = 4, Equivalent Cone Angle = 20 deg, Swirl Angle = 10 deg, Re = 2.5×10^5

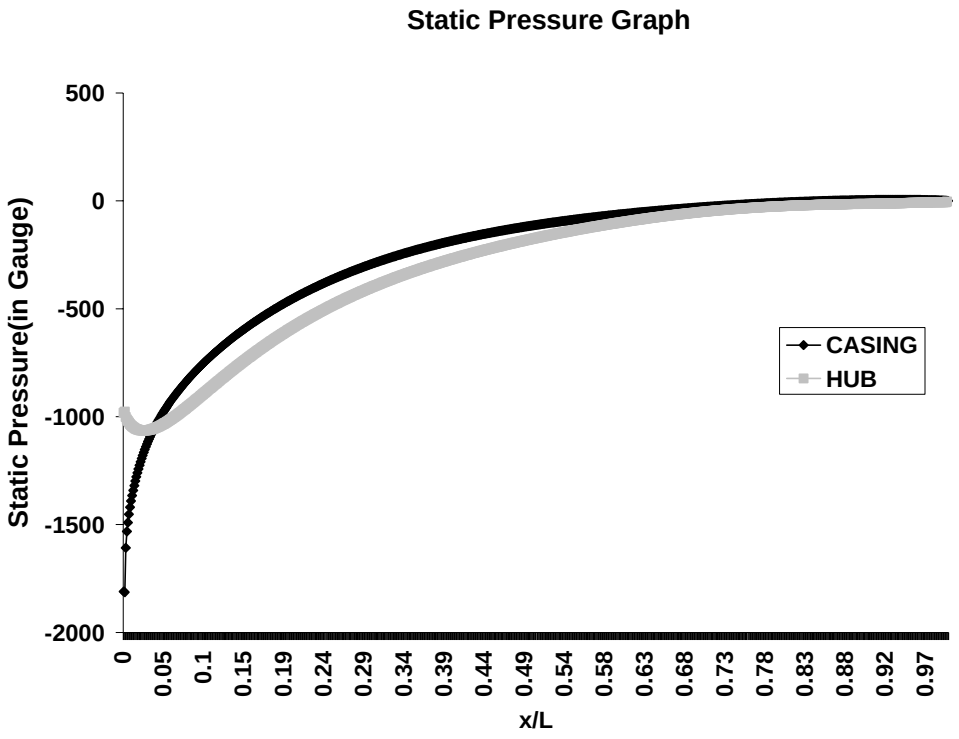

Fig 45

AR = 4, Equivalent Cone Angle = 20 deg, Swirl Angle = 15 deg, Re = 2.5×10^5

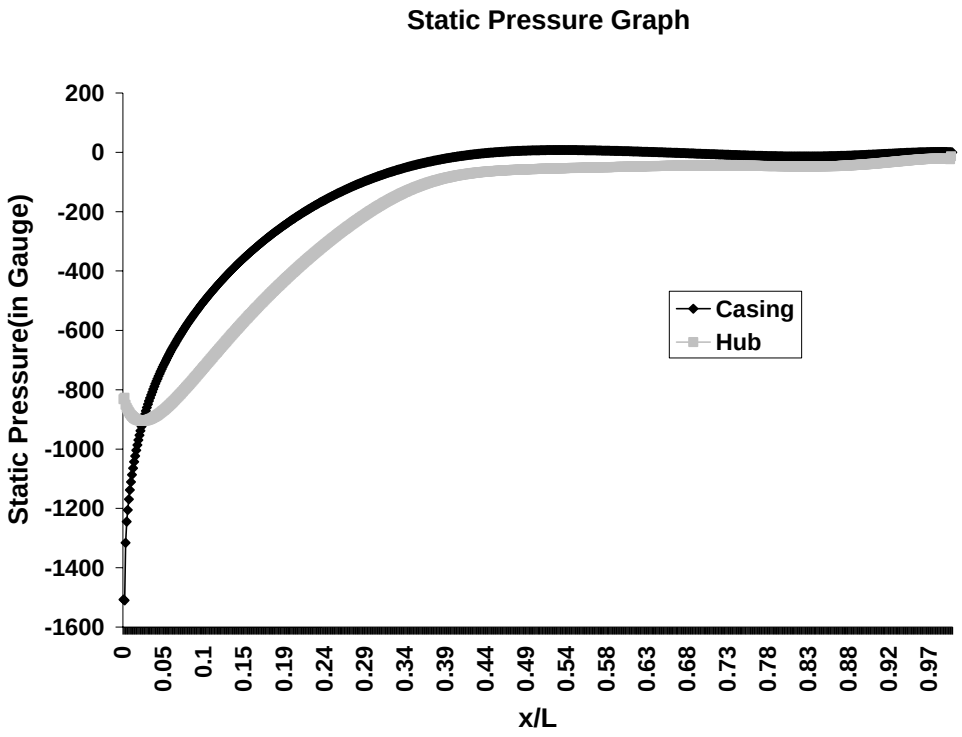

Fig 46

AR = 4, Equivalent Cone Angle = 20 deg, Swirl Angle = 20 deg, Re = 2.5×10^5

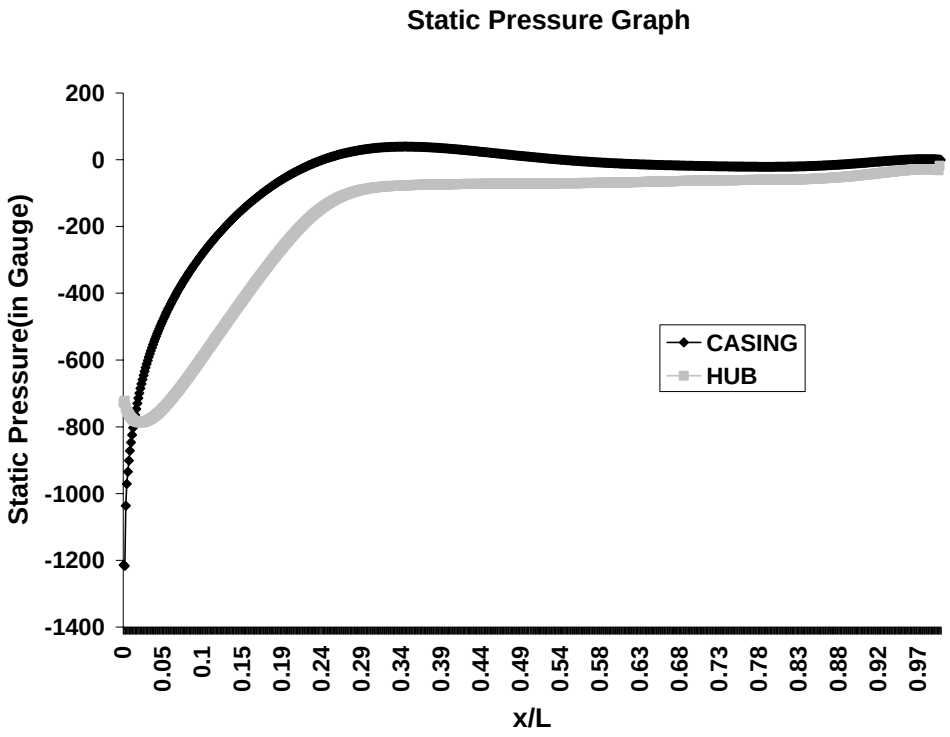

Fig 47

AR = 4, Equivalent Cone Angle = 20 deg, Swirl Angle = 25 deg, Re = 2.5×10^5

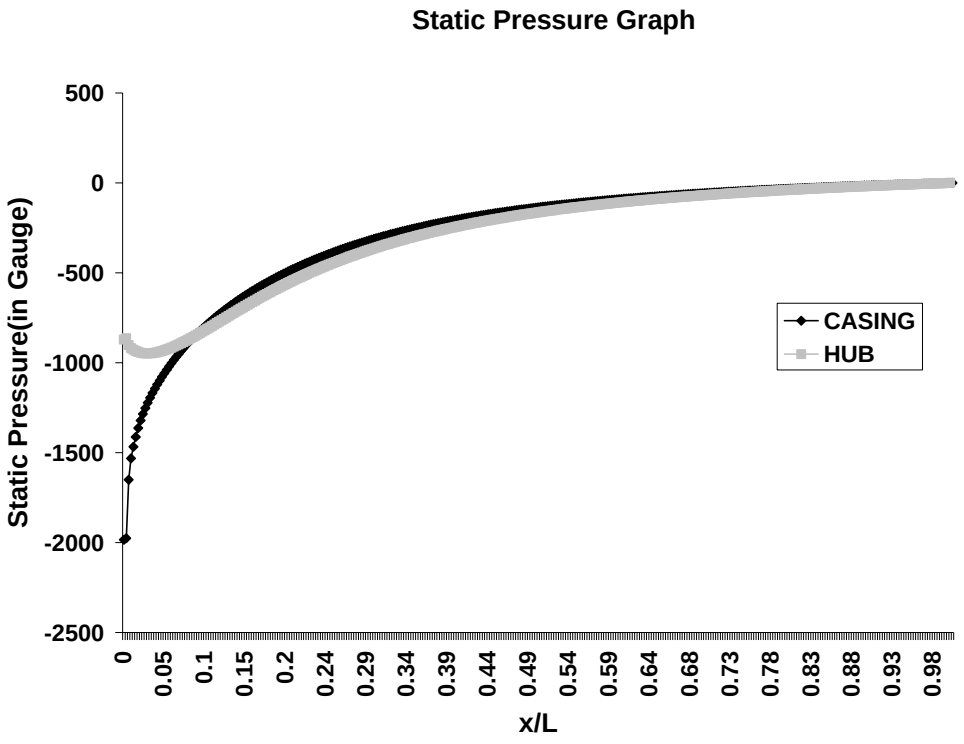

Fig 48

AR = 4, Equivalent Cone Angle = 25 deg, Swirl Angle = 0 deg, Re = 2.5×10^5

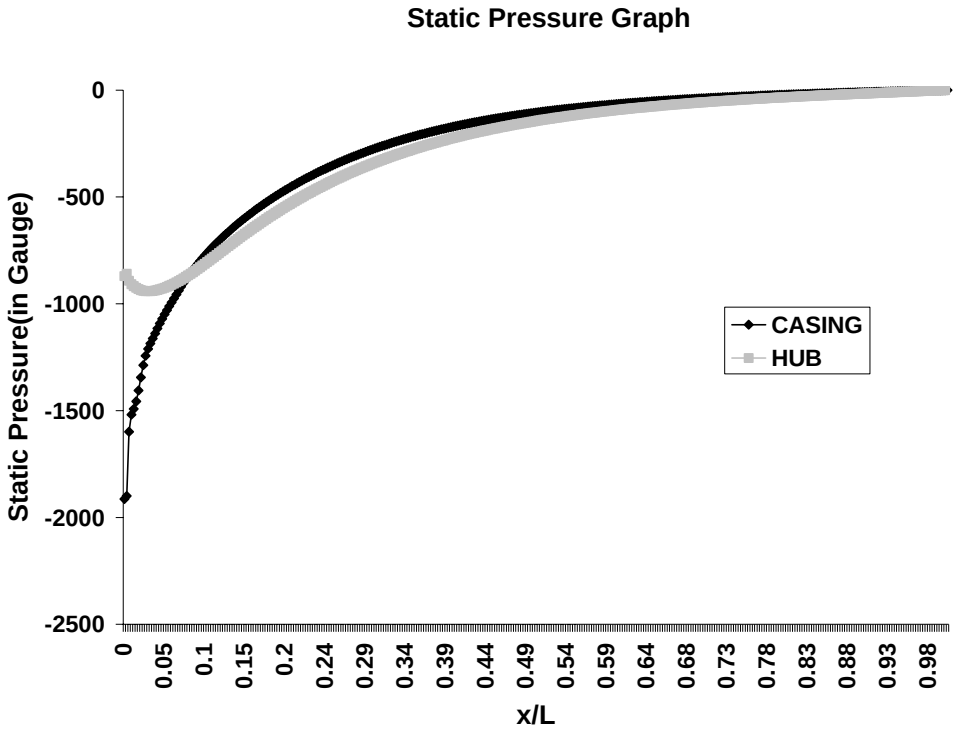

Fig 49

AR = 4, Equivalent Cone Angle = 25 deg, Swirl Angle = 5 deg, Re = 2.5×10^5

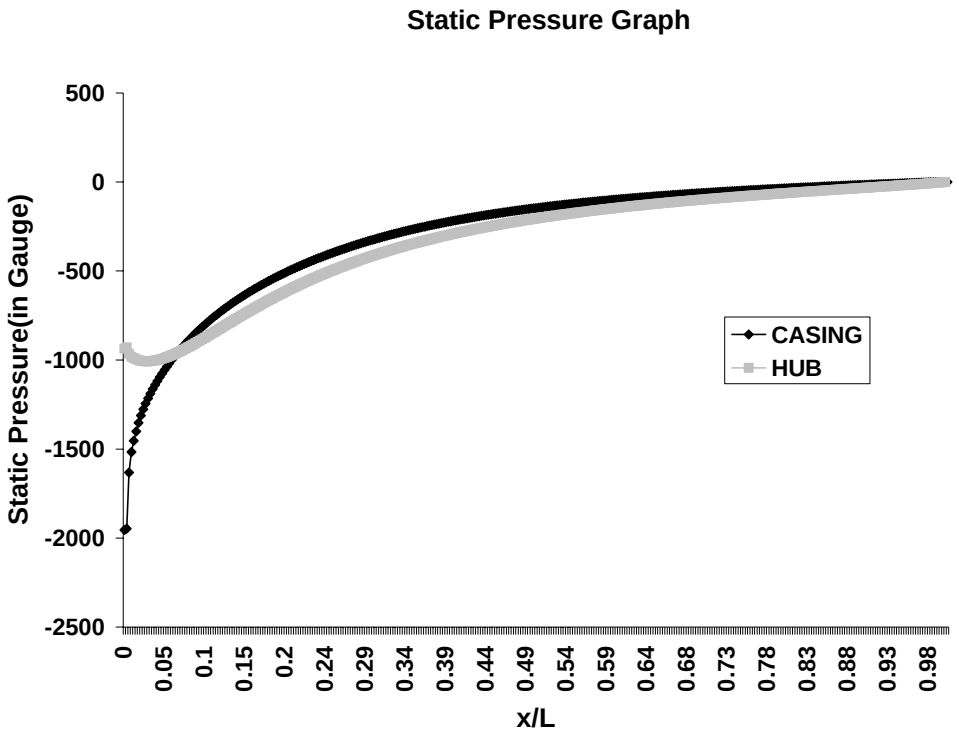

Fig 50

AR = 4, Equivalent Cone Angle = 25 deg, Swirl Angle = 10 deg, Re = 2.5×10^5

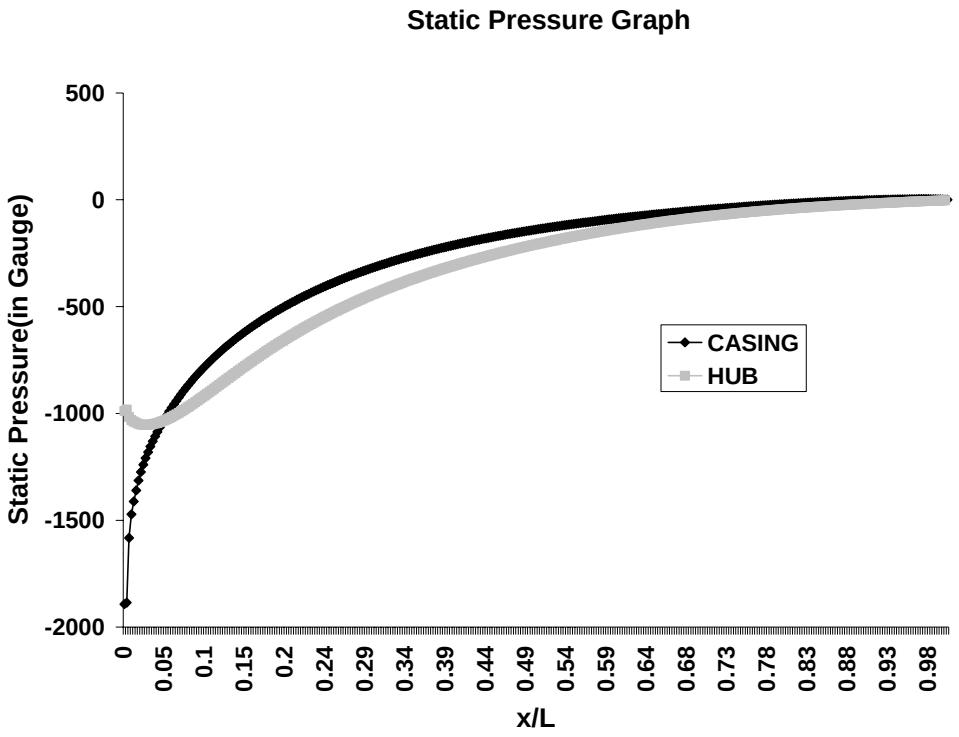

Fig 51

AR = 4, Equivalent Cone Angle = 25 deg, Swirl Angle = 15 deg, Re = 2.5×10^5

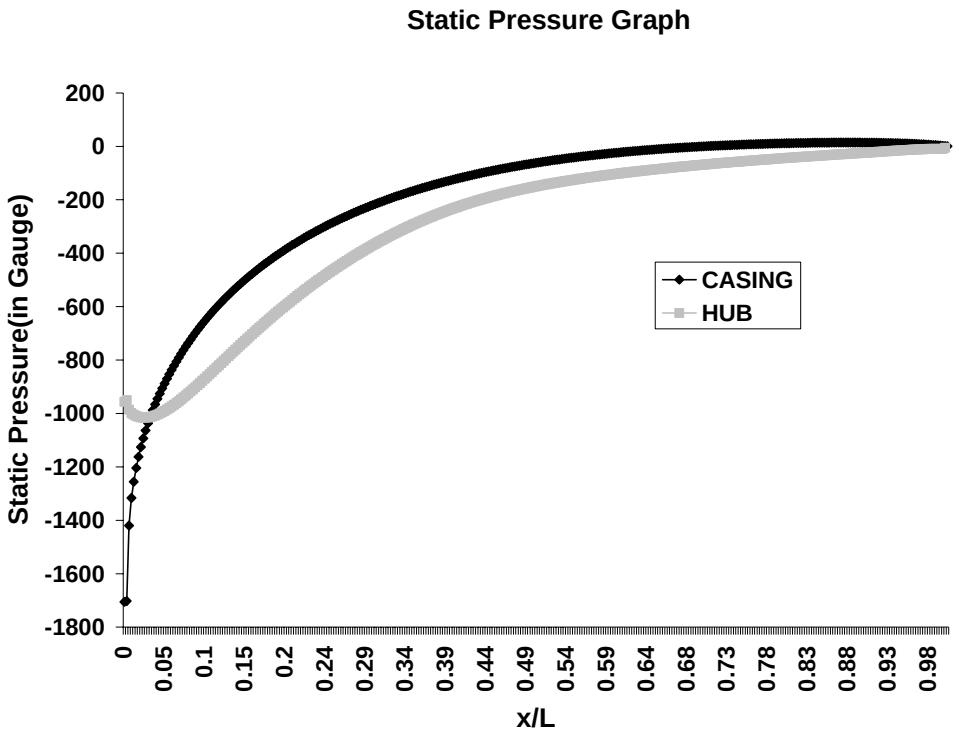

Fig 52

AR = 4, Equivalent Cone Angle = 25 deg, Swirl Angle = 20 deg, Re = 2.5×10^5

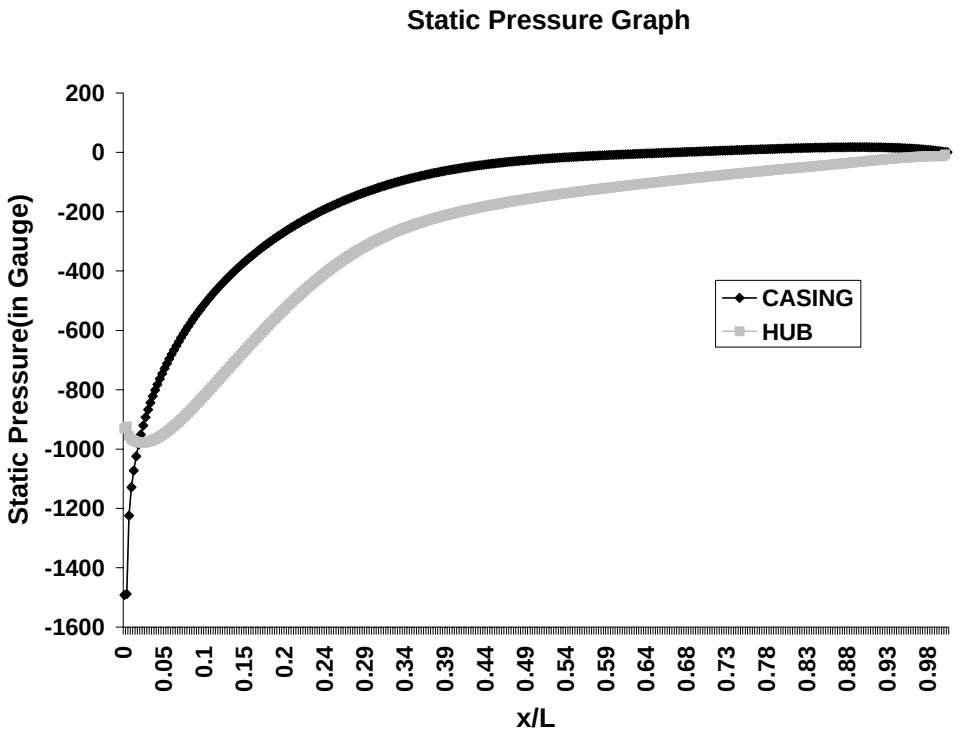

Fig 53

AR = 4, Equivalent Cone Angle = 25 deg, Swirl Angle = 25 deg, Re = 2.5×10^5

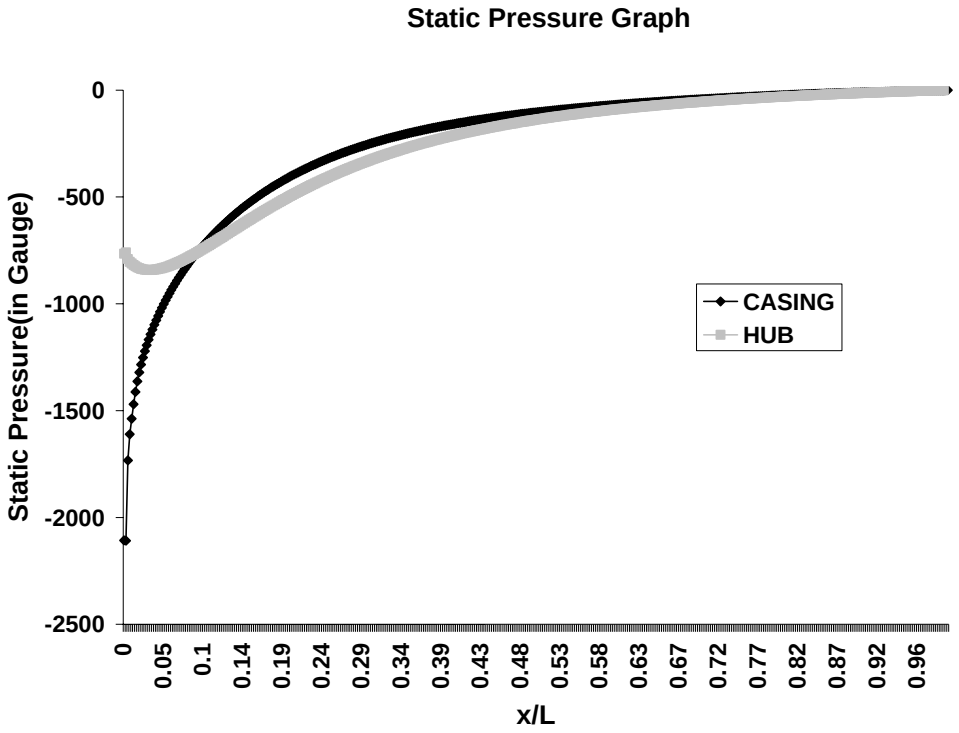

Fig 54

AR = 4, Equivalent Cone Angle = 30 deg, Swirl Angle = 0 deg, Re = 2.5×10^5

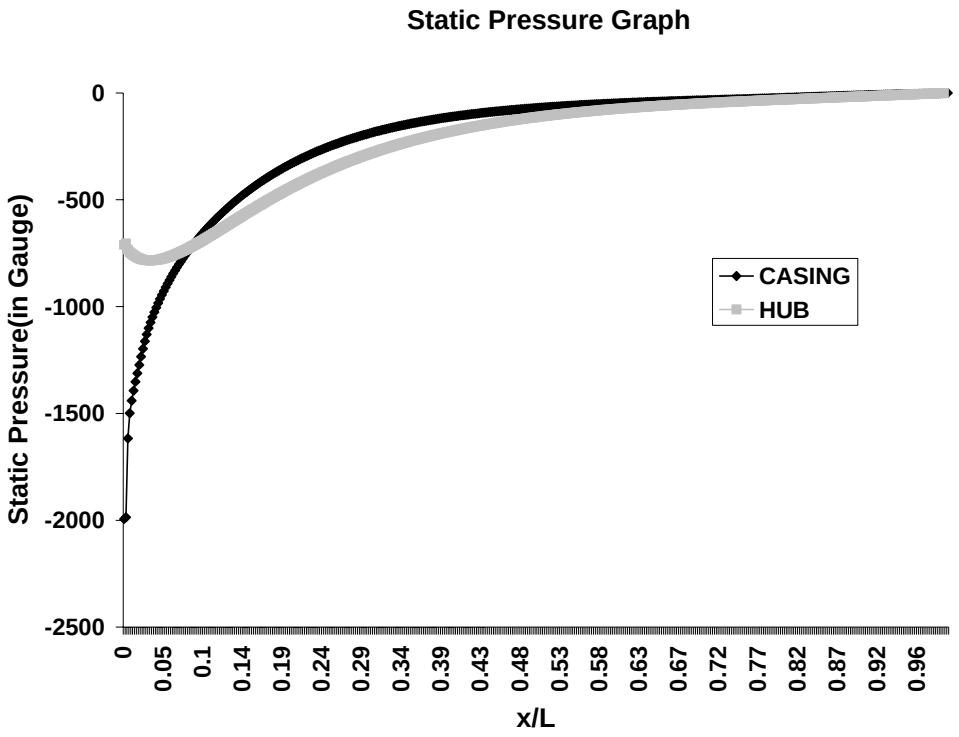

Fig 55

AR = 4, Equivalent Cone Angle = 30 deg, Swirl Angle = 5 deg, Re = 2.5×10^5

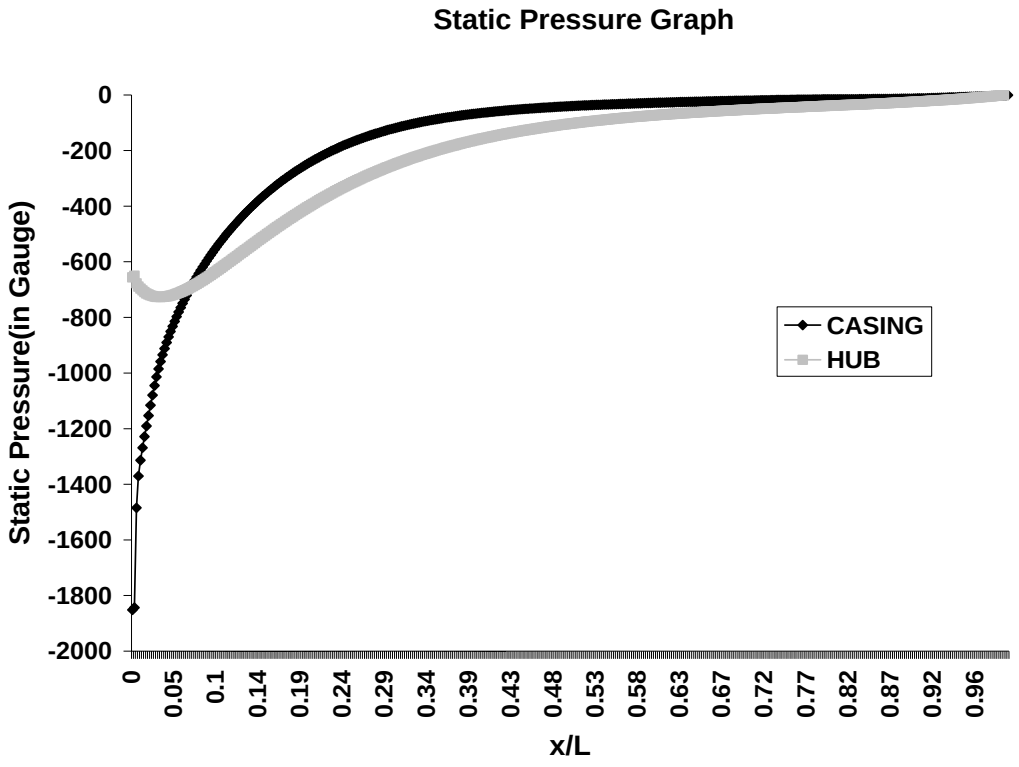

Fig 56

AR = 4, Equivalent Cone Angle = 30 deg, Swirl Angle = 10 deg, Re = 2.5×10^5

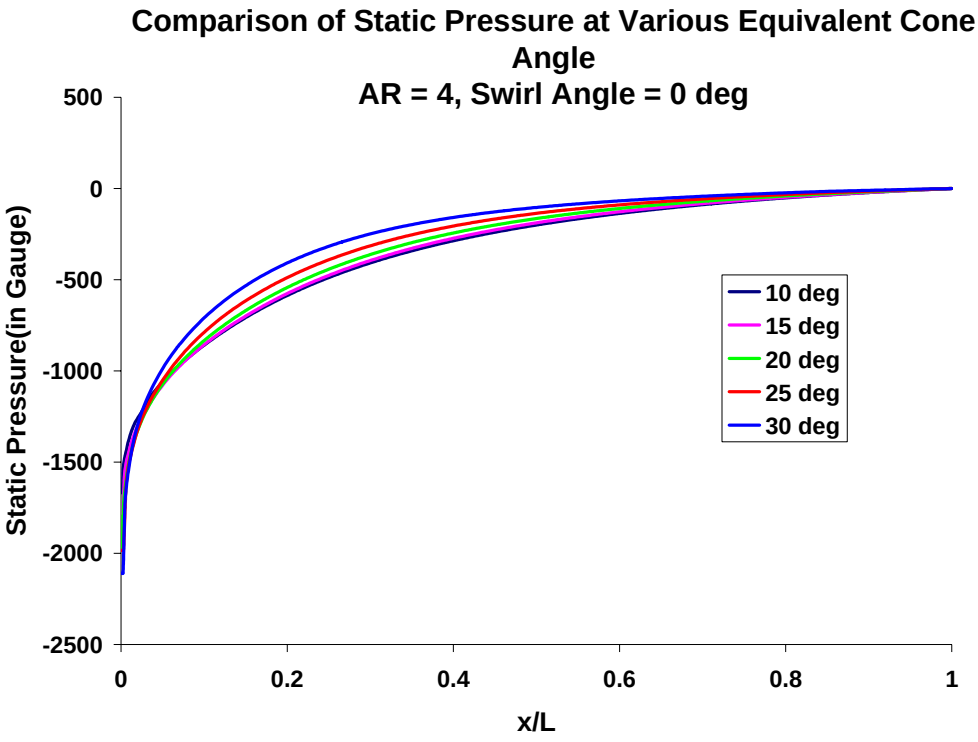
Comparison of Static Pressure at Various Equivalent Cone Angle
AR = 4, Swirl Angle = 0 deg
Static Pressure(in Gauge)
500
0
-500
-1000
-1500
-2000
-2500
0
0.2
0.4
0.6
0.8
1
x/L
10 deg
15 deg
20 deg
25 deg
30 deg

Fig 57

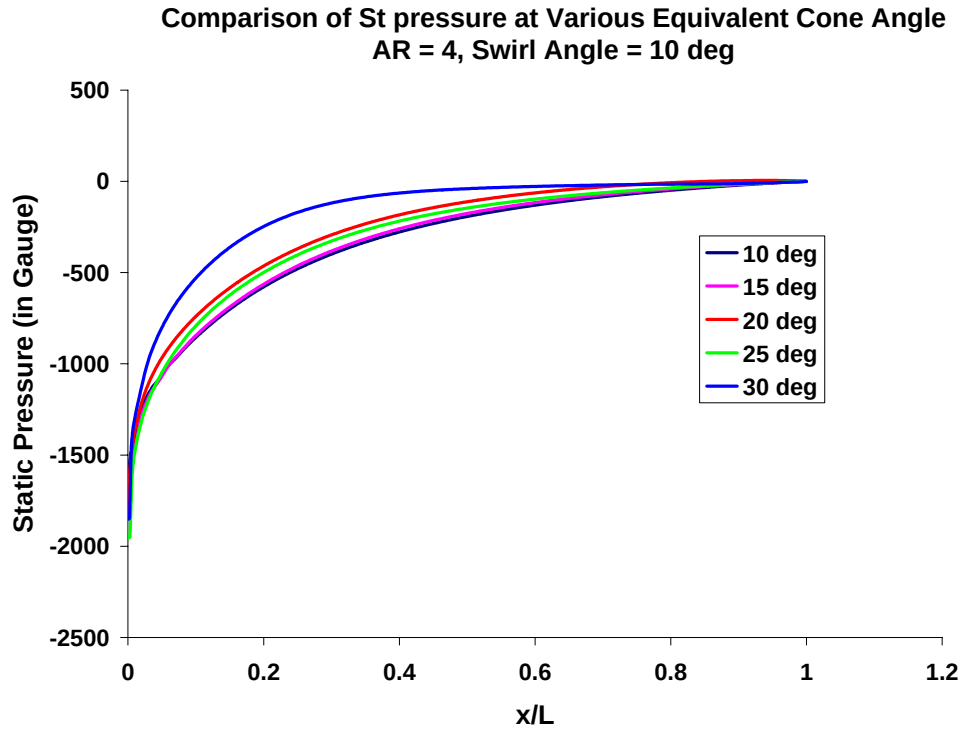
Comparison of St pressure at Various Equivalent Cone Angle
AR = 4, Swirl Angle = 10 deg
Static Pressure (in Gauge)
500
0
-500
-1000
-1500
-2000
-2500
0
0.2
0.4
0.6
0.8
1
1.2
x/L
10 deg
15 deg
20 deg
25 deg
30 deg

Fig 58

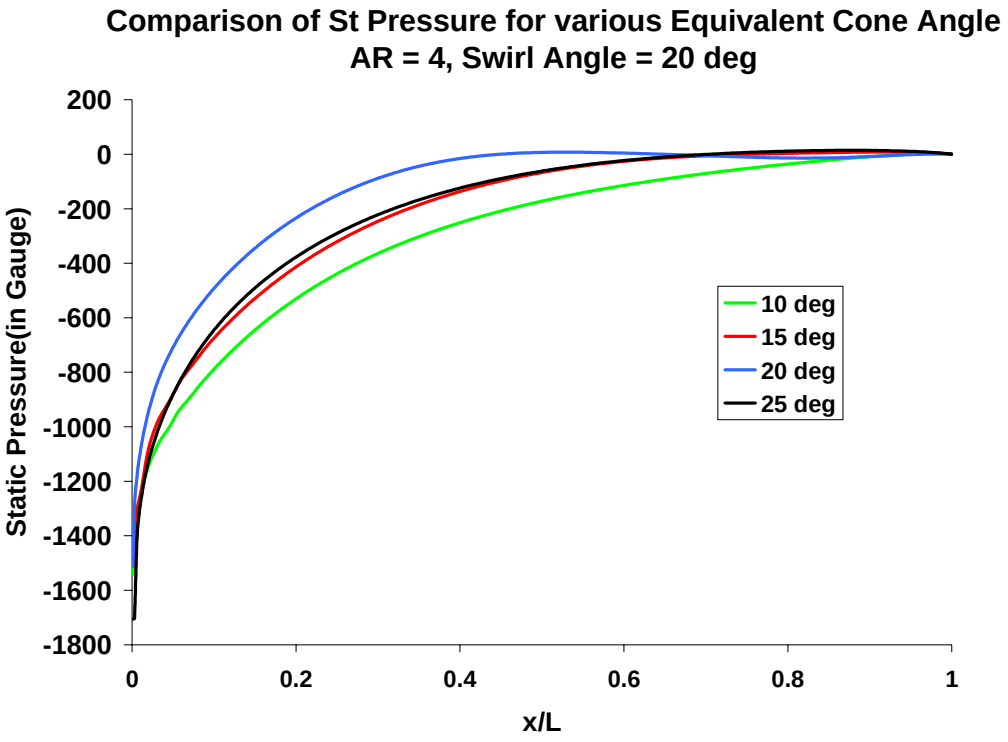
Comparison of St Pressure for various Equivalent Cone Angle
AR = 4, Swirl Angle = 20 deg
Static Pressure(in Gauge)
200
0
-200
-400
-600
-800
-1000
-1200
-1400
-1600
-1800
0
0.2
0.4
0.6
0.8
1
x/L
10 deg
15 deg
20 deg
25 deg

Fig 59

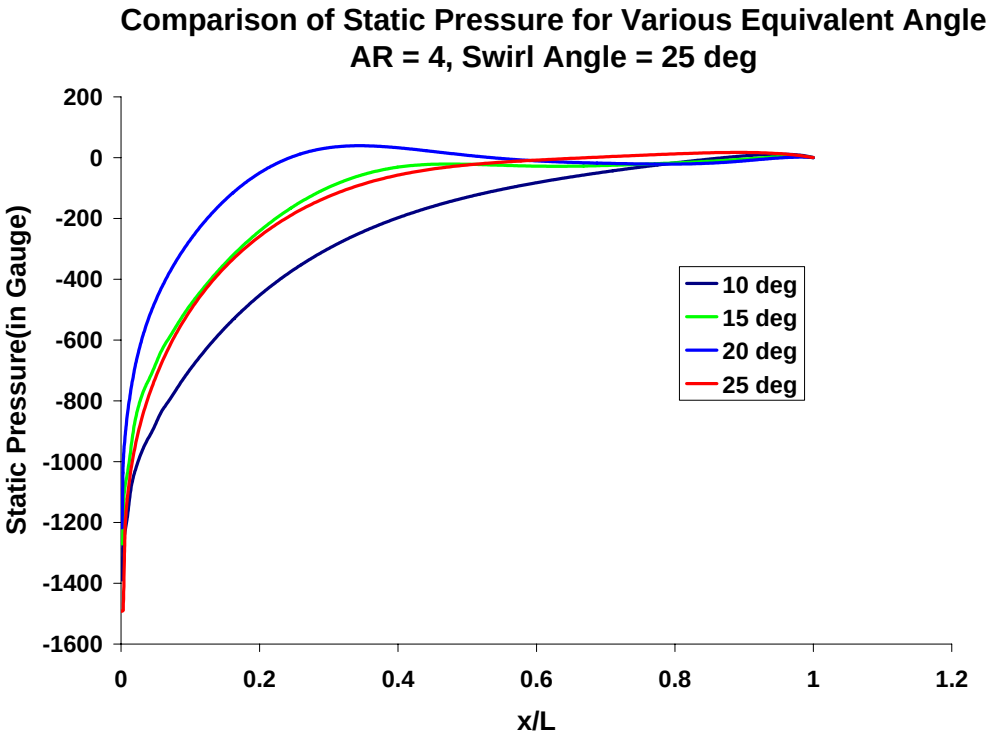
Comparison of Static Pressure for Various Equivalent Angle
AR = 4, Swirl Angle = 25 deg
Static Pressure(in Gauge)
200
0
-200
-400
-600
-800
-1000
-1200
-1400
-1600
0
0.2
0.4
0.6
0.8
1
1.2
x/L
10 deg
15 deg
20 deg
25 deg

Fig 60

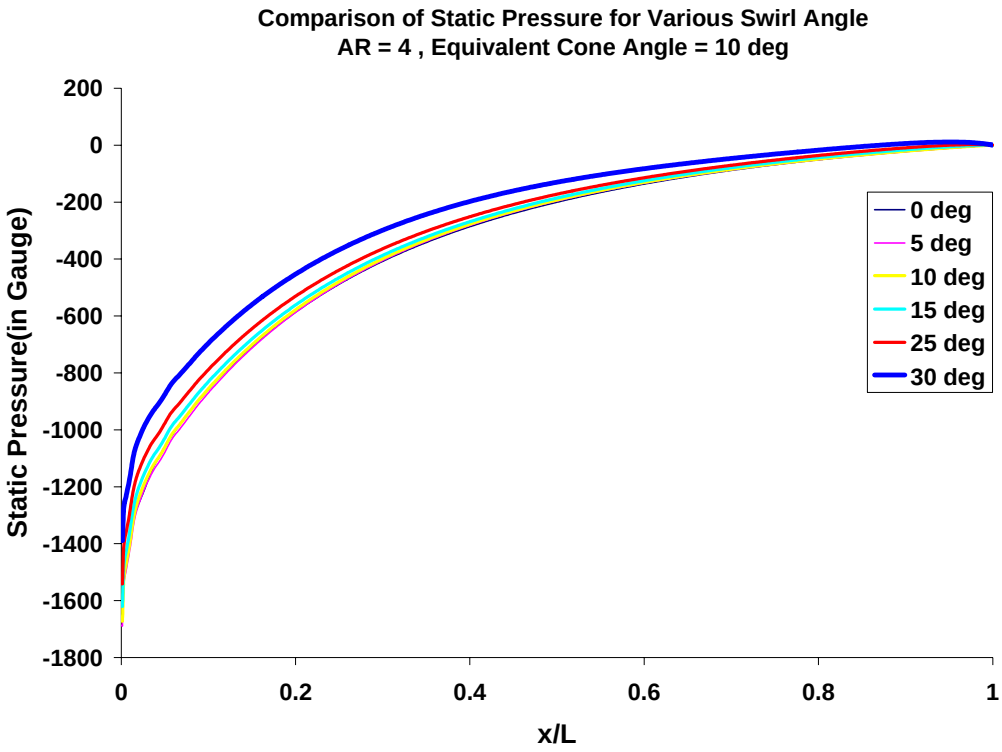
Comparison of Static Pressure for Various Swirl Angle
AR = 4 , Equivalent Cone Angle = 10 deg
Static Pressure(in Gauge)
200
0
-200
-400
-600
-800
-1000
-1200
-1400
-1600
-1800
0
0.2
0.4
0.6
0.8
1
x/L
0 deg
5 deg
10 deg
15 deg
25 deg
30 deg

Fig 61

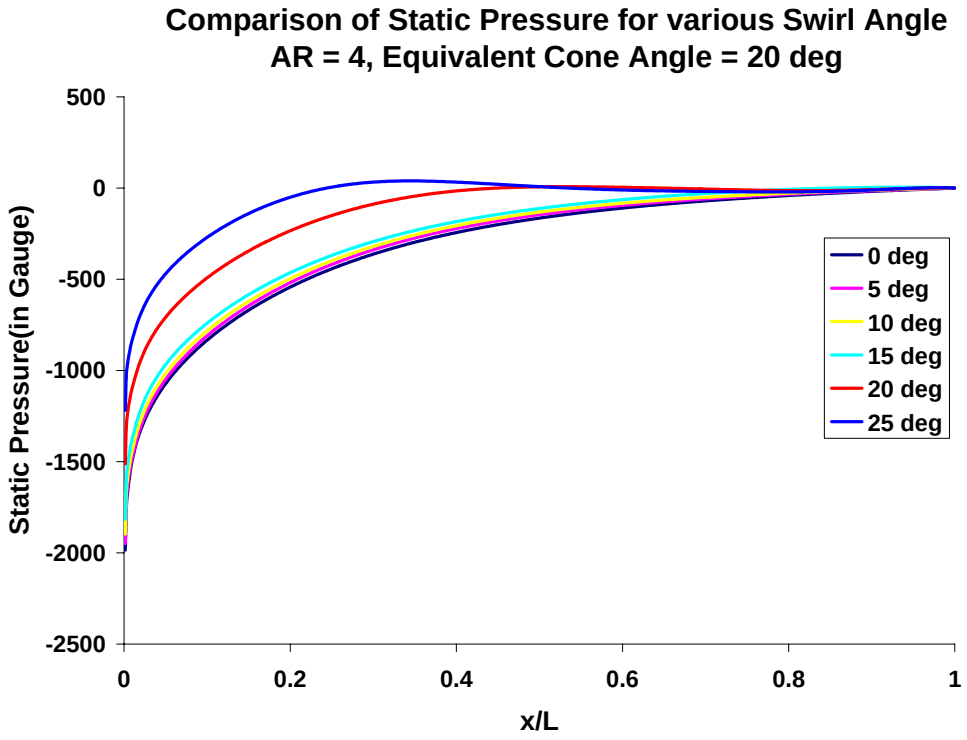
Comparison of Static Pressure for various Swirl Angle
AR = 4, Equivalent Cone Angle = 20 deg
Static Pressure(in Gauge)
500
0
-500
-1000
-1500
-2000
-2500
0
0.2
0.4
0.6
0.8
1
x/L
0 deg
5 deg
10 deg
15 deg
20 deg
25 deg

Fig 62

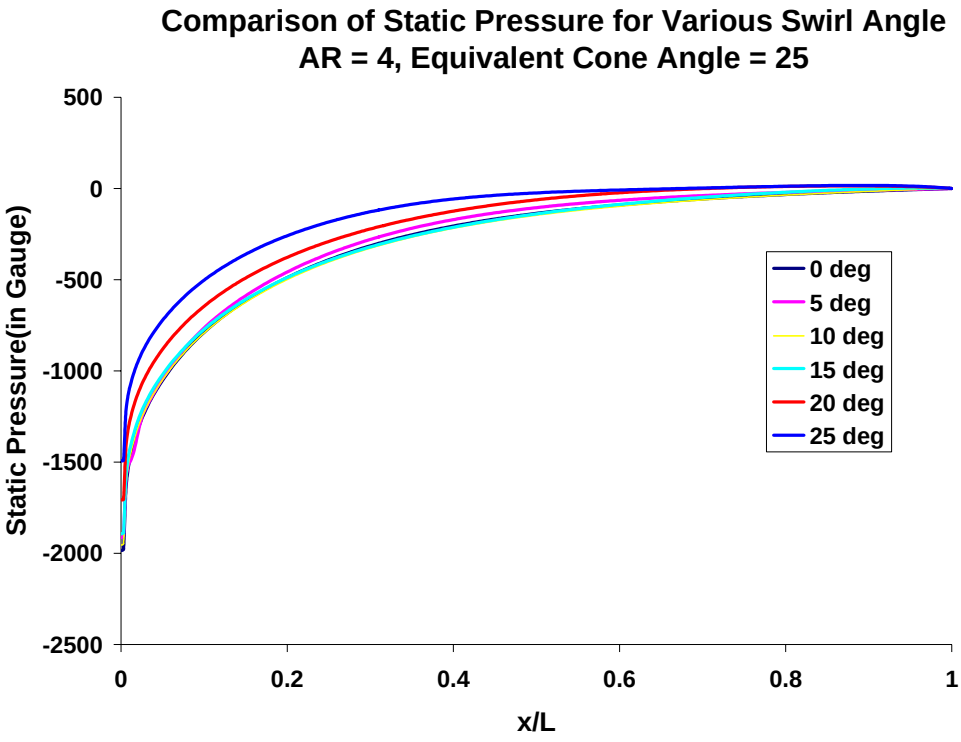

Fig 63

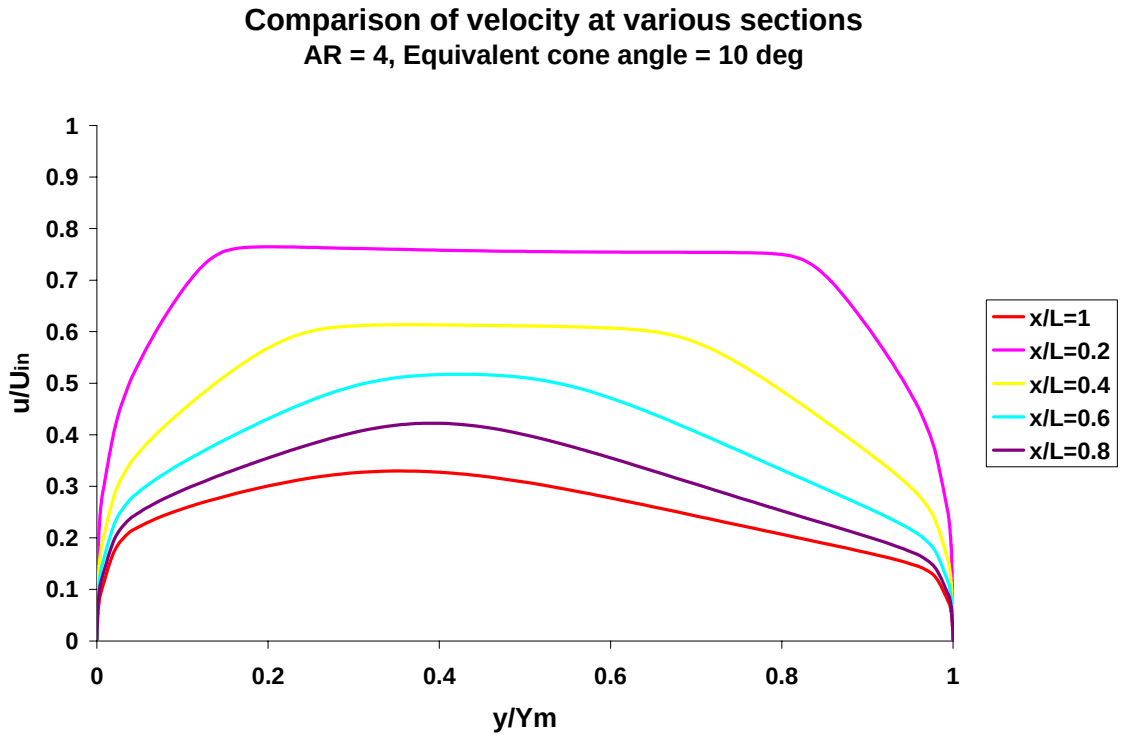

Fig 64

AR=4, Equivalent Cone Angle = 10 deg, Swirl Angle = 0 deg

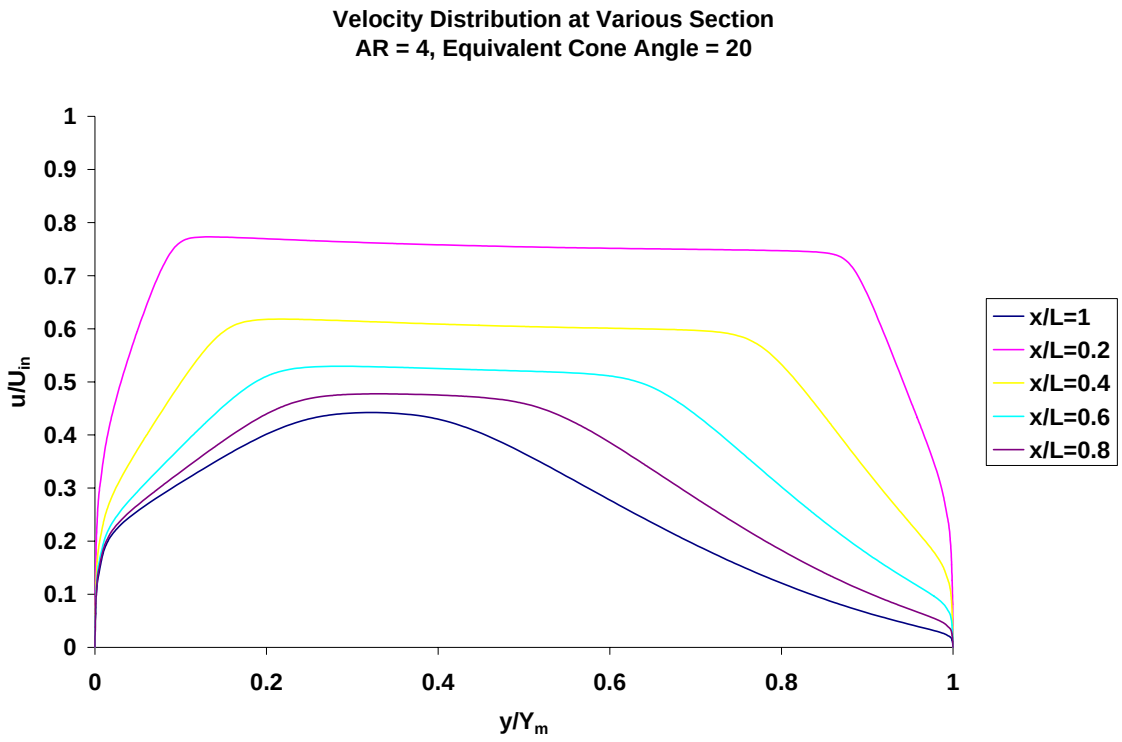

Fig 65

AR=4, Equivalent Cone Angle = 20 deg, Swirl Angle = 0 deg

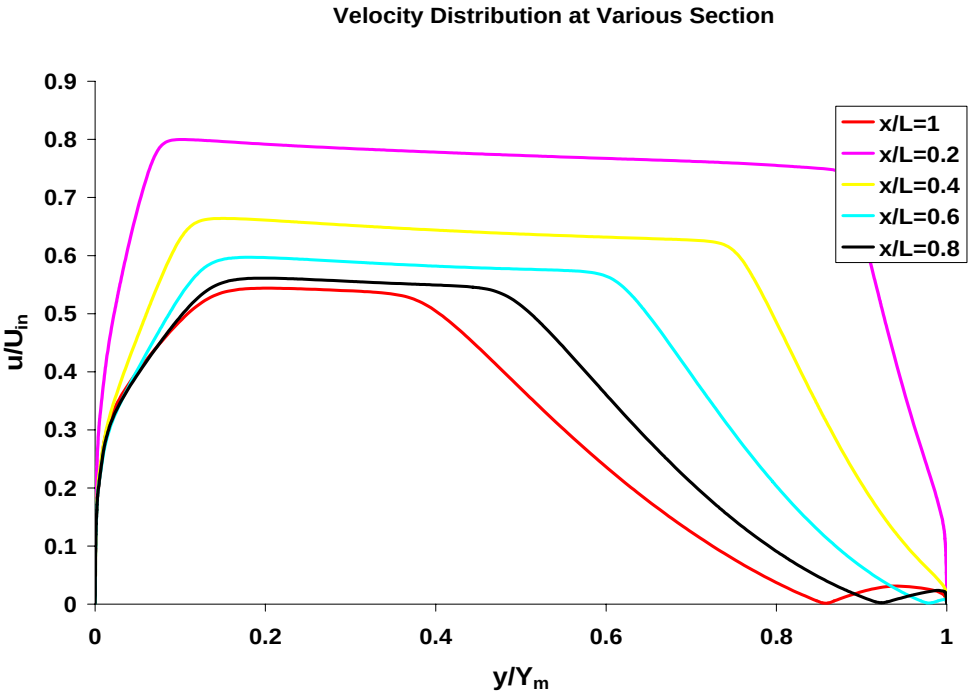

Fig 66 AR=4, Equivalent Cone Angle = 30 deg, Swirl Angle = 0 deg

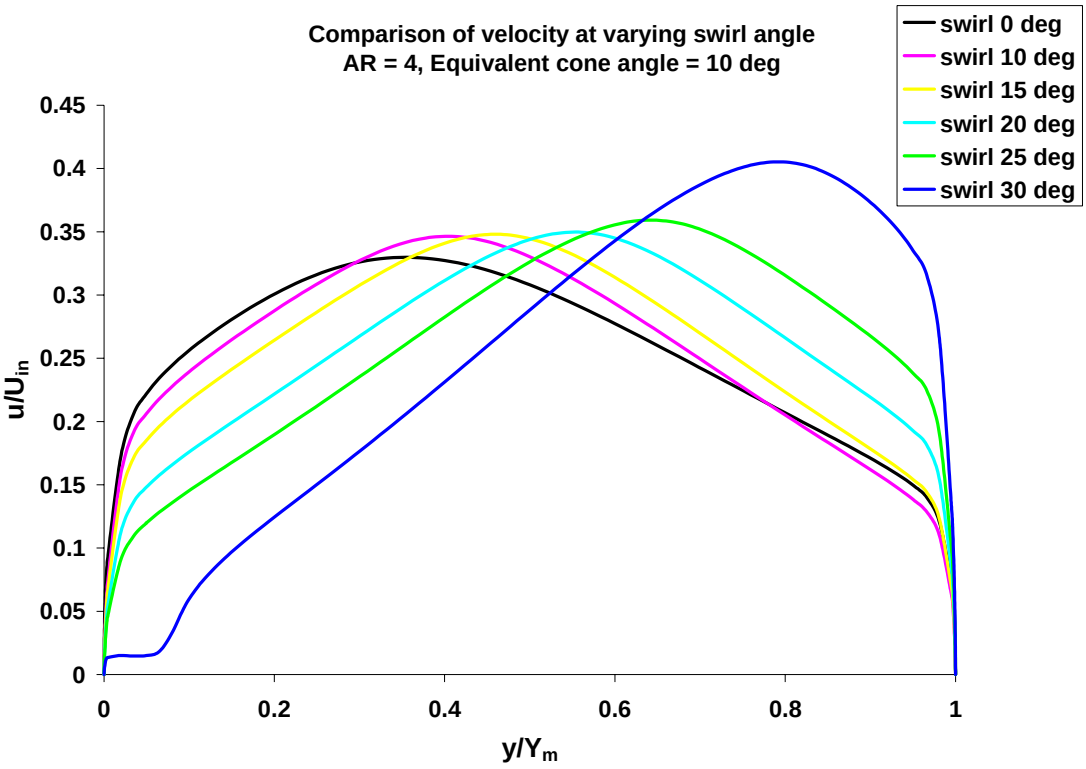
Comparison of velocity at varying swirl angle
AR = 4, Equivalent cone angle = 10 deg
swirl 0 deg
swirl 10 deg
swirl 15 deg
swirl 20 deg
swirl 25 deg
swirl 30 deg
0.45
0.4
0.35
0.3
0.25
0.2
0.15
0.1
0.05
0
u/U_in
0
0.2
0.4
0.6
0.8
1
y/Y_m

Fig 67

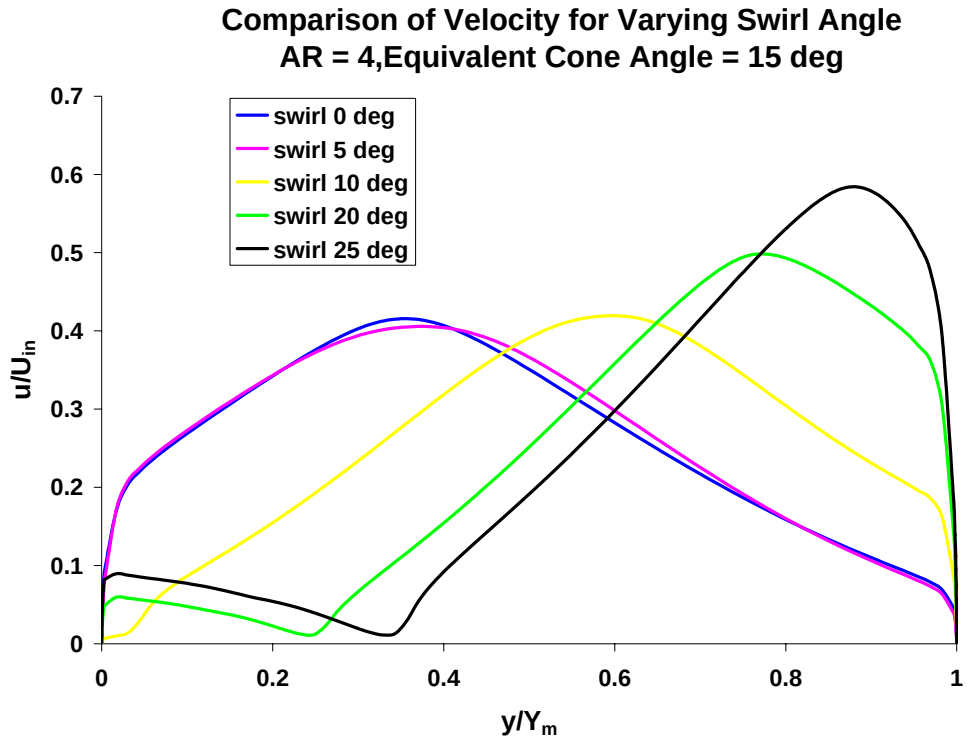
Comparison of Velocity for Varying Swirl Angle
AR = 4,Equivalent Cone Angle = 15 deg
swirl 0 deg
swirl 5 deg
swirl 10 deg
swirl 20 deg
swirl 25 deg
0.7
0.6
0.5
0.4
0.3
0.2
0.1
0
u/U_in
0
0.2
0.4
0.6
0.8
1
y/Y_m

Fig 68

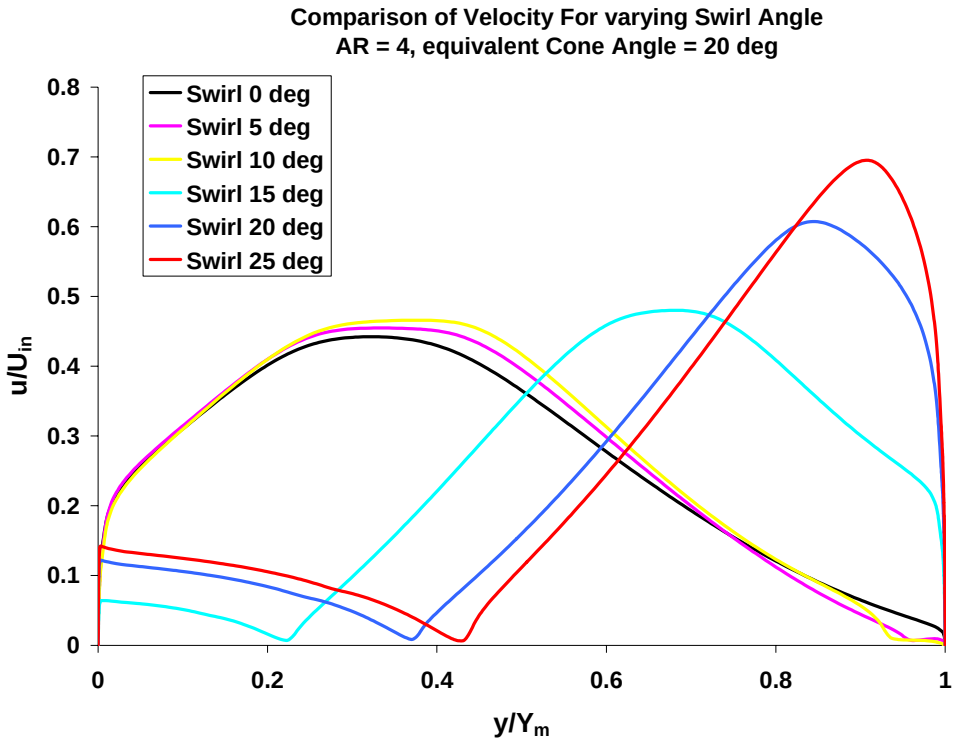
Comparison of Velocity For varying Swirl Angle
AR = 4, equivalent Cone Angle = 20 deg
Swirl 0 deg
Swirl 5 deg
Swirl 10 deg
Swirl 15 deg
Swirl 20 deg
Swirl 25 deg
u/U_in
y/Y_m
0
0.1
0.2
0.3
0.4
0.5
0.6
0.7
0.8
0.2
0.4
0.6
0.8
1

Fig 69

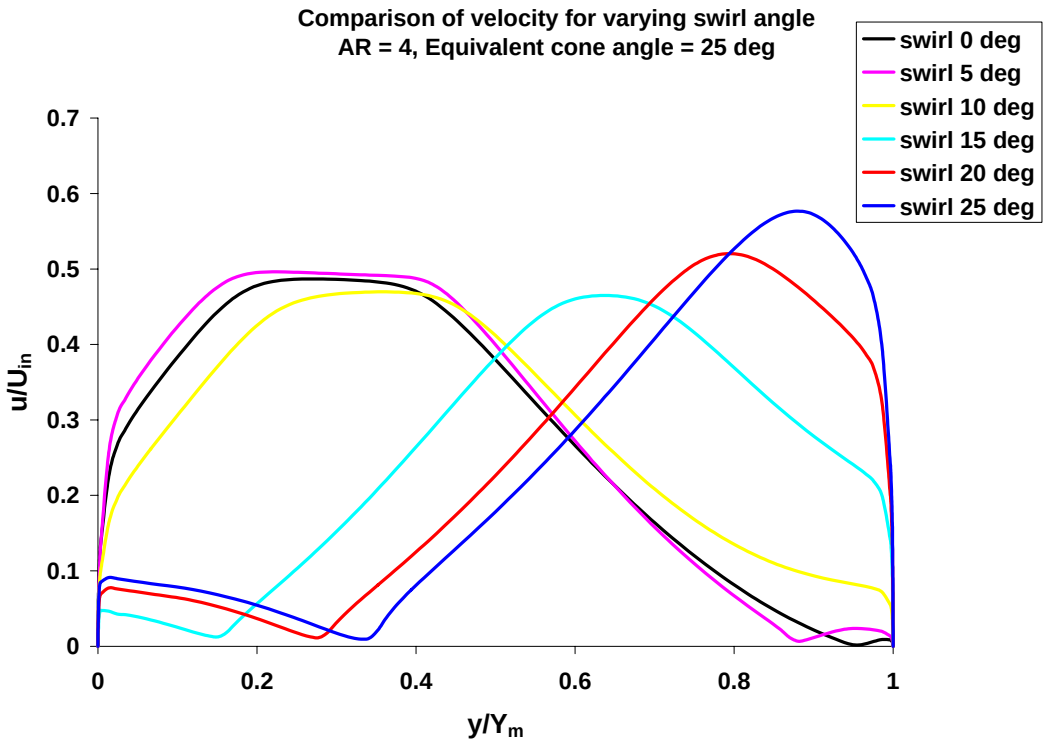
Comparison of velocity for varying swirl angle
AR = 4, Equivalent cone angle = 25 deg
swirl 0 deg
swirl 5 deg
swirl 10 deg
swirl 15 deg
swirl 20 deg
swirl 25 deg
u/U_in
y/Y_m
0
0.1
0.2
0.3
0.4
0.5
0.6
0.7
0.2
0.4
0.6
0.8
1

Fig 70

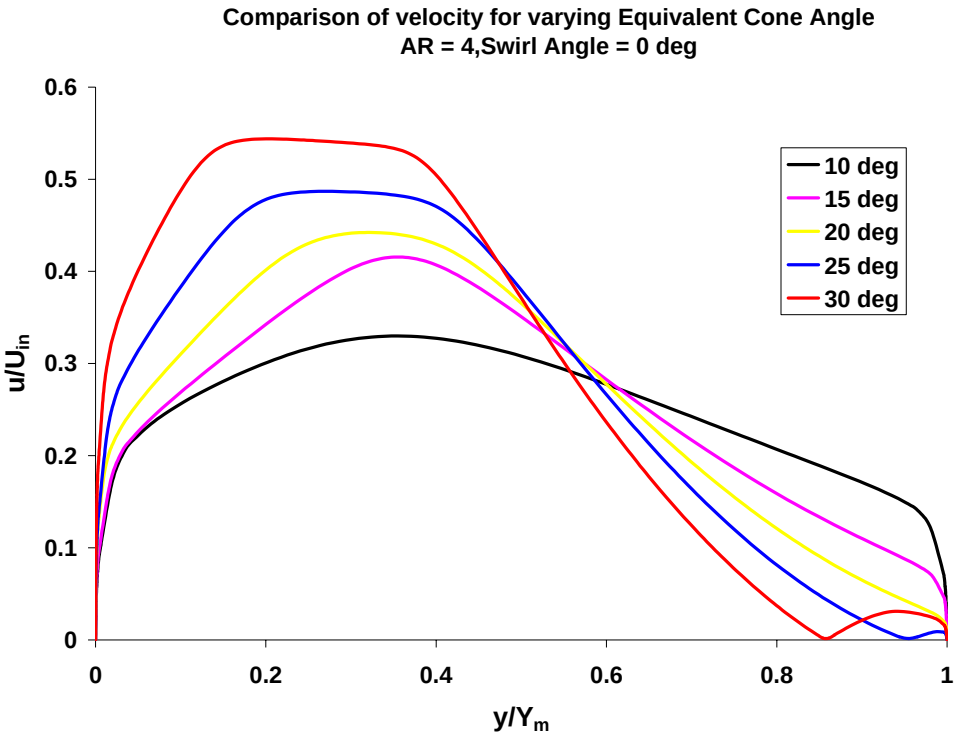
Comparison of velocity for varying Equivalent Cone Angle
AR = 4,Swirl Angle = 0 deg
u/U_in
y/Y_m
0.6
0.5
0.4
0.3
0.2
0.1
0
0
0.2
0.4
0.6
0.8
1
10 deg
15 deg
20 deg
25 deg
30 deg

Fig 71

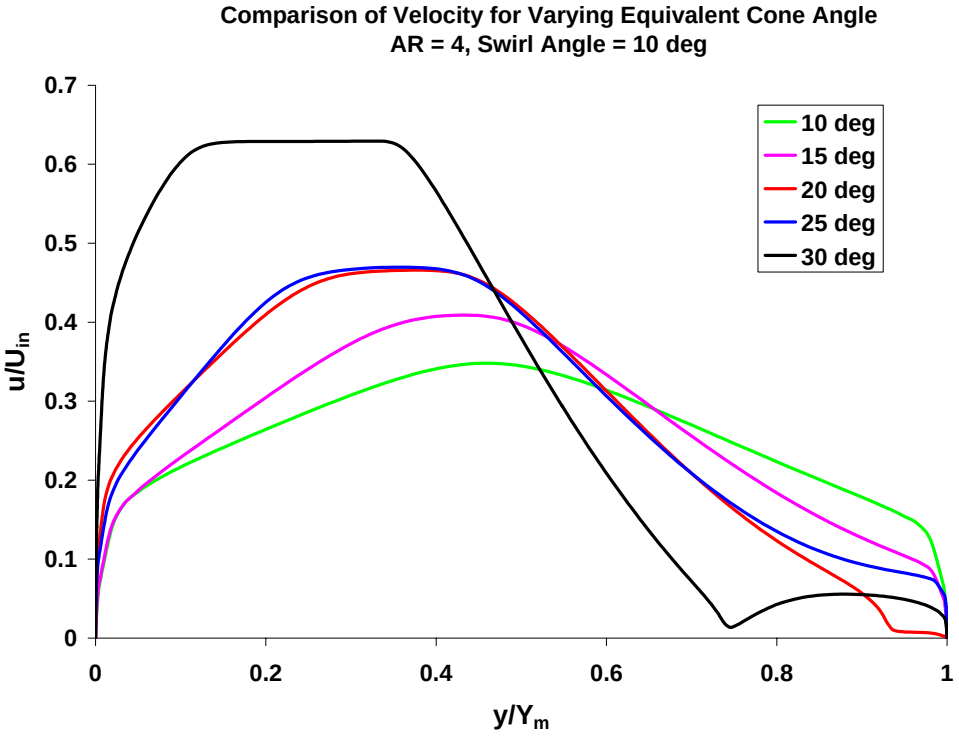
Comparison of Velocity for Varying Equivalent Cone Angle
AR = 4, Swirl Angle = 10 deg
u/U_in
y/Y_m
0.7
0.6
0.5
0.4
0.3
0.2
0.1
0
0
0.2
0.4
0.6
0.8
1
10 deg
15 deg
20 deg
25 deg
30 deg

Fig 72

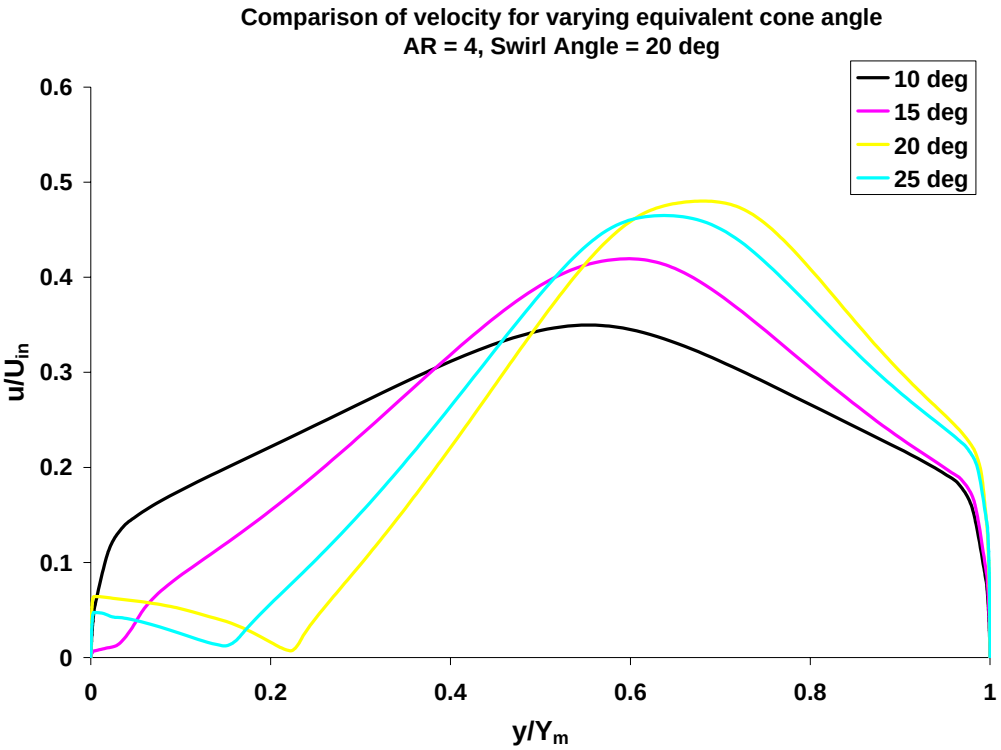
Comparison of velocity for varying equivalent cone angle
AR = 4, Swirl Angle = 20 deg
10 deg
15 deg
20 deg
25 deg
u/U_in
y/Y_m
0
0.1
0.2
0.3
0.4
0.5
0.6
0.2
0.4
0.6
0.8
1

Fig 73

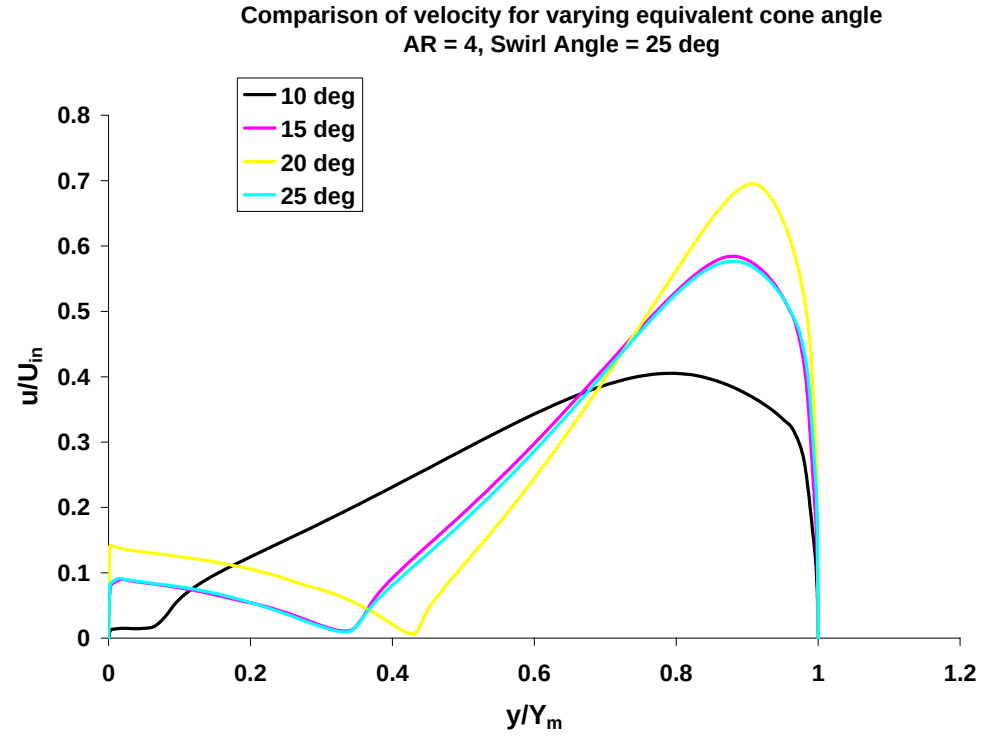
Comparison of velocity for varying equivalent cone angle
AR = 4, Swirl Angle = 25 deg
10 deg
15 deg
20 deg
25 deg
u/U_in
y/Y_m
0
0.1
0.2
0.3
0.4
0.5
0.6
0.7
0.8
0.2
0.4
0.6
0.8
1
1.2

Fig 74

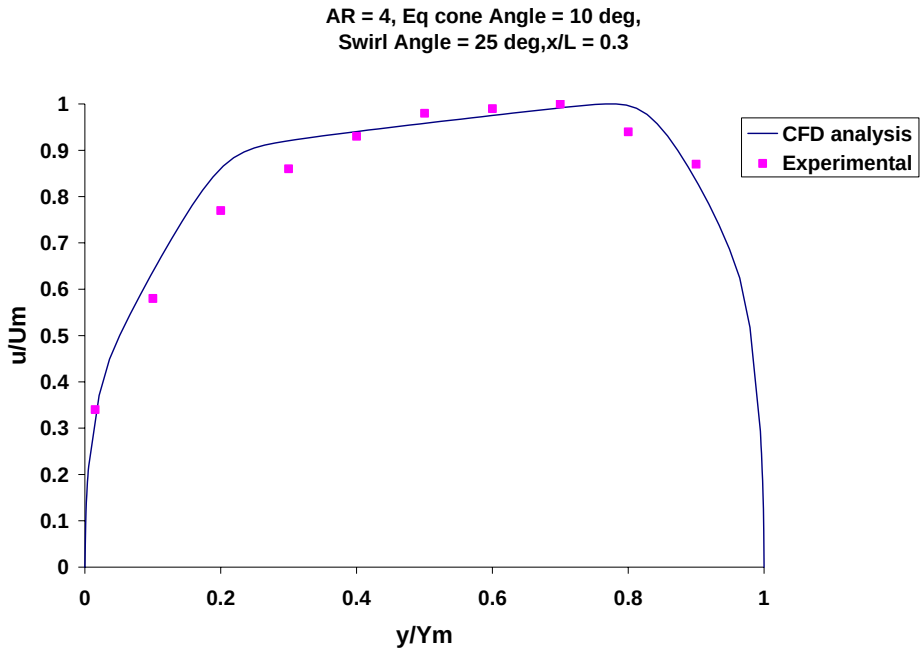

Fig 75 Validation of Fluent Code

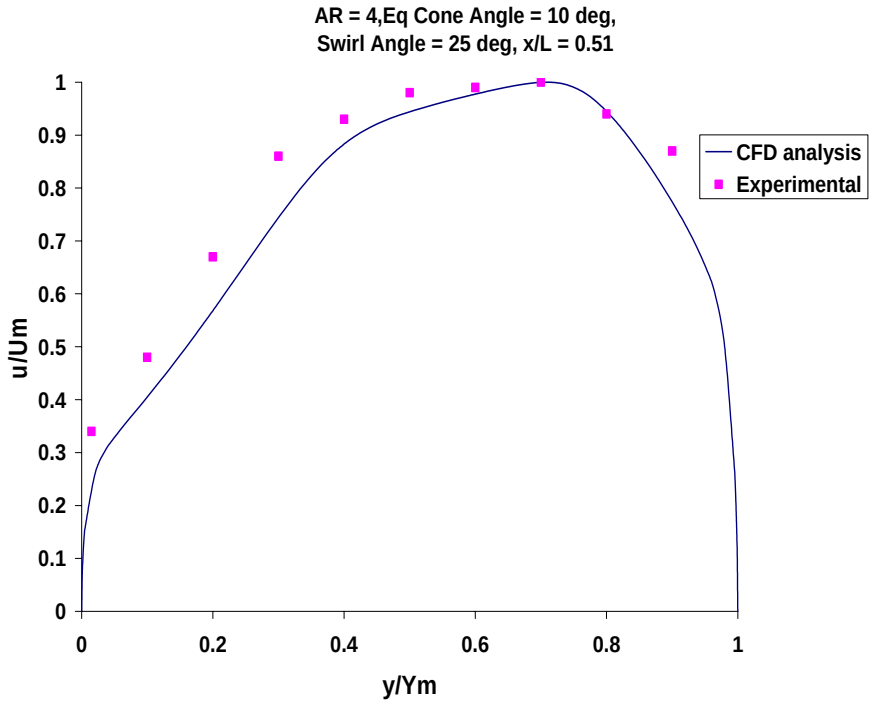

Fig 76 Validation of Fluent Code

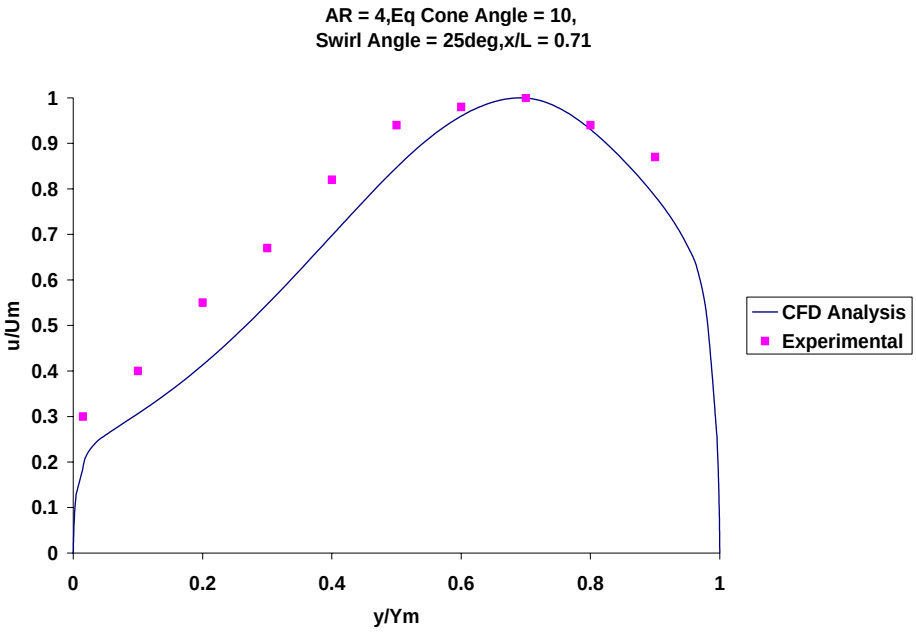

Fig 77 Validation of Fluent Code